

**STRUCTURAL AND FUNCTIONAL REMODELING OF NEURONAL CIRCUITRY
SURROUNDING IMPLANTED ELECTRODES**

By

Joseph William Salatino

A DISSERTATION

Submitted to
Michigan State University
in partial fulfillment of the requirements
for the degree of

Biomedical Engineering—Doctor of Philosophy

2019

ABSTRACT

STRUCTURAL AND FUNCTIONAL REMODELING OF NEURONAL CIRCUITRY SURROUNDING IMPLANTED ELECTRODES

By

Joseph William Salatino

Microelectrode arrays designed to map and modulate neuronal circuitry have enabled greater understanding and treatment of neurological injury and disease. However, poor biological integration remains a significant barrier to the longevity and stability of electrodes implanted in the brain, where gliosis and neuronal loss are commonly attributed to instability and loss of signal over time. However, these metrics do not reliably predict signal loss, and device failure modes remain elusive. Here, this work provides fundamental insight into *biological mechanisms* that contribute to these failure modes, as well as develops genetic engineering strategies to improve the biointegration of brain implants.

While signal-generating neurons have traditionally been considered the important target cells for implanted electrodes, it has become increasingly appreciated that glia remodel the structure and function of neuronal networks following injury, where recent work has uncovered mechanisms relevant to the injuries and ensuing gliosis caused by the implantation of chronic devices. Chapter 2 disseminates important considerations for glial reactivity on device performance and provides a framework for topics explored in subsequent Chapters. Although decades of work has demonstrated that cortical injury generates long-term remodeling of excitatory/inhibitory synapses (the connections which facilitate the propagation of information between neurons) and ion channels (the transmembrane proteins responsible for generating neuronal signals), these mechanisms

have not been investigated around implanted arrays; however, the consequences of these events hold significant implications for the long-term recording stability of implanted devices. Chapter 3 reveals novel changes in both excitatory and inhibitory synaptic circuitry surrounding implanted microelectrodes, where early elevations in excitatory synapses are followed by a shift to inhibitory tone in the chronic setting. A novel subtype of glia is also identified local to the device interface. Chapter 4 reveals a novel relationship between electrophysiological recordings and ion channel expression surrounding implanted arrays over time, where a loss of sodium channel expression and gain in potassium channel expression corresponds with a loss of recorded signals over time. Together, this work supports a trend from hyper- to hypo-excitability, which temporally coincides with signal variability and loss observed with chronic devices.

The previous chapters provide fundamental insight into major circuit changes at the interface that inform both basic-science knowledge and new strategies for improving the biointegration of brain implants. We are developing new approaches to reveal the mechanistic role of these factors in affecting recorded signals over time. Chapter 5 covers ongoing work that includes the development and validation of innovative strategies to deliver genetic material at the interface *in vivo* to yield entirely new avenues of research with opportunities to regulate gene expression and/or introduce new genetic material to rewire the interfacial network. Future directions are discussed with opportunities to unmask key circuit-remodeling effects that impair device performance as well as inform the seamless integration of brain implants.

Copyright by
JOSEPH WILLIAM SALATINO
2019

This dissertation is dedicated to my exceptional family; especially, my parents Denise and Bill Salatino and grandparents Mary and Vito Salatino, who have provided invaluable support and inspiration for my academic and professional pursuits.

ACKNOWLEDGMENTS

None of this would have been possible without the exceptional support of my advisor, Dr. Erin Purcell. She has been the major driving force behind my academic and professional achievements. As the first graduate student in her lab, everything I have learned has come first-hand from her. She has devoted significant efforts to develop my research techniques, scientific acumen, and writing skills in ways that have been invaluable. She has continued to push me to expand my research repertoire, attend supplemental conferences, collaborate with excellent cross-disciplinary and multi-institutional teams, and sustain productivity with publications and conference presentations. Above all else, she has supported my goals to achieve my career aspirations unconditionally. Needless to say, I am very grateful for the gift of her support and wouldn't be here without it. In addition, my committee has provided valuable support and insights to guide my work, and I would like to thank Dr. Brian Gulbransen, Dr. Wen Li, and Dr. Galit Pelled for all of their time and effort.

I have many individuals to thank for guidance and intellectual contributions to my work over the years. Steve Suhr (of Biomilab, LLC) has provided invaluable feedback, direction, and experimental contributions to my work, including a plethora of molecular biology insights, tools and experimental data over the years. His expertise and insights have been critical to my research from the very start, and our countless discussions on startups and the business aspects of science have contributed to my professional development immensely over the years. Marie-Claude Senut (of Biomilab, LLC) has also provided invaluable feedback and contributions to my experimental work and, much like Steve, has taught me a tremendous amount both in- and outside of the lab from the beginning. They are

truly an exceptional couple and I am very grateful for their expertise, generosity, and friendship. Kip Ludwig (of UW Madison) has been a tremendous role model and colleague throughout my PhD. Beyond learning from his expertise in writing the Nature BME review article together, Kip has continued to invest his time in me with ongoing career advice over the years that has immensely shaped my career progression to this point. He has also been tremendously supportive of my work and accomplishments – all of which I cannot express my gratitude enough for. Nick Langhals (of NIH) taught me valuable knowledge regarding extracellular electrophysiology analysis. The summer I started, he consulted for the lab and spent many hours with me running through code and data that I am very grateful for. Nick also bestowed advice that has benefitted me in navigating the field of neural engineering and my career. TK Kozai (of U Pitt) has been another great role model and colleague over the years. Beyond learning from his expertise in writing the Nature BME review together, TK has provided continued insights into my work and valuable advice that contributed to the trajectory of my research.

Several other individuals directly contributed to this experimental work. Bailey Winter has written elegant MATLAB scripts for data analysis and contributed to surgical and histological data collection for numerous projects during her Bachelor's and Master's degrees; I am grateful for her many contributions. Sam Daniels quickly mastered the numerous techniques necessary to contribute to all aspects of my work. His contributions are most evidenced in the final chapter of this dissertation and will continue to build off of this work most directly moving forward, which I am excited to see the outcome of with his dissertation. I am grateful for all of his contributions over the past year and a half. Bronson Gregory (of the Lee Cox Lab) has spearheaded the brain slice electrophysiology and two-

photon experiments in Chapter 5. It has been a great pleasure working with him and watching him generate a high-impact dataset with this novel “high-risk, high-reward” technique. John Seymour (of UMich) has been an exceptional collaborator in providing state-of-the-art fabricated polyimide devices for the brain slice project spearheaded by Bronson. For remaining contributors, Matthew Drazin contributed to data collection for Chapter 3, Arya Kale contributed to data collection for Chapter 4, Stefanos Palestis contributed to signal processing for Chapter 4, and Akash Saxena contributed to signal processing in Chapter 5. Cort Thompson, as an original lab member, has provided countless intellectual contributions and, most recently, has been developing methods to perform RNAseq with excised tissue around devices (with tissue from Chapter 4). I am grateful for his contributions and eager to see the results of his work.

I would like to thank the rest of the Purcell Lab members over the years for their support (especially, Monica Setien-Grafals as we forged a path into the new BME program together), as well as the Department of Biomedical Engineering (especially, Mark Worden, Christopher Contag, and Dana Spence) for the opportunity to enroll as the first graduate student in the new department and for the exceptional experience it has provided.

Finally, I have to thank my exceptional family for all of their support, including my parents, grandparents, aunts, uncles, and cousins, who have all provided outstanding support and inspiration over the years.

TABLE OF CONTENTS

LIST OF TABLES	xii
LIST OF FIGURES.....	xiii
CHAPTER 1 INTRODUCTION	1
Founding principles of neurotechnology	1
Understanding motor cortex.....	1
Probing single-cell electrophysiology.....	3
Neuroprosthetic control via motor cortex: the advent of brain-machine interfaces	4
Barriers to effective integration.....	7
Gliosis and neuronal loss	7
Unknowns regarding residual neuronal function.....	10
Dissertation organization.....	11
CHAPTER 2 GLIAL RESPONSES TO IMPLANTED ELECTRODES IN THE BRAIN	14
Abstract.....	14
Introduction	14
Astrocytic responses to device insertion.....	17
Consequences of glial encapsulation.....	24
Neurostimulation.....	24
Extracellular recordings.....	26
Neurochemical sensing	29
Glia as an active modulator of signal transmission.....	30
Modulation of neuronal excitability.....	30
Modulation of synaptic transmission.....	33
Synaptogenesis and silencing.....	33
Modulation of network activity	37
Neuronal synchrony	38
Glial-activation challenges and design considerations.....	39
Glia as an effector of clinical devices.	39
Consequences of higher-density arrays and multiple implants.	42
Biomaterials and glial activation.....	43
Improved softness.....	44

Smaller feature sizes.....	46
Surface modification.....	47
Effects at the molecular level.....	48
Outlook.....	50
Acknowledgments.....	53
CHAPTER 3 FUNCTIONAL REMODELING OF SUBTYPE-SPECIFIC MARKERS SURROUNDING IMPLANTED NEUROPROSTHESES.....	54
Abstract.....	54
Introduction.....	56
Results.....	58
Shift in excitatory/inhibitory (VGLUT1/VGAT) expression surrounding devices over time.....	58
A reactive astroglial subtype contributes to elevated VGAT positivity.....	60
Progressive loss of VGLUT1 is coupled to loss of CamKii α + neurons.....	60
Discussion.....	63
Methods.....	67
Surgery.....	67
Histology.....	67
Image Analysis.....	69
Statistical Analysis.....	70
Acknowledgments.....	71
CHAPTER 4 ALTERATIONS IN ION CHANNEL EXPRESSION SURROUNDING IMPLANTED MICROELECTRODE ARRAYS.....	72
Abstract.....	72
Introduction.....	73
Results.....	77
Ion channel expression evolves over time.....	77
Alterations in ion channel expression accompany signal loss.....	84
Early observations suggest Kv7.2 expression modulates excitatory synaptic transporters.....	85
Discussion.....	88
Methods.....	95
Surgery.....	95
Extracellular electrophysiology.....	95
Histology.....	96
Cell culture and transfection.....	97

Statistical analysis.....	97
Acknowledgments	98
CHAPTER 5 ONGOING WORK AND FUTURE DIRECTIONS: NEW APPROACHES AND OPPORTUNITIES TO EXPLORE THE INTERFACE.....	99
Abstract.....	99
Unpacking mechanisms of plasticity: new approaches to explore the interface	99
Approaches to unmask plasticity at the interface: brain slice electrophysiology	100
Approaches to validate the delivery of genetic material to neural cells: in vitro optimization.....	102
Approaches to perturb plasticity at the interface: delivering genetic material in vivo.....	103
Synthesizing approaches for investigation.....	108
Unpacking gliotransmission at the interface: exploring impacts on synaptic transmission and neural circuit function	108
Exploring inflammatory pathways that impact gliotransmission	109
Exploring the impacts of gliotransmission on neural circuit function	112
Synthesizing mechanisms: new targets for intervention strategies.....	116
Outlook.....	122
REFERENCES	125

LIST OF TABLES

Table 4.1 Motivation for ion channel selection.	76
---	-----------

LIST OF FIGURES

- Figure 1.1 | Localization of motor function anterior to central sulcus in apes.** Grunbaum and Sherrington report circumscribed localization of motor functions anterior of central sulcus in higher anthropoid apes (gorilla, chimpanzee, and orang). Fig. reproduced from³..2
- Figure 1.2 | Overlapping boundaries between motor and sensory functions in human cerebral cortex.** Penfield describes overlapping boundaries for somatic motor and sensory representations with respect to central sulcus, still corroborating motor is largely represented anterior and sensory posterior. Figs. reproduced from⁴.....3
- Figure 1.3 | Volitional control of motor cortex units by Macaca Mulatta after operant conditioning.** Example of isolated units from motor cortex using a microelectrode and their associated increase in firing rates based upon visual and auditory cues after operant condition. Figure reproduced from¹³.....5
- Figure 1.4 | Quantitative immunohistochemistry and accompanied histological images of neuronal loss and gliosis.** Examples of quantitative immunohostchemistry performed around implanted microelectrodes in the rat motor cortex at 4 weeks post-implantation. Figure reproduced from³⁴.....8
- Figure 2.1 | (Box 2.1) Non-neuronal responses to brain injury..... 18**
- Figure 2.2 | Traditional electrode arrays incite gliosis. a-f,** Devices (a-c) are shown above the associated histology images (d-f). **a,** Michigan-style array⁷⁸. **b,** Utah-style array⁷⁹. **c,** DBS lead⁸⁰. **d,** Rat histology from a Michigan-style MEA (4 week), with labelled astrocytes (GFAP, green) and microglia (ED1, red)³⁴. **e,** Primate with Utah array implanted, with microglia labelled (IBA1, red)⁷⁷, at 17 weeks. **f,** Human DBS lead implant (mean ~38 months for all subjects), with labelled astrocytes (GFAP, magenta), microglia (IBA1, cyan), and all cell nuclei (CyQuant = yellow)^{*76}. Scales bars, 100 μm (**a, d, f**); 1 mm (**b**); 2 mm (**c**); 28 μm (**e**). * = injury (**d, e, f**). 19
- Figure 2.3 | In vivo multiphoton imaging of the glial response to MEA implantation.** Astrocytes and oligodendrocytes (Sulfarhodamine101, false-colored purple in **a**), neurovasculature (intravascular Sulfarhodamine101, red in all panels), and microglia (CX3CR1-GFP, green, in all panels) are shown. **a,** Microglia display an amoeboid morphology and encapsulate two shanks of a 4x4 Neuronexus array 6 hours following implantation⁷⁵. **b,** Microglia form a compact scar around two shanks of a 1x3 Blackrock array at 2 months post-implantation. **c,** Microglia activation and lamellipodia ensheathment of an implanted silicon/silicon-oxide microelectrode. **d,** Microglia avoid the silicon/silicon-oxide microelectrode surface when covalently coated with neurocamouflage protein L1CAM. Scale bars, 100 μm . Panel **b** adapted from ref. ⁶⁷. Panels **c-d** adapted from ref. ⁸⁵..... 21

Figure 2.4 | Evidence for a negative impact of increased gliosis on recording quality. a–d, Representative images from four animals demonstrate the range of endpoint histological outcomes (from ‘good’ to ‘poor’, left to right). The figure has been generated after additional analysis on data collected in a previous study³⁰. Neuronal nuclei (NeuN, green) and astrocytes (GFAP, red) surrounding probe tracts are shown, and the associated average neuronal and non-neuronal density data are listed (area binned cell counts, neuronal density (ND) and non-neuronal density (NND), in cells · mm⁻²). Recording segments with signal-to-noise-ratio (SNR) values representative of the average value for each animal are depicted (the SNRs calculated from peak-to-peak noise result in lower values than root-mean-square noise)^{30,117}. Recording quality improved with decreased NND and increased ND/NND (p<0.05, Spearman’s rho, n = 6). Impedance increased with increased NND (p<0.05, Spearman’s rho, n = 6). Animals in a and c were drug-treated while b and d correspond to the controls. Scale bar, 100 μm..... 27

Figure 2.5 | Potential mechanisms of the active modulation of neurotransmission by glia. **A)** Insertional trauma incites reactive gliosis and impacts neuronal function through modifications to the local neurochemical environment. Punctured cellular membranes release ATP into the local extracellular space, whereby activated microglia and astrocytes are recruited to release glutamate, cytokines and ATP. The resulting signaling cascades ultimately reinforce reactive gliosis and impact local neuronal health and function. The dashed box indicates the region of synaptic silencing depicted in b. Neuronal excitotoxicity is another potential consequence of reactive signaling. **B)** As injured cells and reactive microglia release excess ATP, activated astrocytes are able to silence neuronal activity through two synaptic mechanisms. (1) Glutamate and ATP release, which generate a..... 35

Figure 2.6 | Next-generation arrays mitigate gliosis. a–f, Devices (a–c) are shown above the associated histology images (d–f). **a,** A mechanically adaptive nanocomposite microelectrode becomes compliant upon implantation²¹⁷. **b,** A hollow-architecture parylene-based microelectrode places sites away from the stiff penetrating shaft, along 4-μm-wide lateral support arms²²⁵. **c,** A syringe-injectable mesh electronics mimics brain parenchyma with sites featured along an interwoven structure²²⁶. **d,** Astrocytes labelled (GFAP, green) around mechanically compliant probe at 8 weeks²¹⁵. **e,** Astrocytes (GFAP, red), microglia (OX42, green), and all cells (Hoechst, blue) labelled around the stiff electrode-penetrating shaft (S) and lateral edge (L) at 4 weeks²²⁵. **f,** Astrocytes labelled (GFAP, cyan) around a syringe-injected mesh (blue) at 1 year²²⁷. Scale bars, 500 μm (a); 100 μm(b, d, f); 250 μm (c); 50 μm (e)..... 45

Figure 2.7 | Opportunities for further enquiry in engineering. Future work will need to uncover the effects of electrode properties on the molecular pathways that shape gliosis, including: (1) The degree of softness and corresponding inflammation from mechanoactivation of glia, and the evolution of the effect on gliosis over time (such as mechanical mismatch, micromotion, and the state of glial reactivity and ‘priming’); (2) The relationship between feature size and architecture on inciting and priming inflammatory gliosis around the injury, and the evaluation of the long-term consequences (such as hyperexcitability, excitotoxicity and degeneration) on device function; (3) The effects of surface modifications (chemistry and topography) on shaping reactive signaling at the

interface (receptor activation and cytokine/gliotransmitter release) and the corresponding consequences on recording and stimulation performance; (4) Targeted approaches to modify immune responses will need to be incorporated to achieve seamless integration, which should be guided by their impact on glial signaling, reactivity and device performance. Traditional devices reproduced from refs. ⁷⁸⁻⁸⁰ and referenced directly in Fig. 1. Next-generation devices reproduced from²¹⁶ (top and bottom)and from¹⁰³ (middle)..... 50

Figure 2.8 | Opportunities for further enquiry in biology. (1) The factors responsible for the ‘tipping point’ between reactive and non-reactive glial states, and the implications of glial priming on the safety of high-density arrays and of multiple implant strategies; (2) The contribution of hyperexcitability to neuronal loss and recorded signal quality, and the underlying relationship with a primed glial state; (3) Glial-mediated neuronal silencing surrounding implants, and the relationship to recorded signals and stimulation thresholds; (4) The relationship between device performance and the time course of glial effects, for insights into the sources of performance variability, plasticity, and placebo effects of device insertion, as well as therapeutic effects and side effects in a broad range of MEA applications. 52

Figure 3.1 | Shift in VGLUT1/VGAT expression surrounding devices over time **A)** Within the first 40µm, VGLUT1 and VGAT are both significantly elevated (**p≤0.001) and VGLUT1 intensity is significantly greater than VGAT (**p≤0.001) (n=12 sections across 3 rats). **B)** VGLUT1 and VGAT are both significantly elevated within the first 40µm (**p≤0.001), with no significant difference between VGLUT1 and VGAT (n=16 sections across 4 rats). **C)** VGAT intensity is significantly elevated (*p≤0.05) and significantly greater than VGLUT1 (*p≤0.05) in the first 40µm (n=19 sections across 4 rats). Companion uninjured contralateral images are shown below each injury image for within-section visual comparison. White asterisks (*) denote injury sites. Scale bar = 100µm. Mean +/-standard error is shown. Figure reproduced¹⁴⁷..... 59

Figure 3.2 | Reactive glial subtype contributes to elevated VGAT over time **A)** At 3 days, VGAT+ glia first emerge distal to the device interface, where arrows indicate examples of GFAP+/VGAT+ cells, **B)** By 7 days, VGAT+ glia have encased the device interface, **C)** After 28 days, VGAT+ glia are scarce, with faint exceptions indicated by arrows. White asterisks (*) denote injury sites. Scale bar = 100µm. Figure reproduced¹⁴⁷..... 61

Figure 3.3 | Progressive loss of VGLUT1 is coupled to loss of CamKiiα+ neurons. CamKiiα expression is significantly more robust at **(A)** 3 days (n=4 sections across 2 rats) compared to both **(B)** 7 days (**p≤0.001) (n=10 sections across 3 rats) and **(C)** 28 days (*p≤0.05) (n=9 sections across 2 rats). These results coincide with initial elevation in VGLUT1 at 3 days followed by a progressive decline over 28 days (**Fig. 3.1**). White asterisks (*) denote injury sites. Scale bar = 100µm. Mean +/-standard error is shown. Figure reproduced¹⁴⁷..... 62

Figure 4.1 | Confocal laser scanning microscopy of ion channel expression surrounding the insertion site. Example images of ion channel expression surrounding the device tract. Immunohistochemistry reveals fluorescently stained ion channels on horizontal

tissue sections taken from layer V of the primary motor cortex using the same secondary antibody. Electrodes illustrated for reference with dimensions to scale (100um x 15um)..78

Figure 4.2 | Spatial differences in expression at each time point: Progressive increase in potassium channel expression is coupled with a reduction in sodium channel expression over 6 weeks. A) Averaged intensity from ion channel expression (normalized to final bin) revealed an increase in potassium channel expression and a loss of sodium channel expression over 6 weeks (p-values comparing 0-40um and 230-270um depicted). **B)** Significance compared between 0-40um of each ion channel. Significance depicted as *p<0.05 and ***p<0.001. “NS” denotes non-significance. Standard error bars depicted in both panels. For each ion channel, there was an average of 7 devices and 21 tissue sections analyzed per time point.80

Figure 4.3 | Temporal differences in expression: Percentage change in expression relative to 1 day values corroborates progressive reduction in sodium channel expression and heightened potassium channel expression over time. A) Averaged percentage change for 1 and 6 week expression values relative to 1 day expression values with standard error bars. **B)** Area under the curve calculated for unit region (0-130um) and LFP region (140-270um) for both 1 and 6 week expression curves, as well as total integrated area calculated for the combined 270um radius.83

Figure 4.4 | Alterations in ion channel expression accompany decline in unit detection. A) Example of putative unit and LFP snippet from microelectrode arrays, accompanied by the quantified data (# of units and LFP amplitude) obtained from bi-weekly recording sessions across subjects (with standard error bars). Average LFP amplitude and # of units plotted on bar graphs for each time point. **B)** Averaged data within 0-40um for intensity ratios are plotted. Nav1.6/Kv7.2 intensity ratio appears to coincide closest with unit detection over the 6 week time course, whereas Nav1.6/Kv4.3 ratio appears to best correspond to LFP amplitude over 6 weeks. In contrast, Nav1.6/Kv1.1 does not appear to correspond to either signal metric.....85

Figure 4 5 | Preliminary observations suggest Kv7.2 knockdown impacts excitatory synapses in culture. A) In vivo results of vesicular glutamate transporter 1 (VGLUT1), using data from a previous report¹⁴⁷, show an elevation in VGLUT1 at 3 and 7 days. **B)** In vitro, cortical neurons transfected with Kv7.2 siRNA show successful transient knockdown of Kv7.2, a similar trend in VGLUT elevation at 3 and 7 days compared to in vivo expression, and an impact on PSD95 in the form of a reduction at 7 days. Taken together, these data suggest that the transient downregulation of Kv7.2 at 1 day in vivo (**Fig. 2A**) may be a mechanism for the upregulation of VGLUT1 at 3 and 7 days in vivo. Two biological replicates were performed for the preliminary in vitro data.86

Figure 5.1 | Schematic of methods for capturing devices in a brain slice preparation. 16-channel, single-shank microelectrode arrays are implanted in the primary motor cortex of adult Sprague Dawley rats for predetermined time points, whereby the brain is rapidly extracted and a vibratome is used to take 300um-thick coronal sections to capture the device in a single slice, whereby that slice is then used to perform patch clamp electrophysiology on

interfacial neurons within the recordable radius of the device interface (<100um). These neurons can additionally be filled with Alexa Fluor dyes for performing dendritic spine imaging, as well as perturbed with molecule uncaging to investigate nuanced changes in synaptic transmission and excitability..... 100

Figure 5.2 | Combining whole-cell brain slice electrophysiology with two-photon dendritic spine imaging: new opportunities for exploring plasticity at the interface. Preliminary work from the Regenerative Electrode Interface Lab (spearheaded by Bronson Gregory with the Lee Cox Group) characterizing both electrophysiology and dendritic spine density in single neurons near the device interface (<100um, A and B, device edge in top left corners) and >500um away (C) at 1 week. Results indicate that near-device neurons have reduced firing properties (A and B) and reduced dendritic spine density (D) compared to both >500um and naïve controls..... 101

Figure 5.3 | Reprogramming glia into neurons: histological and electrophysiological evidence of neuronal conversion in vitro. Early observations indicate that the ASCL1 transgene is capable of producing cells with neuronal morphology and marker expression (TUJ1, SYN) from astrocyte cultures. Delivery of NeuroD1 (ND1) or Neurogenin-2 (NGN2) produced TUJ1 positivity (red) without accompanying morphological changes. POU3F and control YFP-infected cultures exhibited no observable conversion to neuronal fate. Scales = 5 um. Reprogrammed astrocytes were capable of eliciting a single spike in response to injected current by Day 9 post-infection, repetitive spiking by Day 21, and mature spike trains by Day 24 (representative traces). Earlier time points were consistently devoid of spiking activity. Control cultures displayed typical glial morphology and were likewise non-responsive to stimulation (not shown). Figure modified from³⁵²....102

Figure 5.4 | Methods to deliver genetic material in vivo. A) Delivery of an AAV-CMV-GFP vector from a cannula (“INJECTION”) to the electrode array (“↑”). B) Acute delivery of BLOCK-iT siRNA reporter using a pulled glass capillary micropipette (alexafluor 555, counterstained with Hoechst). C) Custom-made NeuroNexus probe with a microfluidic channel affixed to the microelectrode shank for chronic delivery. D) Delivery of AAV-GFAP-mCherry at the tip of the electrode array using the custom NeuroNexus device (counterstained with GFAP using alexafluor 488). A and B not published, C and D reproduced from³⁵¹..... 104

Figure 5.5 | Preliminary ion channel knockdown in vitro to systematically screen for impacts on excitatory synapses. Ion channels were knocked down in rat cortical neurons with siRNA for the respective channels. After harvesting the RNA, cDNA was made using an RNEasy kit and Taqman probes were used to quantify RNA for the respective sequences. Results indicate that Kv7.2 most robustly impacts excitatory synapses (VGLUT and PSD95 upregulation) and hyperexcitability (Nav1.6 upregulated, and Kv7.2/Kv4.3/Kv1.1 downregulated) at 1 week. N=3 biological repeats for each condition. 105

Figure 5.6 | Preliminary knockdown of Kv7.2 in vivo with accompanied recordings over 1 week. Preliminary data shows successful knockdown of Kv7.2 in vivo relative to scramble (SCR) siRNA control as determined by quantitative immunohistochemistry (n=3

devices per condition). Additionally, accompanied recordings (n=4 devices per condition) indicate reduced unit detection from the Kv7.2 knockdown condition relative to SCR control. 107

Figure 5.7 | TLR activation produces hyperexcitability in neighboring neurons via astrocytes. The following depicts mechanisms by which TLR activation and resulting glial signaling induces neuronal hyperexcitability. Figure reproduced from³⁶⁴..... 110

Figure 5.8 | Structural and functional remodeling of neuronal circuitry by glia: mechanisms to inform electrode injury models. Depiction of device-related mechanisms of neural circuit remodeling. For both structural and functional impacts, a corresponding table depicts potential glial mechanisms that may drive the remodeling observed around implanted electrode arrays in this work (continued on next pages)..... 118

Figure 5.9 | Future outlook: designing intervention strategies to improve device performance by targeting glial mechanisms. Based on the data and methods reported in this dissertation, it will be possible to design intervention strategies aimed at improving device function by modulating glial mechanisms that impact neural circuit remodeling and, in turn, device performance. Several steps will be necessary to this end: (1) It will be important to investigate glial mechanisms that contribute to remodeling of ion channels around implanted electrodes (by modulating them via siRNA, etc. with methods described in this chapter), and to identify causal relationships to recording quality (with potential candidates for glial mechanisms outlined in Fig. 5.7, and methods to assess impacts on neural circuit remodeling and device performance in Figs. 5.1-5.5); (2) It will be important to investigate glial mechanisms that contribute to the remodeling of synaptic circuitry around devices, and to identify causal relationships to signal quality; (3) Finally, any mechanisms identified that causally impact signal quality can then be used to guide intervention strategies aimed at modulating the specific glial mechanisms responsible. 122

CHAPTER 1 | INTRODUCTION

Founding principles of neurotechnology

Understanding motor cortex

In the late 19th century, Gustav Fritsch and Eduard Hitzig discovered that electrical stimulation of the dog frontal cortex could reproducibly evoke contralateral movements, laying a foundation for motor neurophysiology by demonstrating electrical excitability, localized motor centers, and topographical organization of the cerebral cortex¹. Soon thereafter, David Ferrier discovered that longer-duration pulses could evoke more complex and coordinated movements compared to the brief twitches observed by Fritsch and Hitzig². In the early 20th century, Sir Charles Sherrington used these methods to map motor function in anthropoid apes (gorilla, chimpanzee, orang), describing a circumscribed localization of motor function in the precentral gyrus (immediately anterior to the central sulcus)³ (**Fig. 1**). This work shifted the school of thought from a unified sensorimotor region of cortex to instead a separation of motor and sensory cortices by the central sulcus.

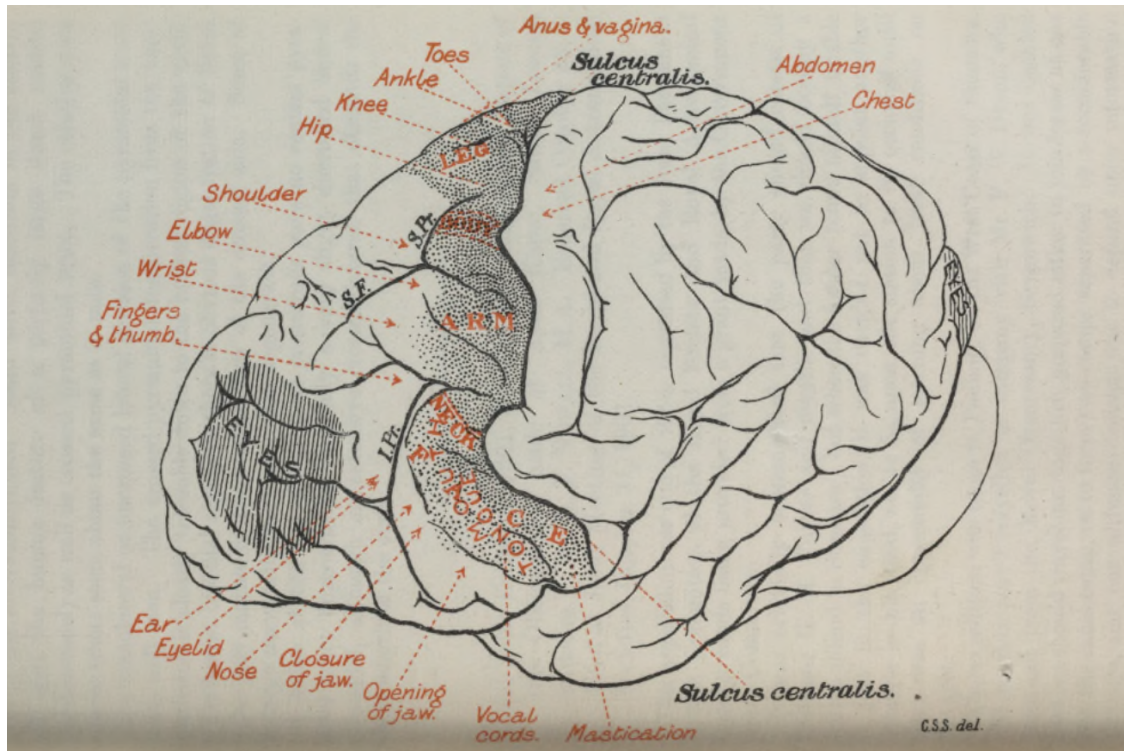


Figure 1.1 | Localization of motor function anterior to central sulcus in apes. Grunbaum and Sherrington report circumscribed localization of motor functions anterior of central sulcus in higher anthropoid apes (gorilla, chimpanzee, and orang). Fig. reproduced from³.

By the mid-20th century, cortical representations were delineated in humans by neurosurgeon Wilder Penfield, who explored topographical organization of motor and somatosensory cortices in hundreds of patients. Despite many modern textbooks portraying his delineations as demarcated boundaries, Penfield emphasized overlapping boundaries between motor and sensory representations⁴ (**Fig. 2**). Penfield also emphasized context-dependent localization of motor centers, and echoed words of Sherrington in highlighting the instability of a “cortical point” with respect to motor function⁴. These early observations and their philosophical underpinnings eluded to the notion of a higher-order involvement of somatosensation in motor cortex function. Indeed, reports on the convergence of afferent sensory

messages in motor cortex began emerging in the second half of the 20th century⁵⁻⁷ as the field of electrophysiology materialized.

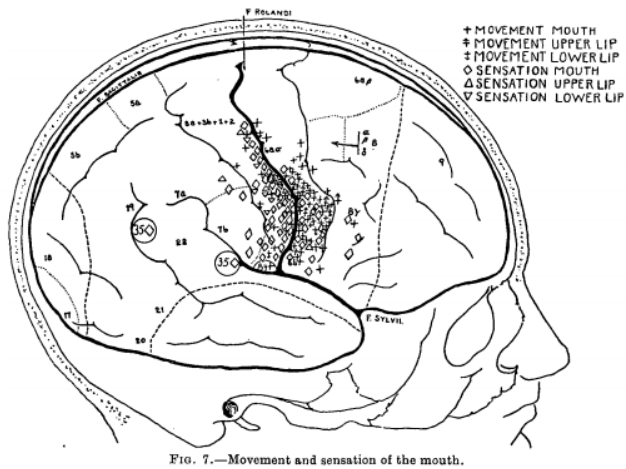


FIG. 7.—Movement and sensation of the mouth.

As may be seen by reference to this figure (fig. 25) movement has a proportionally larger representation anterior to the central fissure and sensation a larger representation posteriorly, and the two areas, motor and sensory, overlap each other consistently and correspond to each other horizontally.

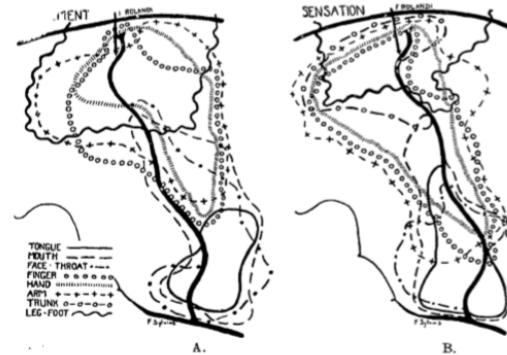


FIG. 25.—Summary of sensory and motor findings in figs. 5 to 20. The lines enclose the areas within which responses were obtained for each subdivision of the body. A. movement. B. sensation.

Figure 1.2 | Overlapping boundaries between motor and sensory functions in human cerebral cortex. Penfield describes overlapping boundaries for somatic motor and sensory representations with respect to central sulcus, still corroborating motor is largely represented anterior and sensory posterior. Figs. reproduced from⁴.

Probing single-cell electrophysiology

Seminal work by Hodgkin and Huxley in 1949 led to the discovery of membrane potential in the large squid axon by internally threading a microelectrode wire to obtain electrophysiological recordings⁸. Here, they discovered a large reversal in membrane potential from rest, later termed an action potential, that was dependent upon ionic concentration distributions and that a “special” mechanism facilitated the selective and high permeability of the membrane to sodium to generate an action potential signal, where the rate of rise and amplitude are determined by the sodium concentration gradient⁸. Further,

this nervous conduction facilitated by specific permeability was determined to be a product of sodium influx to drive the rising phase and potassium efflux to repolarize the membrane with the falling phase⁹. This discovery, which gave rise to the field of electrophysiology, was followed up by rapid progress toward understanding the underlying mechanisms of membrane permeability and excitability. Bert Sakmann and Erwin Neher used pulled micropipettes to perform patch clamp electrophysiology on individual cells and channels to resolve voltage-dependent permeability of ion channels in excitable membranes, where their work pioneered single channel current recordings to mechanistically study ion channel properties and their involvement in membrane excitability (including ligand- and voltage-gating properties, etc.)¹⁰⁻¹². Here, a fundamental understanding of electrophysiology gave rise to new principles for exploring systems neuroscience with *in vivo* extracellular electrophysiology.

Neuroprosthetic control via motor cortex: the advent of brain-machine interfaces

With the burgeoning field of electrophysiology and a growing understanding of sensorimotor function, work began utilizing the electrophysiological signals to further explore motor cortex function and utilize its activity for controlling external devices. This was achieved through performing extracellular electrophysiology, where electrodes placed in the extracellular space of the brain allowed for recordings to be made of action potentials from multiple neurons within close vicinity (termed “spikes” or “units”). Seminal work by Eberhard Fetz in 1969 performed extracellular recordings from Macaca Mulatta using a microelectrode wire to condition the firing of units in motor cortex based upon visual and auditory feedback (using a visual dial or clicking sound, respectively)¹³. This operant

conditioning, which uncovered the capacity for volitional control of single motor cortex units, was demonstrated by the monkey's ability to increase firing rates of specific isolated units by as much as 500% after training (Fig. 1.3).

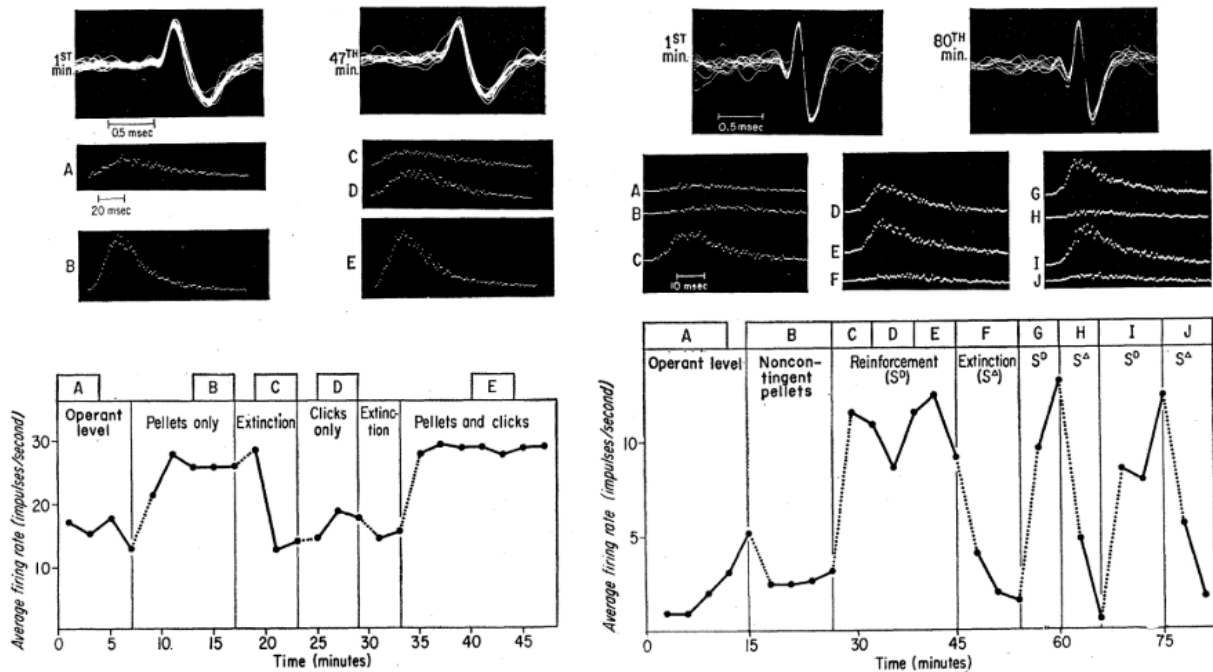


Fig. 1 (left). Firing rate of precentral cortex cell as a function of reinforcement schedule. During operant level and extinction periods neither food nor click feedback was presented. During pellets only period the highest firing rates were reinforced with delivery of a food pellet, without click feedback. During clicks only period a click was presented for each firing of the cell; finally, both pellets and clicks were provided. Interspike interval histograms above the graph show the relative number of intervals from 0 to 125 msec occurring during the specified 4-minute segments of the session. Several superimposed examples of the cell's action potential from the first and last minute of the session are illustrated at top (9). Fig. 2 (right). Firing rate of a precentral cell in a session with visual feedback and noncontingent reinforcement. Each point represents the average firing rate for the preceding 3-minute interval. During operant level and extinction (S^A) periods, no food or feedback was provided. During the noncontingent pellets period, the meter was illuminated and pellet delivery and meter deflection were determined by a tape recording of a previous session. The only change from noncontingent pellets to reinforcement (S^D) period was the correlation of pellet delivery and meter deflection with the activity of the monitored cell. In succeeding periods reinforcement (S^D) alternated with extinction (S^A). Interspike interval histograms taken during the specified time segments show the number of intervals between 0 and 62.5 msec, all at the same vertical scale. Several superimposed action potentials from the first and last minute of the session are shown at top (9).

Figure 1.3 | Volitional control of motor cortex units by Macaca Mulatta after operant conditioning. Example of isolated units from motor cortex using a microelectrode and their associated increase in firing rates based upon visual and auditory cues after operant condition. Figure reproduced from¹³.

Soon thereafter, progress was made toward developing microelectrode arrays with higher throughput by spanning multiple distances in cortex to facilitate the control of external prosthetic devices (often termed “neural prostheses” or “brain-machine interfaces”). In the 1970’s and 1980’s, Kenneth Wise and David Anderson pioneered batch fabrication techniques for reproducibly fabricating silicon-micromachined electrode arrays. This led to the introduction of the “Michigan-array” with multiple sites spanning the shank to acquire greater numbers of units spanning cortex in a high-throughput, reproducible fashion compared to traditional handmade microwire electrodes¹⁴⁻¹⁶. Shortly thereafter, the “Utah-array” was developed to improve resolution along the electrode depth, instead of the lateral spread achieved with single-shank multi-site Michigan-arrays, where the Utah-array consists of 10x10 shanks with electrode sites only at the tips.

Through the use of implanted microelectrode arrays, methods have been developed to decode information from motor cortex that can be used to control brain-machine interfaces. In the 1980’s, seminal work discovered that individual neurons in M1 fire in response to a specific direction (cosine tuning)¹⁷. This work was later expanded upon to uncover a context-dependency of the tuning (e.g., velocity, distance, etc.)¹⁸. In addition, kinesthetic and proprioceptive feedback has been identified to modulate motor cortex, where inclusion of these sensory modalities has dramatically improved brain-machine interface performance¹⁹⁻²¹. These advances enabled the first clinical brain machine interfaces, which were first reported in 2006²². This successful interface restored function, but with only binary output²², whereas by 2012 this same “BRAINGATE” technology had already advanced to restore 7-degrees of freedom²³. By 2016, the functional reanimation of

a paralyzed limb was made possible through closed loop stimulation of peripheral muscles driven by motor cortex decoding²⁴. More broadly, activity from motor cortex has also been used to restore function in closed-loop strategies for deep brain stimulation²⁵. These advances highlight the significance for utilizing implanted microelectrode arrays to detect and decode electrical activity from motor cortex.

This progress over the past half-century has generated significant advances in our ability to decode motor cortex function for restoring lost function. While these microelectrode arrays demonstrate enormous potential for understanding and treating intractable neurological injuries, their stability and longevity are severely hindered by the foreign body response that ensues following implantation²⁶⁻³⁰.

Barriers to effective integration

Gliososis and neuronal loss

Early observations at the turn of the 21st century linked histological evidence of neuronal loss around implanted electrodes to a deficit in resolvable units with the same devices³¹. This was coupled with observations from the field of a compact astrocytic sheath that formed around electrodes, which was reported to have heightened GFAP+ immunoreactivity that persisted for the duration of the implant to isolate the device from the brain³². Two generalized glial responses were further extrapolated, where an “acute” exacerbated astrocytic and microglial response was subsequently reduced to a baseline level of gliosis across all chronic time points (by 4, 6 & 12 weeks)³³. This baseline level of gliosis was

considered to be due to the presence of a chronically indwelling object³³. Finally, these observations were synthesized with seminal work by Biran et. al, where methods to quantify both neuronal loss and gliosis were used to inform device integration as a function of distance using immunohistochemistry³⁴ (**Fig. 1.4**). Significant neuronal loss at 4 weeks occurred within the first 100um compared to stab control, which did not fully resolve until ~500um, and a significant loss of neurofilament extended out beyond 200um. In addition, GFAP+ immunoreactivity was most elevated within the first 100um but extended out 500um.

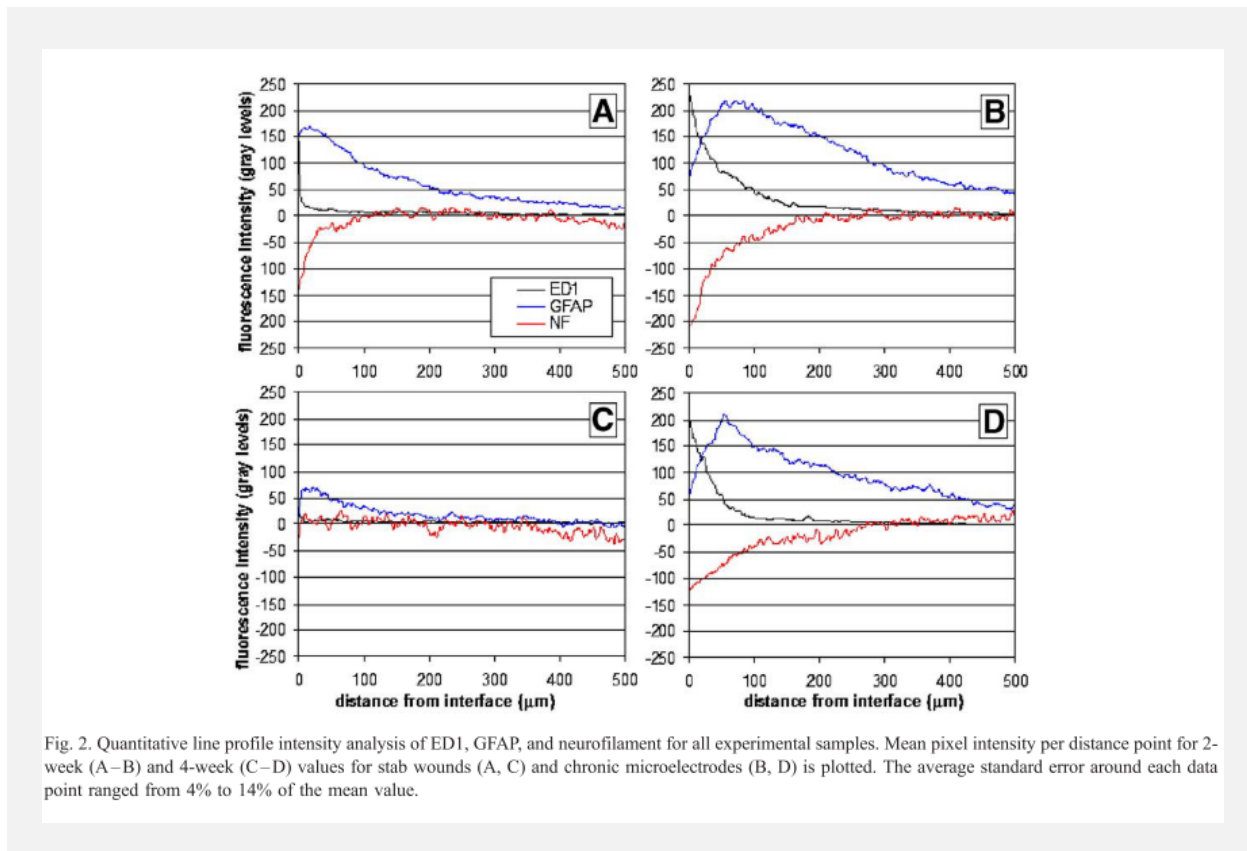


Figure 1.4 | Quantitative immunohistochemistry and accompanied histological images of neuronal loss and gliosis. Examples of quantitative immunohistochemistry performed around implanted microelectrodes in the rat motor cortex at 4 weeks post-implantation. Figure reproduced from³⁴ (continued on next page).

Figure 1.4 (cont'd)

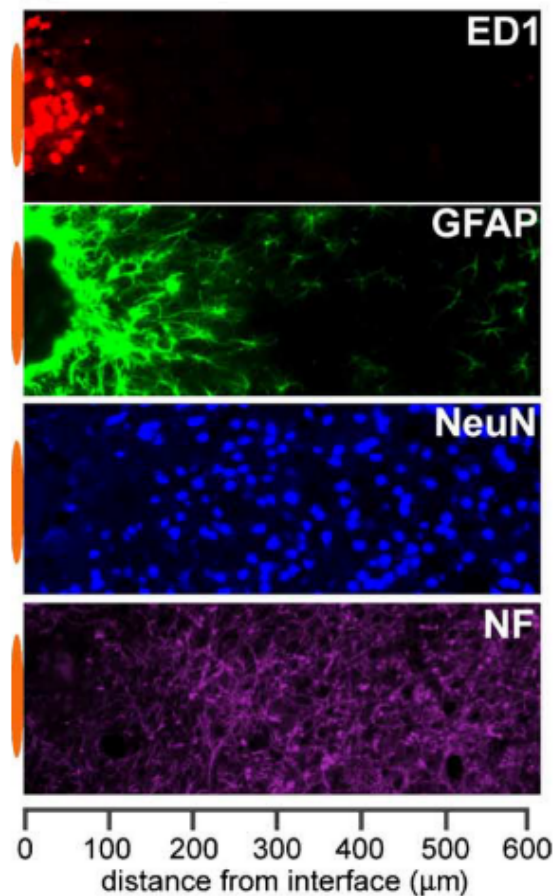


Fig. 6. Stratification of cellular immunoreactivity using cell-type-specific markers at the microelectrode–brain tissue interface. Representative images collected from two adjacent sections of an animal with a 4-week microelectrode implant illustrate the general appearance of the foreign body response characterized by minimally overlapping inflammatory (ED1) and astrocytic (GFAP) phenotypes adjacent to the implant interface. The area of inflammation and intense astrocyte reactivity contains a reduced number of NeuN⁺ neuronal bodies and a loss of neurofilament (NF) density. The position of the microelectrode is illustrated by the orange oval (drawn to scale) at the left of each image. Images were captured in grayscale and pseudocolored for illustration.

Critical insights from this work provided a framework for the relative radius in which device implantation affects neuronal loss, which addressed timely work describing the “recordable radius” for implanted microelectrodes³⁵. Here, seminal work by Henze et. al³⁵ demonstrated that the radius in which single units could be resolved by an implanted electrode array was

130um (by performing simultaneous intracellular and extracellular recordings), where optimal clustering of units occurred only within $\sim 40\mu\text{m}$ ³⁵. Therefore, significant neuronal loss observed by Biran within the first 100um demonstrated to the field that neuronal preservation within the recordable radius could be a critical gap moving forward to improve the long-term recording quality of implanted microelectrode arrays. Since then, significant efforts in electrode design have been focused on using these methods as guiding principles to assess biocompatibility of devices (i.e., assessing NeuN density and GFAP reactivity within the recordable radius) (see several reviews³⁶⁻³⁸).

Unknowns regarding residual neuronal function

While progress has been made in characterizing the loss of neuronal density surrounding implanted microelectrode arrays, it remains to be shown whether changes in the function of *remaining neurons* occurs that could affect recorded signal quality. Henze et. al reported an interesting observation in their seminal study, which described a significant under-sampling of neurons (~ 1 in 6 *at best*) given the density in the hippocampal region they were recording from acutely. They attributed this to “silent” neurons, which begs the question of whether electrode injury could be affecting the *function* of residual neurons at the device interface. This would coincide with decades of experimental work unpacking changes in excitability, synaptic transmission, and connectivity of neurons following traumatic brain injuries, where injury-induced hyperexcitability can lead to seizures and epileptogenesis in the short-term and widespread inhibition in the long-term³⁹⁻⁴³ (**Fig. 1.5**). Therefore, it appears within reason that similar remodeling events could occur following electrode insertion injury and potentially contribute to the instability and loss of signals with chronic devices.

Dissertation organization

This dissertation covers work that reveals major circuit-remodeling effects following the implantation of microelectrodes in the brain that can be used to inform the design of next-generation devices and intervention strategies aimed at achieving stable recording performance with chronic devices.

It has become increasingly appreciated that glia remodel the structure and function of neuronal networks following injury, where recent work has uncovered mechanisms that are relevant to the injuries and ensuing gliosis caused by the implantation of chronic devices. Chapter 2 covers a first-author, cross-institutional review article published in *Nature Biomedical Engineering* that disseminates important considerations for glial reactivity on device performance and provides a framework for topics explored in subsequent Chapters. Co-authors include Kip Ludwig and TK Kozai.

Based on work performed in other injury models, it has become increasingly clear that long-term remodeling of excitatory and inhibitory synapses (the connections which facilitate the propagation of information between neurons) occurs following the event of a cortical trauma, the consequences of which have significant implications for long-term recording stability of implanted microelectrode arrays. Chapter 3 covers first-author work published in *Journal of Neurophysiology* identifying novel changes in both excitatory and inhibitory synaptic circuitry surrounding implanted microelectrodes. The results support a trend from early hyperexcitability to chronic hypoexcitability, which has significant

implications for signal loss commonly observed with chronic devices. Co-authors include Bailey Winter and Matthew Drazin.

Chapter 4 covers first-author work uploaded to *bioRxiv*, and under preparation for journal submission, revealing the relationship between electrophysiological recordings and ion channel expression surrounding implanted microelectrode arrays over time, which expands upon preliminary work reported in a co-authored, cross-institutional publication in the *Journal of Neural Engineering*. The results showing a loss of sodium channel expression and gain in potassium channel expression supports the previously described trend from hyper- to hypoexcitability and corresponded with the loss of signal observed in the same devices. Co-authors and contributors to this work include Arya Kale, Stefanos Palestis, and Steven Suhr.

The previous chapters provide fundamental insight into major circuit changes at the interface that inform both basic-science knowledge and new strategies for improving the biointegration of brain implants. We are developing new approaches to reveal the mechanistic role of these factors in affecting recorded signals over time. Chapter 5 covers ongoing work that includes the development and validation of innovative strategies to deliver genetic material at the interface *in vivo* to yield entirely new avenues of research with opportunities to regulate gene expression and/or introduce new genetic material to reprogram cellular identity and rewire the interfacial network (includes work published in *Micromachines*, an *IEEE Life Sciences Conference Proceeding* paper, and ongoing work that expands upon previous chapters). These approaches offer the unique opportunity to unmask

key circuit-remodeling effects that impair device performance as well as inform the seamless integration of brain implants. In addition, this chapter highlights opportunities for future directions to unpack mechanisms that impact neuronal circuit function and device performance; these include exploring inflammatory mechanisms that shape neuronal function and gliotransmission impacts on local synaptic transmission and circuit function. Co-authors and contributors to this work include Bronson Gregory, Bailey Winter, Samuel Daniels, Akash Saxena, and Steven Suhr.

CHAPTER 2 | GLIAL RESPONSES TO IMPLANTED ELECTRODES IN THE BRAIN

Abstract

The use of implants that can electrically stimulate or record electrophysiological or neurochemical activity in nervous tissue is rapidly expanding. Despite remarkable results in clinical studies and increasing market approvals, the mechanisms underlying the therapeutic effects of neuroprosthetic and neuromodulation devices, as well as their side effects and reasons for their failure, remain poorly understood. A major assumption has been that the signal-generating neurons are the only important target cells of neural-interface technologies. However, recent evidence indicates that the supporting glial cells remodel the structure and function of neuronal networks and are an effector of stimulation-based therapy. Here, we reframe the traditional view of glia as a passive barrier, and discuss their role as an active determinant of the outcomes of device implantation. We also discuss the implications that this has on the development of bioelectronic medical devices.

Introduction

There are more connections between neurons in the human brain than there are stars in our galaxy⁴⁴, and there are at least a dozen specific neuronal subtypes in the brain that are recognized as unique on the basis of their distinctive functional and morphological characteristics^{45,46}. There is also growing recognition that non-neuronal supporting cells are more diverse and dynamic than previously appreciated, with distinct classes and subclasses of glia actively shaping the structure and function of neural circuitry⁴⁷. Although such

complexity is a likely requisite for the ability to internalize, integrate, and respond to the continuous streams of information that the brain must process, it also makes the effective treatment of neurological disorders especially challenging. In recent years, the development and design of new implantable-device technologies to read-out and write-in electrical and chemical signals to and from the nervous system have created unprecedented opportunities to understand normal brain function and to ameliorate dysfunction resulting from disease or injury.

Although research and clinical applications of implanted electrode arrays continue to experience rapid growth, their usage has outpaced the clear understanding of the mechanisms underlying their benefits, side effects, and modes of failure. Originally a precision academic-research tool to measure and modulate neural circuitry at sub-second and sub-millimeter resolution, implanted electrode arrays have increasingly been used in the clinic to treat an expanding array of medical conditions. Reports in the late 1980s and early 1990s demonstrated compelling preliminary clinical efficacy of deep brain stimulation (DBS) for tremor as a safer alternative to thalamotomy or pallidotomy in medically intractable Parkinson's Disease⁴⁸. Although the mechanisms underlying its benefits remain the subject of debate⁴⁹, DBS has since been approved by the U.S. Food and Drug Administration for Parkinson's disease, essential tremor, obsessive compulsive disorder, dystonia, and refractory epilepsy⁴⁸. Therapeutic indications presently being pursued in clinical studies are rapidly expanding, and include Alzheimer's disease, depression, Tourette's syndrome, deafness, blindness, and strategies to promote plasticity in cases of severe stroke or tinnitus⁴⁹. Electrophysiological and neurochemical recordings have gained

traction as a diagnostic tool, as an enabling technology for brain/machine interfaces in paralysis patients, and as biomarkers to inform strategies for closed-loop stimulation devices⁵⁰.

The successful use of chronically implanted neuroprostheses is predicated on the ability to reliably modulate or record signals from surrounding neurons over time (preferably, for many years). This is true for the broad range of clinical and research applications pursued, and for the variety of methods of read-out or write-in of neural activity employed (such as optical or electrical) ⁵¹. However, problems arising from small signal amplitudes and from signal instability plague implanted recording arrays, limiting their long-term function^{26,35,52-54}. Signal amplitudes typically shift on a daily basis²⁷, compromising the likelihood that spike detection crosses the required threshold . This can, in turn, affect apparent firing rates, contributing to the non-stationarity that burdens the use of these signals for prosthetic control²⁶. Studies across animal models often report progressive losses in signal detection in the weeks following implantation^{27,31}. In recordings taken from human subjects, significant changes in unit amplitudes were observed on an intraday basis²⁶. Many of these shifts seen to be related to device micromotion (based on simultaneous effects observed across electrode sites)²⁶, but the vast majority were attributed to a physiological origin (85%). Likewise, in applications that stimulate the central nervous system , desensitization can occur following chronic microstimulation, and inexplicably large placebo effects can follow implantation of non-functional devices^{55,56}. A variety of factors, both biological and non-biological, have been proposed to contribute to observations of instability in neural recordings and to the variable thresholds of

neurostimulation^{52,57}. Amongst these, suboptimal biocompatibility and suboptimal integration with surrounding tissue remain a significant limitation to reliably transfer information to and from the brain through implanted electrode arrays.

Astrocytic responses to device insertion

Historically, neurons have been viewed as the information-processing cells of the central nervous system (CNS), because of their specialized capability to generate transient spikes in membrane potential (so-called action potentials). The presence or absence of these spikes serve as the putative ones and zeros of the neural code, where the detection or stimulation of these signals by implanted electrode arrays is the primary mode of device–neuron communication. However, neurons are outnumbered three-to-one by supporting glial cells in the brain⁵⁸, and recent data has suggested that glia are capable of both transmitting and receiving synaptic signals as well as of producing profound effects on the local neurochemical environment⁵⁹. These observations of complex functional roles belie the simple structural role implied by the origin of the term glia (Greek for ‘glue’)⁶⁰. The foreign-body response to electrode arrays implanted in the brain is typified by glial encapsulation surrounding the device, where reactive glia ensheath the implant in a layered structure which can measure tens to hundreds of microns in thickness (**Figs. 2.2 and 2.3**). Heterogeneous types of glia respond to injury (**Figure 2.1**), with reactive astrocytes being notable for their effects on the health, function and connectivity of neural networks.

Box 2.1 | Non-neuronal responses to brain injury

Non-neuronal cells in the brain include specialized supportive cells (such as astrocytes, microglia, oligodendrocytes and NG2-glia) and neurovascular cells (such as pericytes and ependymal cells), and structural connective tissue cells (such as meningeal fibroblasts). Of these, the most studied in response to brain implants are microglia and astrocytes, because of their prominent role in the encapsulation of devices. Pericytes and NG2-glia have also gained recent attention because of their suggested reparative potential following injury⁶¹⁻⁶⁵. Also, blood-borne myeloid cells (such as monocytes and leukocytes) can infiltrate on BBB disruption, and their involvements around devices have been investigated and discussed elsewhere^{66,67}. The foreign-body response to neural implants has been comprehensively discussed in refs. ^{38,68,69}.

Pericytes, which form the basement membrane of capillaries and regulate blood flow, immediately respond to injury by disrupting the permeability of the blood-brain barrier and by constricting cerebral blood flow, which can lead to larger volumes of cellular damage^{70,71}. It has been proposed that these cells have reparative potential through association with neurogenic niches^{64,65}.

NG2-glia were historically recognized as oligodendrocyte precursors found to be inhibitory to axonal outgrowth⁷². More recent evidence of functional synapses between neurons and NG2-glia has reframed this view: NG2-glia are now regarded as a unique class of glia that can actively participate in neural-network formation^{61,63}. NG2-glia actively proliferate and arrive at injury sites within 24 hours of the insult, their responses are pronounced around devices at 1 week, and subsequently return to baseline responses ~4 weeks following injury^{63,73}. These cells can be a source of gliogenesis^{61,63,74} and may also have neurogenic potentia^{61-63,74}.

Microglia are the resident macrophages in the brain responsible for initiating the foreign-body response through the release of excitatory and inflammatory factors. They are the first responders to injury, rapidly adopting an activated, amoeboid morphology, then proliferating, migrating, and encapsulating the device⁷⁵.

Astrocytes activated by microglial signaling visibly respond to injury at ~1 week by proliferating, hypertrophying, upregulating intermediate filaments (such as glial fibrillary acidic protein, GFAP), encapsulating the device, and releasing factors to further promote the foreign-body response. By ~4-6 weeks they begin to form a dense scar around the device that can last for years^{69,76,77}.

Figure 2.1 | (Box 2.1) Non-neuronal responses to brain injury.

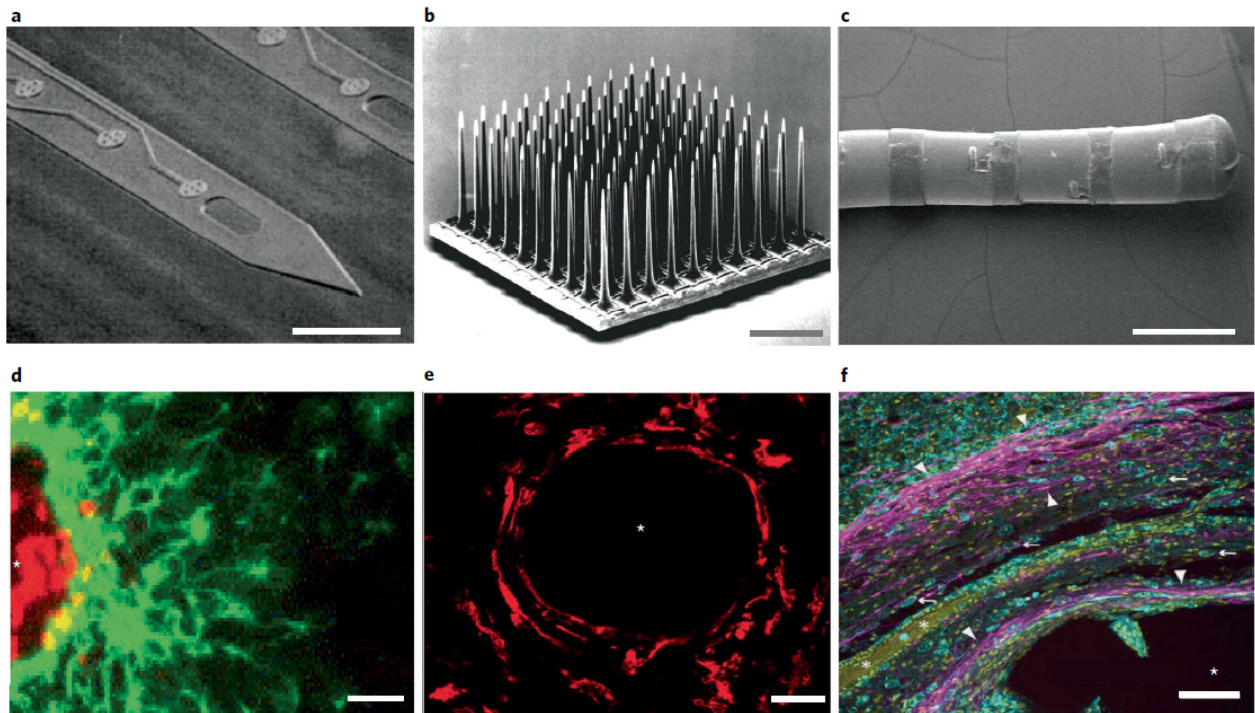


Figure 2.2 | Traditional electrode arrays incite gliosis. **a–f**, Devices (**a–c**) are shown above the associated histology images (**d–f**). **a**, Michigan-style array⁷⁸. **b**, Utah-style array⁷⁹. **c**, DBS lead⁸⁰. **d**, Rat histology from a Michigan-style MEA (4 week), with labelled astrocytes (GFAP, green) and microglia (ED1, red)³⁴. **e**, Primate with Utah array implanted, with microglia labelled (IBA1, red)⁷⁷, at 17 weeks. **f**, Human DBS lead implant (mean ~38 months for all subjects), with labelled astrocytes (GFAP, magenta), microglia (IBA1, cyan), and all cell nuclei (CyQuant = yellow)⁷⁶. Scales bars, 100 μm (**a**, **d**, **f**); 1 mm (**b**); 2 mm (**c**); 28 μm (**e**). * = injury (**d**, **e**, **f**).

Astrocytes are the most abundant cell in the brain⁸¹ and are so-named for their stellate morphology. They are responsible for regulating neurovascular blood flow, neurotransmitter activity, and the composition of the extracellular environment, and provide metabolic support under physiological and pathological conditions⁴³. They participate in communication as a third member of the traditional synapse (the ‘tripartite synapse’), through the release of gliotransmitters (glutamate, ATP, D-serine) in response to hundreds of synaptic inputs. Hence, they are responsible for the storage, processing and transfer of synaptic information across neuronal networks in the brain⁵⁹. The diversity of

their roles is reflected in the recent identification of distinct subclasses of astrocytes that are characterized by differences in gene expression, function and reactive states during CNS injury^{43,47,81,82}. Gradients of damage-associated cues regulate the expression of extracellular-signaling molecules, intracellular transducers, and of transcription factors that instruct subtype specification⁸³. Heterogeneous subtypes range from inflammatory phenotypes, which produce cytokines and chemokines, to phenotypes with an active role in inter-neuronal signal transmission (such as neurotransmitter release, sensing, or re-uptake)⁸¹ and in blood-flow regulation⁶⁹. Therefore, differential responses arising as a consequence of astrocyte reactivity, in addition to their physiological roles in the uninjured brain, need to be considered when evaluating the effects of astrogliosis on therapeutic outcomes and device performance. Brain injury, pathology and electrical stimulation generate considerable modifications to the physiological nature and consequences of glial signaling, with reactive astrogliosis implicated in both neuroprotective and neurodegenerative outcomes^{83,84}.

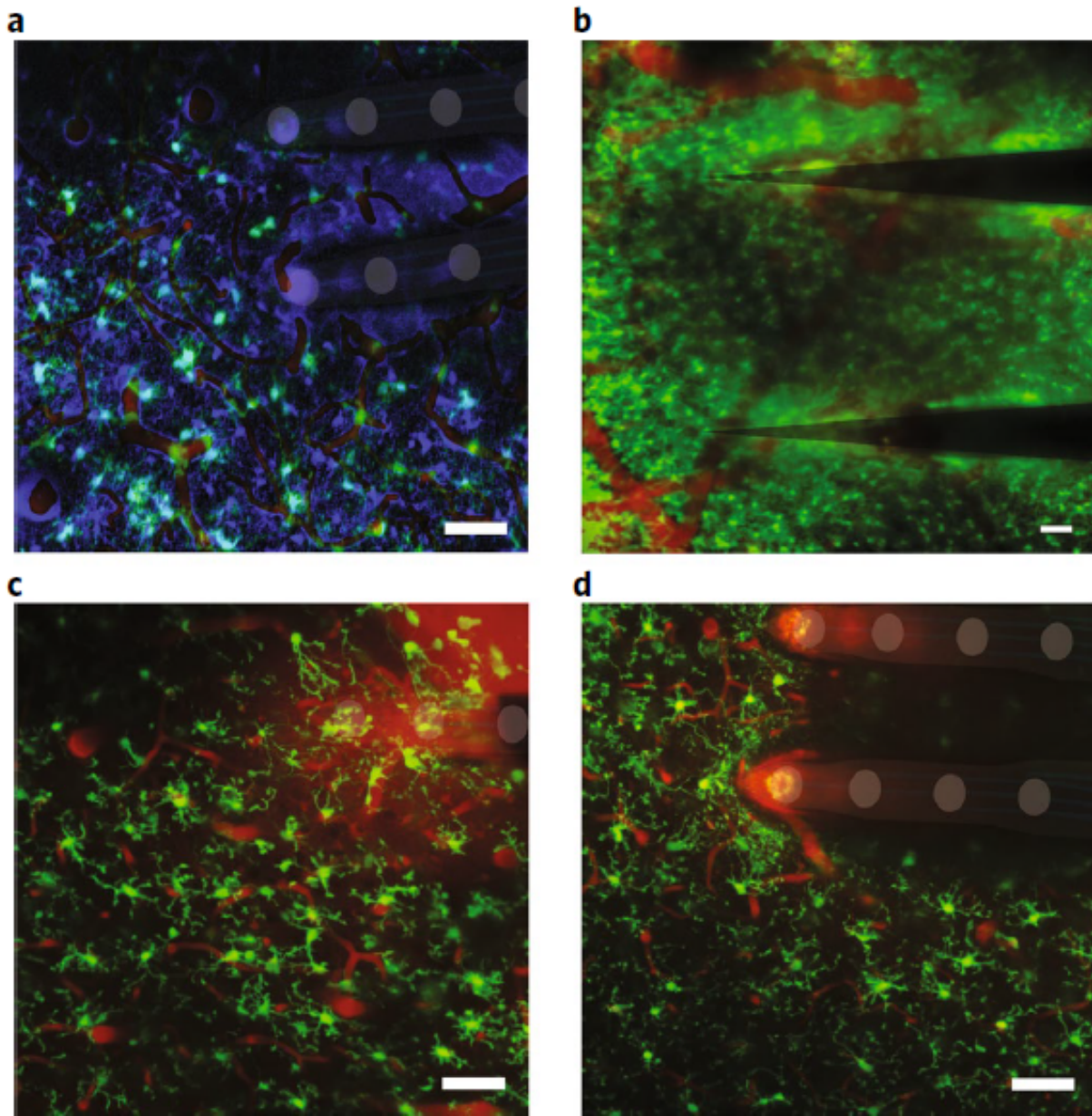


Figure 2.3 | In vivo multiphoton imaging of the glial response to MEA implantation. Astrocytes and oligodendrocytes (Sulfarhodamine101, false-colored purple in **a**), neurovasculature (intravascular Sulfarhodamine101, red in all panels), and microglia (CX3CR1-GFP, green, in all panels) are shown. **a**, Microglia display an amoeboid morphology and encapsulate two shanks of a 4x4 Neuronexus array 6 hours following implantation⁷⁵. **b**, Microglia form a compact scar around two shanks of a 1x3 Blackrock array at 2 months post-implantation. **c**, Microglia activation and lamellipodia ensheathment of an implanted silicon/silicon-oxide microelectrode. **d**, Microglia avoid the silicon/silicon-oxide microelectrode surface when covalently coated with neurocamouflage protein L1CAM. Scale bars, 100 μm . Panel **b** adapted from ref. ⁶⁷. Panels **c-d** adapted from ref. ⁸⁵.

Disruption of the blood–brain barrier (BBB) is inevitable during device implantation⁸⁶ (**Fig. 2.3**). The influx of blood-serum proteins (including albumin and fibronectin) activate inflammatory pathways of nearby glial cells, including microglia and astrocytes⁶⁹ (**Fig. 2.3a**). Microglia become activated, divide, and migrate to the implant to release pro-inflammatory cytokines. This activation of microglia and the loss of ramified processes prevent these cells from undertaking their important ‘resting-state’ activities, such as normal modulation of synapses^{69,87}. In turn, the upregulation of pro-inflammatory cytokines drives nearby neurons towards excitotoxicity and neurodegeneration. Simultaneously, the loss of nearby oligodendrocyte precursor cells (also called NG2 cells) leads to the proliferation, migration, and differentiation of distant NG2 cells into astrocytes⁸⁸, increasing the activated astrocyte population (**Fig. 2.1**). Astroglial reactivity around the implant leads to increased expression of connexin-43 (Cx43), an astroglial hemichannel and gap-junction known to facilitate the spread of inflammation^{89–91}. In turn, inflammation leads to the recruitment of blood-borne monocytes and neutrophils through the intact BBB, and to the formation of multinucleated giant cells⁶⁷. In addition, this inflammation alters the expression level of matrix metalloproteinases, together leading to further breakdown of the BBB and facilitating the influx of blood-serum proteins, red blood cells, and leukocytes⁶⁹. BBB disruption also leads to lower oxygen and nutrient delivery, as well as to impaired removal of neurotoxic waste products, including reactive oxygen species generated during the breakdown of red blood cells in the parenchyma⁶⁹. This increase in metabolic, oxidative, and osmotic stress further drives inflammation in nearby cells⁶⁹. As expected, there is growing literature pointing to the idea that lasting BBB disruption around electrodes is

implicated in long-term signal instability^{66,68,69,92}. Together, this underscores an important role for BBB disruption in attracting and sustaining gliosis following device implantation.

After arrival, astrocytes can act as either effectors or affectors of device function. In the wake of the discovery of DBS and of expanding applications for similar devices, there has been growing interest in the role of glial cells in the effects and side-effects of therapeutic stimulation, as well as in the progressive deterioration of the ability of electrodes to stimulate and record effectively^{30,93-96}. Historically, the evaluation of the glial contribution to performance outcomes has been limited to the formation of an encapsulating scar around implanted electrodes (**Fig. 2.2**). For stimulation therapies, this often led to the simplistic view that the encapsulating scar was a passive physical barrier, where one could simply 'turn up the current' to offset any impact of the glial response, until hitting a threshold limit for safe electrical stimulation. For diagnostics and therapies depending on recording electrodes, the impact of the glial response was typically assessed by correlating measured tissue-electrode impedance to the quality of recorded neuronal activity⁹⁷. However, more recent data have associated the chronic glial response to functional changes in neural circuit behavior and to progressive neurodegeneration within the vicinity of implanted electrodes^{84,98,99}, painting a more complicated picture of the glial contribution to the injury response. Likewise, newer data suggests that glia are an effector in stimulation-based therapeutic outcomes^{93,100}. Isolating the structure-function relationship between glial reactivity and the remodeling of local neuronal circuits is central to understanding the fundamental mechanisms underlying therapeutic effects and device-failure modes. Here, we

consider the influence of astroglia on device function, both as a passive barrier to device–tissue communication and as an active influence on neuronal signaling.

Consequences of glial encapsulation

Neurostimulation.

The barrier nature of gliosis has traditionally been assessed through in vivo measurements of the impedance of the tissue/electrode interface, and modelled using static circuit elements. However, the electrode/tissue interface, especially in the presence of reactive gliosis, cannot be fully defined by these traditional methods. In vivo impedance measurements are sensitive to a variety of factors in addition to glial encapsulation, including potential cellular encapsulation of the reference electrode, protein adsorption on electrode sites, and the characteristics of the ionic environment at the electrode/electrolyte interface (such as diffusion, resistance to charge transfer, and double-layer capacitance)^{101,102}. Likewise, impedance can be especially difficult to interpret for emerging biomaterials with high ratios of electrochemical surface area to geometric surface area, for which the surface topography and chronic glia–surface interaction remain difficult to characterize¹⁰³. Even for simple surfaces, faradaic reactions such as platinum dissolution occur at low levels of stimulation¹⁰⁴, and increase as a function of increasing stimulation intensity¹⁰⁵. Charge transfer via faradaic reactions risks damage to both electrodes and neighboring tissues¹⁰⁶. Similarly, the extracellular tissue resistance between cells comprising the glial scar, and the combined resistance and capacitance of their cellular membranes, can be altered as a function of stimulation intensity^{95,107,108}. Given the nonlinear

contributions of these elements, the accuracy of the volume of neural-tissue activation of a chronically healed-in electrode predicted by computational models is difficult to verify. Moreover, the impacts of these nonlinear elements in chronic settings on stimulation strategies such as high-frequency stimulation to induce neural block¹⁰⁹, on asymmetrical waveforms to inactivate neural tissue close to the electrode¹¹⁰, and on thresholding techniques to activate specific neural classes/elements remains unclear¹¹¹.

For stimulation applications, the barrier nature of gliosis is reflected in models of the effective volume of tissue activated, where greater gliosis reduces the number of neurons stimulated¹¹⁰. The stimulation paradigm affects the impact of the glial barrier: in constant-voltage stimulation, voltage is controlled and the actual current delivered to tissue varies as the tissue response evolves (increased impedance due to gliosis reduces the stimulation delivered). Although glial encapsulation is known to change in the weeks immediately following implantation, it is generally assumed that reactive gliosis reaches a steady state three to six months post-implantation^{96,112}. For constant-voltage stimulation paradigms, the day-to-day changes in impedance caused by consolidation of the glial scar during the first three to six months post-implantation may dramatically alter the effective current reaching neural tissue⁹⁴. As a result, most device manufacturers have moved towards constant-current stimulation paradigms where the charge density delivered by the stimulating electrode does not depend on day-to-day changes in impedance of the tissue/electrode interface^{113,114}.

Extracellular recordings.

The impact of glial encapsulation on the quality of signals recorded in vivo remains ill-defined, as studies that investigate histology, impedance, and recording quality for the same system are rare. Nevertheless, a few lines of indirect evidence support the idea that glial encapsulation acts as a barrier to signal detection by implanted electrodes^{92,97,115}. Astrogliosis, as identified by increased glial fibrillary acidic protein (GFAP) immunoreactivity, was associated with reduced recording quality of Utah-style arrays implanted in the rat cortex in a study that investigated the relationship between histology and recording quality⁹². Another study found a correlation between increased impedance and the presence of GFAP-positive astrocytes (signal quality was not assessed, however)¹¹⁶. An inverse relationship between recording quality and impedance measurements over a chronic time course was also observed, but a direct assessment of histology was not reported⁹⁷. In a study which assessed impedance, recording quality, and quantitative histology within the same set of chronically-implanted animals³⁰, the data revealed a negative correlation between non-neuronal density (NND) and signal quality, and a relatively weaker, positive correlation between NND and 1-kHz impedance (**Fig. 2.4**).

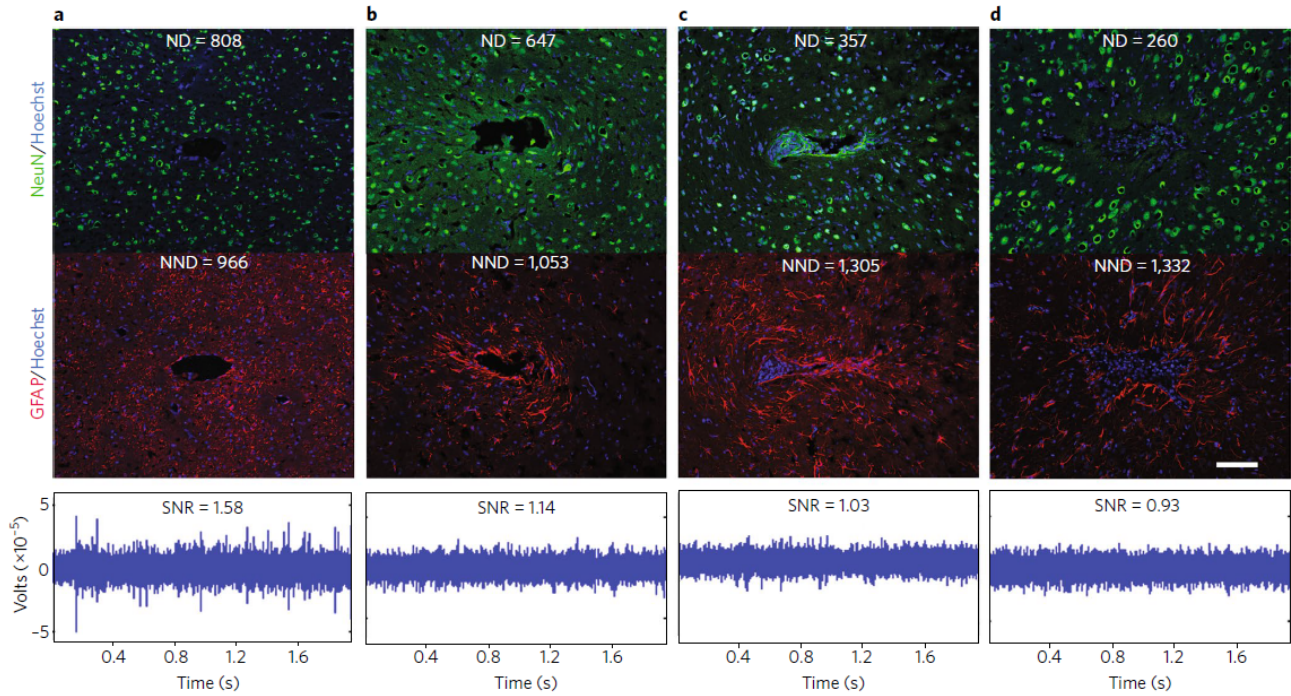


Figure 2.4 | Evidence for a negative impact of increased gliosis on recording quality. a–d, Representative images from four animals demonstrate the range of endpoint histological outcomes (from ‘good’ to ‘poor’, left to right). The figure has been generated after additional analysis on data collected in a previous study³⁰. Neuronal nuclei (NeuN, green) and astrocytes (GFAP, red) surrounding probe tracts are shown, and the associated average neuronal and non-neuronal density data are listed (area binned cell counts, neuronal density (ND) and non-neuronal density (NND), in cells · mm⁻²). Recording segments with signal-to-noise-ratio (SNR) values representative of the average value for each animal are depicted (the SNRs calculated from peak-to-peak noise result in lower values than root-mean-square noise)^{30,117}. Recording quality improved with decreased NND and increased ND/NND ($p < 0.05$, Spearman’s rho, $n = 6$). Impedance increased with increased NND ($p < 0.05$, Spearman’s rho, $n = 6$). Animals in a and c were drug-treated while b and d correspond to the controls. Scale bar, 100 μm .

These data suggest that glial encapsulation is an underlying cause of both increased impedance measurements and a concomitant reduction in recording quality (in support of a barrier role). However, the relationship between impedance and recording quality is complex, with multiple potential confounders and often inconsistent correlation between metrics^{118,119}. For example, inter-animal and intra-day variability in recorded signal and impedance correlations have been reported, where a ‘simple’ relationship between

impedance and unit activity could not be defined¹¹⁹. Loss of insulation integrity is an important factor in determining measured impedance values, and several results underscore the potential contribution of device integrity in determining performance outcomes^{120,121}. Furthermore, drug treatments that reduce glial activation and decrease impedance do not necessarily translate to an improvement in recording quality³⁰. Additionally, modelling data suggest that glial scarring may have a large impact on impedance values but minimal impact on signal amplitude¹²². Interpreting impedance values measured in vivo and their relationship to recorded signal quality and histology, is then confounded by the dual influence of mechanical integrity and glial encapsulation on recorded values. Also, the assimilation of reported effects across studies is undermined by inconsistencies in the analysis methods used. Moreover, impedance measurements are an imperfect surrogate for the measurement of action potentials generated by a nearby neuron. Impedance measurements are typically taken at 1 kHz or across a frequency spectrum, and consist of continuous sinusoids in the 5–25 mV range delivered by back-end instrumentation. In contrast, extracellular potentials are generated by the movement of ions across a cellular membrane and are caused by the gating of ion channels during an action potential, are not continuous in nature, consist of multiple frequency components, and are in the range of tens to hundreds of microvolts, depending on the distance and orientation with respect to the extracellular recording electrode^{123,124}. New methods of assessing the barrier effect of gliosis in vivo, in concert with complementary approaches to assess individual glial-encapsulated sites (such as in vivo imaging, controlled perturbations of glial reactivity surrounding sites, and improved computational models) will be required to determine the impact on long-term recording quality. Similarly, the view of the glial sheath as a passive barrier needs to be

reconciled with an expanding body of evidence for direct action of glia on neuronal health and excitability.

Neurochemical sensing.

In addition to electrically isolating devices from neuronal signals, glial encapsulation may pose a communication barrier between implanted sensors and the local neurochemical environment. Neurochemical sensing has become a commonplace application of implanted electrodes in research studying synaptic transmission^{125,126} and is an emerging approach in clinical diagnostics of neurological disease¹²⁷. When coupled with implanted drug-delivery or neuromodulation devices, it can serve as a source of feedback, enabling personalized and smart neuroprosthetic therapies^{50,127}, and providing a foundation for future closed-loop applications (for example, low neurotransmitter levels triggering the delivery of electrical or chemical-based therapy). Although the spatiotemporal resolution of these devices is superior to the alternative approach of microdialysis¹²⁸, their lifetime is limited due to factors such as the electrochemical stability of the interface and the reliability of the transduced output measurement over time¹²⁸.

Relatively limited histological examination has been reported for neurochemical sensors¹²⁸, and further studies are necessary to clarify the impact of glia on the function of neurochemical sensing⁶⁹. Given that effective diffusion of the chemical species to the electrode is a rate-limiting factor in the performance of neurochemical sensors¹²⁹, the diffusion barrier posed by astrogliosis¹³⁰ could be a key factor limiting the temporal resolution achievable by these devices. Also, although neurons are typically assumed to be

both effector and affected cells of neurotransmitter release, an increasing body of evidence demonstrates that glia are capable of neurotransmitter release and uptake⁸¹. For example, an investigation into the source of glutamate in neurochemical sampling by microelectrode arrays reported only ~40–50% of measured glutamate to be of neuronal origin in the rat prefrontal cortex¹³¹. Likewise, non-vesicular glial mechanisms accounted for the majority of extracellular glutamate detected in the rat prefrontal cortex using microdialysis¹³². Glia can influence the local neurochemical environment and produce related effects on the excitability of local neurons, affecting the interpretation and quality of data collected from implanted sensors and stimulators.

Glia as an active modulator of signal transmission

An increasing body of literature demonstrates that reactive glia directly influence the signal-generating capabilities of local neurons by influencing the excitability of individual cells, the synaptic transmission of signals between them, and the broader population activity detected within a network. In this section, we explore the mechanisms of these effects and consider the potential influence on the signals detected or generated by implanted devices.

Modulation of neuronal excitability.

Neuronal signaling is enabled by the conduction of ionic charge carriers across the cell membrane through specialized transmembrane proteins known as ion channels¹³³. The function and expression of ion channels is shaped by a variety of factors, including the ionic composition of the intracellular and extracellular environments as well as events occurring

during individual stages of protein synthesis (such as transcription, translation, post-translational modification, assembly with ancillary subunits and alternative splicing). The glial–neuronal signaling pathways, in which autocrine/paracrine amplification loops for cytokine release are generated following injury, have the potential to affect these processes in several ways, ultimately influencing the excitability of individual neurons.

A downstream influence of glial–neuronal signaling is the efflux of potassium and the accumulation of glutamate in the extracellular environment surrounding neurons. Astrocytes have a primary role in maintaining the homeostasis of the ionic and chemical composition of the extracellular environment; their active clearance of potassium and glutamate from the extracellular space produces a net inhibitory effect on nearby neurons that dampens excitability^{59,134}. In a mouse model deficient in astroglial connexins and astroglial coupling, hyperexcitability, synaptic unsilencing, and increased synaptic release arose within the local neuronal network⁹⁰. Glial scar tissue bears upregulated expression of connexins¹³⁵, indicating tight astroglial network formation in the wake of the injury response to neural prostheses. By extension, astroglial scar formation may favor enhanced buffering of excitatory accumulation of extracellular potassium and glutamate, ultimately ‘quieting’ the local neuronal population surrounding a device.

Additionally, glia are known to release cytokines in response to injury, which may influence neuronal function through direct impacts to ion-channel expression and physiology. Reactive glia, including astrocytes and microglia, release potentially neurotoxic, inflammatory cytokines following device implantation^{34,136}, including interleukins 1 and 6

(IL-1 and IL-6), tumor necrosis factor alpha (TNF α), and monocyte chemoattractant protein 1 (MCP-1)¹³⁷. These events may initiate cell death pathways and impair recording performance⁹⁹, where preventing IL-1 β activation showed significant improvement in neuroprosthesis performance¹³⁸. Released cytokines can also result in a change in neuronal function, since alterations in ion-channel expression have been shown to follow exposure to inflammatory cytokines (IL-1 β , TNF- α , IL-6) in models of traumatic brain injury^{139,140}. Alterations in channel currents may occur on both short- and long-term timescales, where short-term effects are most probably attributed to alterations in gating characteristics or post-translational modifications to channel proteins, whereas longer-term impacts may be related to changes in channel expression¹³⁹. Acute effects (within 24 hours) tend to favor hyperexcitability whereas longer-term impacts (days or weeks after exposure or injury) tend to favor loss of excitatory sodium^{141,142} and calcium currents^{143,144} in the central nervous system, a trend which has been interpreted as the progressive dampening of the excitability of affected neurons in order to promote neuroprotection and prevent excitotoxicity¹⁴⁵. Impaired excitability would limit the detection of neuronal activity by investigational recording devices and elevate the stimulation thresholds required for clinical neuromodulation devices. Relating the underlying inflammatory pathways to performance outcomes of implanted devices will require further efforts, and targeted intervention strategies will be necessary for restoring network-level excitability to maintain long-term function in implanted devices.

Modulation of synaptic transmission.

Device implantation necessarily disrupts the connectivity of the surrounding network, and can remodel synaptic organization through multiple mechanisms. Gliosis and related changes in the local neurochemical environment can affect synapse formation and function following injury, influencing signal generation by the interfaced network. The impact on synaptic transmission mirrors that of intrinsic excitability, favoring a shift from hyperexcitability to hypoexcitability over time.

Synaptogenesis and silencing.

Astrocytes can direct the formation and maintenance of synapses through multiple signaling pathways (this has been reviewed extensively elsewhere¹⁴⁶). However, the influence of reactive glia on the synaptic remodeling surrounding implanted devices is only beginning to be explored. A recent report of initially heightened excitatory synaptic transporters was followed by a chronic elevation in markers of inhibitory transmission surrounding electrode arrays implanted in rat brains¹⁴⁷. BBB breach due to device insertion may be an initiating signal for these events, on the basis of evidence that astrocyte-induced excitatory synaptogenesis follows injury¹⁴⁸. Furthermore, heightened glutamatergic transmission subsequently activates astrocytic release of transforming growth factor beta 1 (TGF- β 1) to induce inhibitory synaptogenesis¹⁴⁹; this parallels the observed excitatory inhibitory shift surrounding implanted devices¹⁴⁷.

An alternative mechanism of injury-induced synaptogenesis is related to a class of matrix associated glycoproteins, known as thrombospondins (TSPs), produced by reactive

astrocytes and microglia^{150,151} (**Fig. 2.5b**). Purinergic signaling and mechanical stimulation, which are both relevant in device implantation, increase TSP production¹⁵². Here, TSP release is responsible for the formation of ultrastructurally normal yet functionally silent synapses^{153,154}, which are characterized by altered expression of glutamate receptors. Silent synapses display normal postsynaptic N-methyl-D-aspartate receptor (NMDAR) density but an absence of postsynaptic α -amino-3-hydroxy-5-methyl-4-isoxazolepropionic acid receptors (AMPARs). Without AMPARs, these excitatory synapses are silent due to magnesium ion blockage of conductive NMDARs, unless they are artificially depolarized to remove the block¹⁵³. Notably¹⁵⁵, TNF- α release by astrocytes can compensate for long-term silence via AMPAR insertion into all synapses of a given neuron¹⁵⁴⁻¹⁵⁶ (a mechanism of network-level homeostatic plasticity known as synaptic scaling¹⁵⁵). However, upregulation of connexins, as occurs in the astroglial scar¹³⁵, has been shown to limit AMPAR insertion and to maintain silent synapses through scaling mechanisms that prevent excitotoxicity⁹⁰. Therefore, synapses formed near the injury scar may be likely to exhibit depressed activity. However, variability in the functional consequences of reactive signaling is to be expected, especially in the context of a chronic, indwelling implant where surrounding gliosis may be aggravated by chronic inflammation, on-going micromotion, or repetitive stimulation.

Figure 2.5 (cont'd)

positive-feedback loop; ATP is rapidly hydrolyzed to adenosine in the synapse, where adenosine is able to act on presynaptic A1Rs to inhibit Ca²⁺ channels and prevent vesicle release (presynaptic silencing), and to act on postsynaptic A1Rs to open K⁺ and Cl⁻ channels and prevent the generation of action potentials (postsynaptic silencing). (2) TSP production and release, which forms ultrastructurally normal, but functionally silent synapses. These postsynaptic terminals lack AMPARs, which are required to alleviate the Mg²⁺ block on NMDARs, therefore preventing effective signal transfer from the presynapse (postsynaptic silencing). A1R, adenosine A1 receptor; P2R, purinergic P2 receptor; GluT, glutamate transporter. Figure reproduced¹⁵⁷.

Synaptic remodeling is shaped by the local neurochemical environment, which is in turn affected by device implantation. Electrode insertion induces significant increases in neurotransmitters in the extracellular environment (glutamate, ATP and adenosine)¹⁵⁸, where likely sources include punctured cellular membranes and mechanoactivation of astrocytes and microglia (**Fig. 2.5a**)⁴³. The resulting gradient serves as a beacon for attracting and reinforcing reactive gliosis^{43,81}, and necessarily affects local synaptic plasticity⁵⁹. Therefore, glial-derived changes in the local neurochemical environment are both neuron-affecting and self-sustaining^{84,98}. Microglia mobilized by extracellular ATP withdraw their processes to assume an amoeboid morphology and converge on the site of injury to release cytokines, glutamate and ATP (ref. ⁴³). Adenosine is produced when ATP is rapidly hydrolyzed in the synapse¹⁵⁹, and has been demonstrated to play a key role in the suppression of synaptic activity. Activation of adenosine receptors inhibits presynaptic calcium-dependent release of neurotransmitters¹⁶⁰ and opens postsynaptic K⁺ and Cl⁻ channels^{161,162}. These events collectively hyperpolarize the post-synapse and prevent synaptic transmission (**Fig. 2.5b**). A reduction in synaptic activity will affect synaptic strength and plasticity¹⁶³, resulting in further alterations to the local synaptic network. To summarize, glial neurotransmitter release may underlie synaptic-silencing mechanisms as

an origin of injury-induced synaptogenesis or of adenosine-mediated suppression of pre- and post-synaptic transmission. Combined with evidence of increased markers of inhibitory synaptic transmission in the chronic setting, device implantation is likely to favor dampened signal transmission in the long term. These plastic silencing mechanisms are likely to be maladaptive for the effective stimulation and recording of neurons near devices. However, they may be adaptive for confining the spread of excitotoxicity and neuronal loss in the wake of implant injury and for reducing the potential for excessive synchrony within the local network.

Modulation of network activity.

Beyond their influence at the level of a single synapse or neuron, astrocytes coordinate activity across broader cohorts of neurons and the connections between them, resulting in network-level modulation. Interconnected astroglia are able to orchestrate synchrony through the integration of signaling within neuronal circuits and across functional regions of the brain⁵⁹. The stimulated actions of a single astrocyte could dictate functional consequences on an entire network of neurons⁵⁹. Artificial synchronous depolarization of astrocytes using optogenetic stimulation resulted in global suppression of neuronal activity in the subthalamic nucleus¹⁶⁴, providing direct evidence of network coordination by glia. Computational models support the available empirical evidence, where astrocytes were identified as critical determinants of the level of synchrony between neighboring neurons in simulated data¹⁶⁵. Gap junctions and hemichannels subserve this function through the rapid trafficking of ions, solutes, and metabolites along astroglial networks, coordinating efforts across distributed spatial domains and providing a framework for modulating synchrony

and plasticity in complete neuronal ensembles⁵⁹. Given evidence for astrocyte coordination of neuronal networks⁵⁹ (albeit controversial¹⁶⁶), reactive gliosis likely impacts not only the generation and transmission of action potentials between single neurons, but also the broader population activity detected and stimulated by electrodes implanted in the brain.

Neuronal synchrony.

The analysis of complex networks has revealed guiding principles for the emergence of synchrony within a network of oscillators, where both the dynamics of the individual oscillators and the architecture of their connectivity are key determinants of function: homogeneity of the oscillators and high coupling strength tend to favor synchrony¹⁶⁷. Astroglial glutamate release is able to strengthen excitatory coupling between neurons by acting on pre- and postsynaptic receptors^{168,169}, resulting in a robust propagation of synchronous activity across networks^{170,171}. Moreover, computational modelling has supported glial mechanisms for synchronizing neuronal activity, where simulated pre-synaptic targeting of glutamate release by astrocytes was sufficient for initiating hypersynchronization and seizure activity¹⁷². On the other hand, computational models have also demonstrated the importance of astrocytes in the desynchronization of neuronal activity, by providing activity-dependent stabilization, as neighboring neurons are prone to hypersynchrony through their intrinsic excitatory coupling¹⁶⁵.

This is supported by the observation that astroglial adenosine release desynchronizes network activity¹⁶⁹. However, these apparently opposing results may be reconciled by considering the reactive state of the astrocyte: astrocytes in an activated, pro-

inflammatory state⁴⁷ may lose their ability to desynchronize local neuronal networks. It was suggested that a loss in the ability of astrocytes to desynchronize neuronal firing may underlie abnormalities in the oscillatory activity associated with brain pathology (such as Parkinson's disease, Alzheimer's disease and epilepsy¹⁷³)¹⁷⁴. Therefore, therapeutic effects of stimulation may evoke astrocyte-mediated changes in network synchrony and plasticity that would otherwise occur under physiological conditions⁵⁹. Taken together, this evidence suggests that glia are a central determinant of network-level activity and may be underutilized as a target cell of neuromodulation therapies that interrupt pathological oscillations.

Glial-activation challenges and design considerations

Glia as an effector of clinical devices.

The serendipitous discovery of DBS to alleviate the symptoms of Parkinson's disease preceded understanding of the mechanisms of therapy. Subsequently, the role of glia as a cellular target of DBS treatment¹⁷⁵⁻¹⁷⁷ has emerged amongst several candidate mechanisms. Gliosis is commonly observed in post-mortem brain tissue from DBS patients^{76,178} and can be more pronounced when surrounding active devices¹⁷⁹ (**Fig. 2.2**). Several DBS models using high-frequency stimulation (HFS) have suggested that astrocytes are effectors for interrupting pathological oscillations in the thalamus¹⁰⁰ and for attenuating tremor⁹³. The release of adenosine or glutamate by HFS¹⁵⁸ can modulate neuronal oscillations from non-synaptic sources^{93,100}, with corresponding astrocytic Ca²⁺-wave propagation occurring in a frequency- and amplitude-dependent manner⁹³. Likewise, neurochemical measurements

taken from DBS patients have correlated adenosine release with both tremor arrest¹⁸⁰ and seizure termination¹⁸¹. Although still at an early stage, evidence is mounting for glial contributions to clinical device efficacy, spanning from neurochemical mediators on implantation to direct effectors of neuromodulation devices. Even in the absence of stimulation, device implantation results in insertional trauma and in ensuing inflammation that can directly modulate network activity and affect clinical outcomes. This is known as the microthalamotomy effect¹⁵⁸, where implantation results in a window of therapeutic efficacy that can last for as long as a year¹⁸⁰, implying injury-induced plasticity. Astrocyte-mediated plasticity is a tightly regulated interaction between glutamate, ATP and cytokine signalling^{163,182} (**Fig. 2.5**), and can lead to either potentiation or depression after injury^{43,163,182}. As an example, reactive inflammatory signaling can alter AMPAR/NMDAR ratios and ion-channel expression/function, and excessive glutamate release can alter the excitatory coupling strength of synaptic networks^{43,59,90,163}. In turn, the resulting plasticity (including synaptogenesis and long-term potentiation or depression¹⁴⁶) shapes long-term network function^{146,163}, where potentiation favors hyperactivity (seizure activity) and depression results in network silencing. For this, recent evidence suggests immediate, local upregulation of markers of glutamatergic transmission surrounding devices after insertion, suggesting a potential mechanism of heightened synchrony and activity detected by recording electrodes¹⁴⁷. However, later upregulation of inhibitory neurotransmission (driven by release of gamma aminobutyric acid, GABA) suggests a shift towards network silencing and limited signal detection¹⁴⁷. This shift from elevated glutamatergic to GABAergic tone around implanted electrodes is likely astrocyte-induced. In this regard, heightened glutamatergic transmission has been shown to activate astroglial release of TGF- β 1 to induce

GABAergic synaptogenesis¹⁴⁹. Therefore, glial signaling after insertion can directly remodel the structure and function of surrounding circuitry, likely affecting the long-term performance of recording devices and the activation thresholds of stimulating devices. These factors will need to be further explored in order to uncover their impact on device efficacy.

A growing body of literature supports the important role of glial cells during electrical stimulation. Several models have demonstrated the direct modulation of plasticity, inflammation, neurogenesis, and cerebrovascular functions by glial cells following neurostimulation^{175,183}. For example, stimulation evokes astrocyte-induced cortical plasticity, as demonstrated in studies using transcranial direct current stimulation (tDCS)¹⁸⁴. Also, optogenetic depolarization of astrocytes led to the release of glutamate, which directly modulates synaptic plasticity (LTD) and motor behaviour¹⁸⁵. Inflammation is likewise modified by stimulation: tDCS can both incite inflammation in the uninjured brain and modulate it following injury¹⁸⁶. Implanted-electrode stimulation upregulates inflammatory receptors (toll-like receptors, TLRs) in microglia¹⁸⁷, favoring a shift to a pro-inflammatory state¹⁷⁴. However, the timing¹⁸⁸ and intensity¹⁸⁹ of stimulation may differentially affect reactivity and inflammation, suggesting a gradient of glial responses¹⁸³. In the context of neurogenesis, neuromodulation is gaining traction as a reparative tool for brain injury and disease^{175,190}. Neurostimulation stimulates neural progenitor proliferation¹⁹¹⁻¹⁹³, directs the migration (galvanotaxis) of neuronal and glial precursors^{190,194-196}, and promotes their differentiation^{192,193,196,197}. Interestingly, tDCS-polarized pro-inflammatory microglia accompany NG2-precursor migration to promote functional recovery after stroke¹⁸⁶. This suggests that the modulation of reactivity and inflammation could potentially be harnessed

for guiding endogenous repair around active electrodes. Finally, astrocytes are key constituents of the neurovascular unit⁷¹, where they release neurochemicals to modulate vasodilation or constriction and provide activity-dependent metabolic support (as demonstrated with electrical^{198,199} and optogenetic²⁰⁰ stimulation). In turn, evidence points to astrocytes as important DBS effectors for improved cerebral blood flow and metabolism in drug-refractory epilepsy²⁰¹. Taken together, glia represent important effectors of clinical devices, where their responses to electrical stimulation are gaining utility as targets to modulate regeneration or repair, cerebrovascular function and inflammation.

Consequences of higher-density arrays and multiple implants.

Monitoring the electrical activity of large numbers of neurons simultaneously with single-cell resolution is an ongoing challenge in neural engineering²⁰², and has motivated the design of increasingly high-density electrode arrays with smaller individual electrode site sizes^{202,203}. Furthermore, as neuromodulation strategies become increasingly sophisticated (as exemplified by closed-loop systems), multiple implants within a single patient or research subject are becoming more common. The potential for injuries induced by multiple implants and/or multi-shank devices to exacerbate inflammation and gliosis should be considered as the field moves towards more distributed sampling approaches. Successive brain injuries engage a state known as glial priming: a condition where glia remain in an activated pro-inflammatory state with upregulated inflammatory markers, heightened sensitivity, resistance to negative feedback mechanisms, and a predisposition to releasing excessive amounts of inflammatory factors on subsequent activation¹⁷⁴. Glial priming can develop over many years following CNS insults including cortical stab-wound injury^{204,205},

as well as in neurodegenerative conditions^{206,207} and ageing^{208,209}. Subsequent (secondary) insults exacerbate glial responses through excessive release of pro-inflammatory IL-1 β , TNF- α , and IL-6 (refs. ^{174,204,210}), which can lead to prolonged inflammation and progressive degeneration^{206,207}. These cytokines can also elicit hyperexcitability and excitotoxicity under primed conditions¹⁷⁴, and have been implicated in susceptibility to seizures and epileptogenesis^{170,211}, all of which bear implications on side-effects not only for experimental models, but also for clinical DBS treatments where patients are inherently predisposed to conditions of pathology, ageing and hyperexcitability prior to the implantation of devices. The extent of glial priming incurred from pathology (such as Parkinson's disease, Alzheimer's disease, epilepsy and stroke) and ageing will need to be considered prior to the implantation of devices that will necessarily exacerbate pro-inflammatory glial priming. Moreover, device-design considerations will need to evaluate the relationship between glial priming and implant-feature sizes, the quantity of sites in high-density arrays, and distributed injuries caused by multiple implants and/or shanks.

Biomaterials and glial activation

The physicochemical properties of electrode materials directly influence glial gene expression, inflammation and chronic gliosis³⁸. Soft, nanoscale and bioactive materials have been incorporated into device design to produce electrode arrays with improved biointegration³⁶. The broad strategies are to reduce the mechanical mismatch between device materials and brain tissue, reduce the footprint (and invasiveness) of the array, enhance surface porosity to mitigate immune responses, or create a biomimetic or bioactive coating that conceals the implant from the foreign-body response³⁶.

Improved softness.

Stiff substrates including silicon exacerbate the activation of both astrocytes and microglia in comparison to softer materials²¹². Currently, silicon remains the most common material substrate for intracortical primate studies^{118,213} and clinical trials of brain/machine interfaces^{97,214}, whereas DBS leads used in patients are primarily made of polyurethane (Fig. 1). Silicon and polyurethane are substantially stiffer than brain tissue (Young's moduli for silicon, polyurethane and brain tissue are $\sim 10^2$, $\sim 10^{-1}$ and $\sim 10^{-5}$ GPa respectively³⁸). Minimizing the mechanical mismatch between the device and neural tissue improves gliosis, inflammation and neuronal preservation^{38,215,216}, and next-generation devices incorporate flexible materials designed to more closely mimic the stiffness of brain tissue (**Fig. 2.6**). Mechanically adaptive materials (initially stiff materials that become compliant upon contact with the physiological environment) significantly reduce glial scarring and inflammation^{215,217-219}. Examples are mechanically compliant nanoparticle polymer substrates for stimuli-responsive designs inspired by the sea cucumber dermis^{215,220-223} (**Fig. 2.6a**), and shape-memory polymer substrates with similarly adaptive characteristics and tunable moduli^{218,219,224}. Polymer blends of silicones and poly(3,4-ethylenedioxythiophene) (PEDOT) are the softest reported materials to record extracellular units, with accompanied reductions in microglial attachment²¹⁶. However, these materials introduce challenges for functional device design and minimally damaging deployment³⁶.

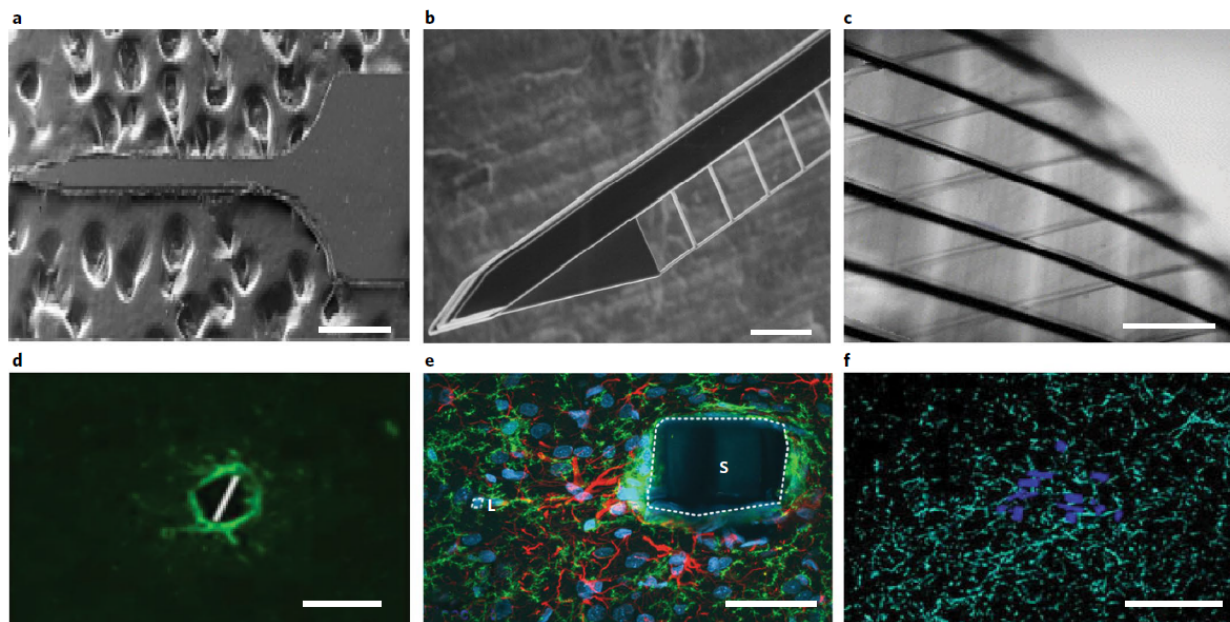


Figure 2.6 | Next-generation arrays mitigate gliosis. **a–f**, Devices (**a–c**) are shown above the associated histology images (**d–f**). **a**, A mechanically adaptive nanocomposite microelectrode becomes compliant upon implantation²¹⁷. **b**, A hollow-architecture parylene-based microelectrode places sites away from the stiff penetrating shaft, along 4- μm -wide lateral support arms²²⁵. **c**, A syringe-injectable mesh electronics mimics brain parenchyma with sites featured along an interwoven structure²²⁶. **d**, Astrocytes labelled (GFAP, green) around mechanically compliant probe at 8 weeks²¹⁵. **e**, Astrocytes (GFAP, red), microglia (OX42, green), and all cells (Hoechst, blue) labelled around the stiff electrode-penetrating shaft (S) and lateral edge (L) at 4 weeks²²⁵. **f**, Astrocytes labelled (GFAP, cyan) around a syringe-injected mesh (blue) at 1 year²²⁷. Scale bars, 500 μm (**a**); 100 μm (**b**, **d**, **f**); 250 μm (**c**); 50 μm (**e**).

Both device architecture and its material composition affect flexibility, since bending stiffness is determined by both the Young's modulus (E) and the dimensions of the material^{36,69,228}. Bending stiffness is proportional to Et^3 (where t is the thickness of a rectangular cross-section), meaning that reduced stiffness scales more rapidly with decreased device dimensions than reductions in modulus. Syringe-injectable, flexible mesh electronics have been shown to interpenetrate the brain parenchyma and record along interwoven neuronal networks (for up to 1 year, with minimal tissue response and sustained recordings)^{226,227} (**Fig. 2.6c**). And an electrode with a 15- μm^2 cross-sectional area is the

smallest chronically implantable extracellular microelectrode so far reported²²⁹. Two-photon imaging surrounding the implant revealed a lack of astrogliosis and minimal disruption of the vasculature. However, reduced stiffness can make softer^{38,230} and sub-cellular devices^{49,70,179} difficult to implant, requiring the use of an insertion tool^{179,180} or dissolvable shuttle^{231,232}. Since new device designs often employ both softer materials and reduced feature sizes, the relative impact of each of these factors on the tissue response can be difficult to interpret. Nonetheless, there is increased interest in the fabrication of electrode arrays with smaller features and softer materials, and potentially concomitant reduced gliosis (**Fig. 2.6**).

Smaller feature sizes.

In addition to enhanced flexibility, reducing device dimensions may diminish gliosis^{103,233,234} by presenting an adhesive surface that is too small to allow cellular attachment^{235–239}. For brain implants, feature sizes below 10 μm lead to reduced gliosis and preserved neuronal density²⁴⁰.

Reduced glial responses were observed with parylene-based Michigan-style arrays combined with the use of an open-architecture design (4- μm -wide feature sizes)²⁰³ (**Fig. 2.6b**). Open-architecture designs have also improved the integration of implanted planar arrays²³³. Ultrasmall, flexible carbon-fiber electrodes with subcellular features (< 10 μm in diameter) have emerged as an approach to mitigate tissue response and to improve long-term recordings¹⁰³. Devices are becoming both smaller and increasingly sophisticated. For example, injectable wireless electronics can carry out electrical recordings, optical

stimulation, temperature sensing and photodetection²⁴¹. Also, the immune response can be mitigated by decreasing implant volume and by increasing surface permeability or porosity, facilitating the dispersion of inflammatory cytokines and preventing their accumulation, as has been achieved with porous coatings²⁴² and web-like mesh electronics²⁴³⁻²⁴⁵. Although advancements in material-based strategies to improve the neuron-electrode interface continue, there is a need to pursue basic-science studies to identify guiding biological principles for improved device design.

Surface modification.

Electrode surface coatings have also become increasingly sophisticated for reducing the foreign-body response to brain implants^{38,246-248}, where materials include hydrogel^{246,249}, silk^{250,251}, bioactive anti-inflammatory surface molecules^{73,248,252}, and biodegradable polymer nanoparticles for the controlled delivery of anti-inflammatory therapeutics^{125,246,253,254}. Coatings are designed to (i) reduce inflammation through drug release, (ii) buffer or disperse inflammatory-cytokine accumulation, (iii) increase the fractal dimensions of the site for reduced impedance, and/or (iv) present a biomimetic surface to mask the implant from being recognized as a foreign body. The controlled release of anti-inflammatories from coatings has shown promise in the reduction of glial encapsulation and impedance^{253,255-257}, but the impact on neuronal health and recorded signal quality is less clear. In recent years, several strategies to increase the fractal dimensions of electrode sites with 'fuzzy' conductive material coatings have been developed to reduce impedance and improve tissue integration^{103,246,247,258,259}. For example, carbon nanotube coatings for metallic-wire electrodes in vivo have led to improved impedance, recording and stimulation

in both rats and monkeys²⁶⁰. Conductive polymer nanoparticles with hydrogel layers for decorating microfabricated electrode arrays with nanostructured surfaces offer the added advantages of improved charge transfer, greater compliance, reduced impedance, and the precise delivery of bioactive species^{254,258,261}. Strategies combining conductive polymer coatings and bioactive treatments lead to lower impedance and reduced gliosis^{38,246,247}. However, the implementation of 'stealth' coatings, such as those based on neuronal cell-adhesion molecules, can alleviate the foreign-body response by both promoting neural growth and by reducing gliosis (**Fig. 2.3c-d**)^{85,216,248}.

Effects at the molecular level.

The characteristics of a material substrate can influence the signaling pathways associated with reactive glia (**Fig. 2.5**). Nanostructured topographical features can increase astroglial ATP release²⁶², downregulate GFAP expression²⁶³, and increase the expression of glutamate transporters and the clearance of extracellular glutamate²⁶⁴. Stiffer substrates have been associated with the activation of microglia (amoeboid morphology, upregulation of CD11b/Ox-42) and of astrocytes (hypertrophy, upregulation of GFAP), as well as their proliferation, migration and adhesion²¹². With regards to gene expression, stiffer materials upregulate the molecular determinants of inflammatory signaling (TLR, IL-1 β , TNF α) in glia²¹². Mediation of these pathways may improve device function; for instance, knock-out of IL-1 β has demonstrated significant improvement to long-term functional recordings¹³⁸. For smaller feature sizes, improvements in gliosis are broadly associated with reduced injury-related inflammation and BBB permeability along with reduced micromotion-related tissue strain²⁴². Still, further details on the relationship between the material characteristics of an

electrode and the inflammatory/molecular effects on reactive glia are needed to establish guiding principles to design fully integrated devices (including intervention strategies and their temporal influence). Future research directions will need to incorporate genetic tools to identify precise targets of design features. For instance, it would be useful to locally knockdown or upregulate specific glial pathways (such as receptor expression and transmitter production or release) in order to determine the consequences of gliotransmission on device performance (including plasticity, network function and neuronal health). And advances in biomaterial science are producing new approaches to modify immune responses that could be leveraged to improve the tissue response to brain implants²⁶⁵⁻²⁶⁷. Uncovering the molecular pathways determining the relationship between glial responses and specific electrode features will facilitate targeted approaches to improved device design (**Fig. 2.7**).

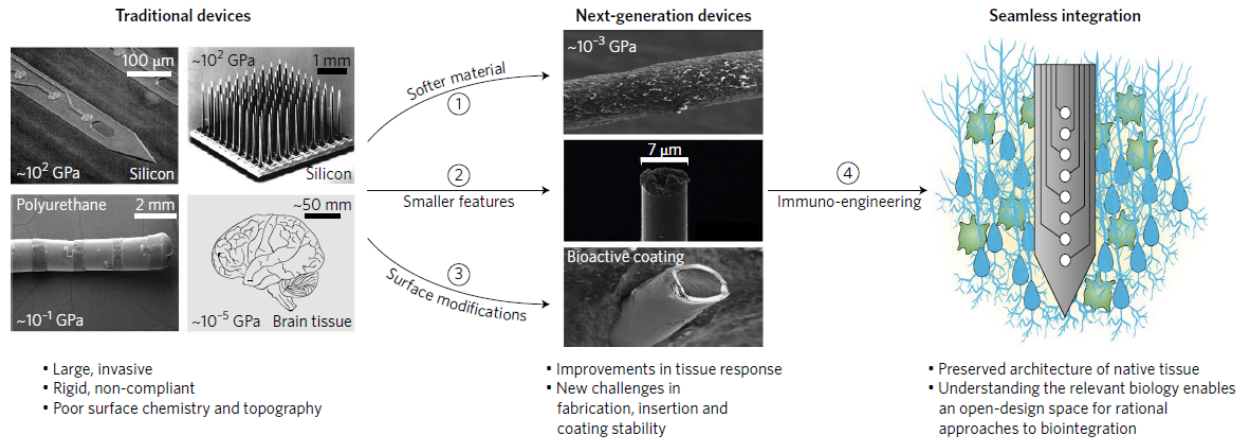


Figure 2.7 | Opportunities for further enquiry in engineering. Future work will need to uncover the effects of electrode properties on the molecular pathways that shape gliosis, including: (1) The degree of softness and corresponding inflammation from mechanoactivation of glia, and the evolution of the effect on gliosis over time (such as mechanical mismatch, micromotion, and the state of glial reactivity and ‘priming’); (2) The relationship between feature size and architecture on inciting and priming inflammatory gliosis around the injury, and the evaluation of the long-term consequences (such as hyperexcitability, excitotoxicity and degeneration) on device function; (3) The effects of surface modifications (chemistry and topography) on shaping reactive signaling at the interface (receptor activation and cytokine/gliotransmitter release) and the corresponding consequences on recording and stimulation performance; (4) Targeted approaches to modify immune responses will need to be incorporated to achieve seamless integration, which should be guided by their impact on glial signaling, reactivity and device performance. Traditional devices reproduced from refs. ^{78–80} and referenced directly in Fig. 1. Next-generation devices reproduced from²¹⁶ (top and bottom) and from¹⁰³ (middle).

Outlook

Although glia have been portrayed as acting as an encapsulating barrier to electrode integration and communication with surrounding neurons, this view does not capture the dynamic role of glia in the functional plasticity of neuronal networks following injury, and the implications of glia for the performance of microelectrode arrays implanted in the brain. A growing body of literature attests to the role of reactive gliosis in the remodeling and reshaping of neural circuitry during healing, yet relatively few reports have linked glial activity to the therapeutic effects of neuromodulation^{93,100} or explored the relationship between glial responses and recording quality^{118,121}. Bridging this gap is a major opportunity

for understanding the function and failure of microelectrode arrays in both research and clinical applications. Four major focus areas deserve further attention (**Fig. 2.8**). First, a better understanding of the glial role in shaping neural plasticity near devices (both at the cellular and network level). This is particularly relevant when interpreting results and developing methods to induce plasticity as a repair strategy. Targeted neurostimulation strategies can reorganize neural networks, potentially bypassing and overcoming neuronal damage or enhancing native function^{268,269}. Additionally, connecting well-described, known mechanisms for the glial influence on neuronal excitability and synaptic transmission to the performance of implants would create new opportunities for improved device design, stimulation protocols and tissue-integration strategies. Second, an in-depth study of glia as the effector of stimulation-based therapy, especially for reconciling the time course of therapeutic effects to potential glial-mediated underlying mechanisms (for instance, the slowly-emerging DBS outcomes that evolve over days and weeks²⁷⁰, or the stimulation-induced depression of neuronal excitability⁵⁵). Third, the heterogeneity of glial responses, on the cellular scale (types and subtypes of glia, and their individual roles) and on spatiotemporal scales (the impacts of time post-implantation and the affected region relative to the electrode). Fourth, the development of electrodes for the seamless integration of clinical devices into brain tissue, including the identification of materials that are sufficiently stiff to allow for precise surgical placement and have the necessary balance of mechanical, chemical and electrical properties to reduce the inflammatory response and chronic gliosis (**Fig. 2.6**). Performance variability is a broad, on-going challenge for both recording and stimulation applications in the research and clinical use of implanted electrode arrays, and understanding the biological underpinnings of inconsistent outcomes will inform the

development of improved neuroprosthetic and neuromodulatory devices. As a regulator of the structural and functional remodeling of neuronal networks, glia are emerging as a dynamic, active determinant of device integration and performance.

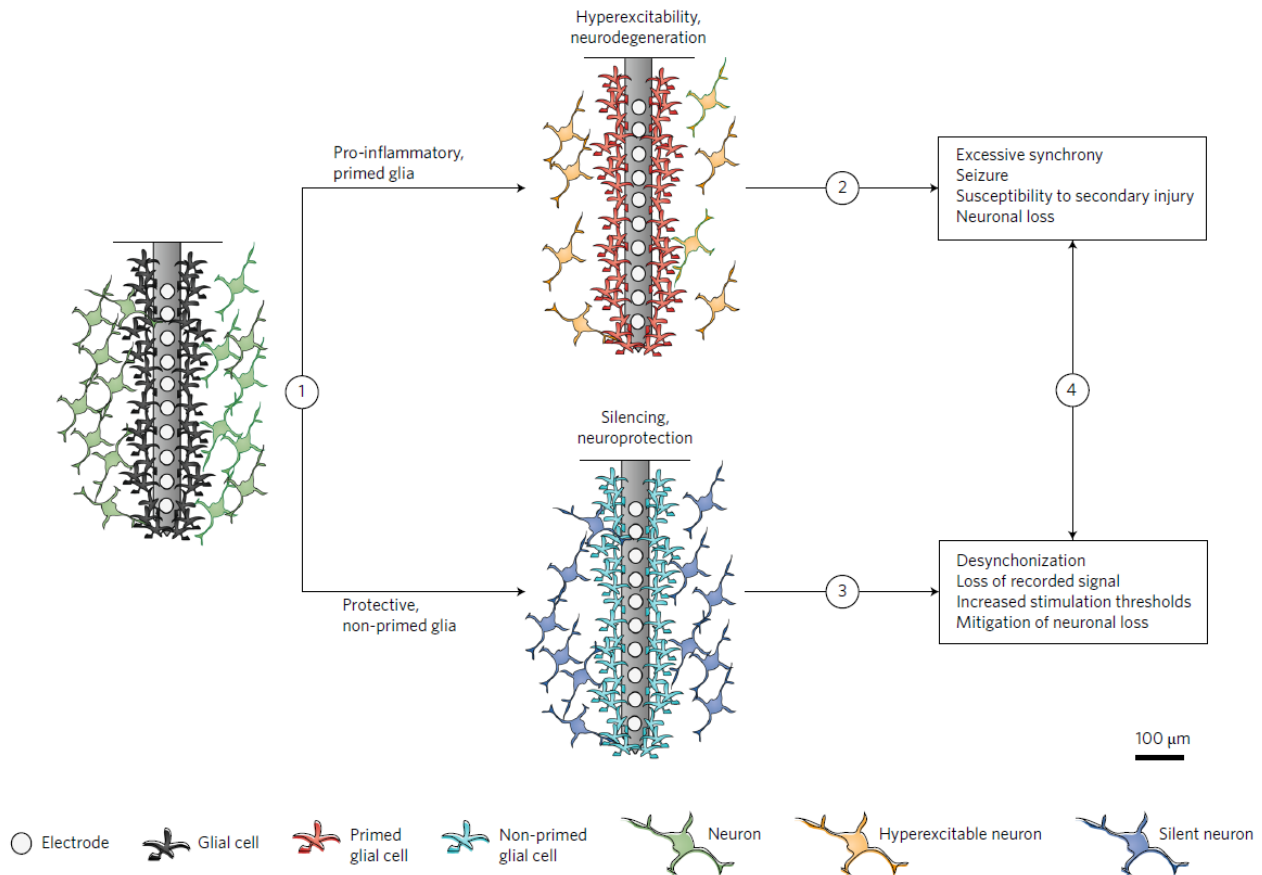


Figure 2.8 | Opportunities for further enquiry in biology. (1) The factors responsible for the ‘tipping point’ between reactive and non-reactive glial states, and the implications of glial priming on the safety of high-density arrays and of multiple implant strategies; (2) The contribution of hyperexcitability to neuronal loss and recorded signal quality, and the underlying relationship with a primed glial state; (3) Glial-mediated neuronal silencing surrounding implants, and the relationship to recorded signals and stimulation thresholds; (4) The relationship between device performance and the time course of glial effects, for insights into the sources of performance variability, plasticity, and placebo effects of device insertion, as well as therapeutic effects and side effects in a broad range of MEA applications.

Acknowledgments

J.W.S. was supported by National Institutes of Health (NIH) 1R21NS094900, T.D.Y.K. was supported by NIH 1R01NS094396, K.A.L. was supported by The Grainger Foundation, and E.K.P. was supported by NIH 1R21NS094900 and 5R03NS095202. The authors thank J. Eles for assistance collecting in vivo imaging data (Fig. 2.2a), D. Thompson and S. Yandamuri for assistance collecting data presented in Fig. 2.3, and M.-C. Senut of Biomilab, LLC, for providing feedback. Co-authors included Kip Ludwig and TK Kozai.

CHAPTER 3 | FUNCTIONAL REMODELING OF SUBTYPE-SPECIFIC MARKERS SURROUNDING IMPLANTED NEUROPROSTHESES

Abstract

Microelectrode arrays implanted in the brain are increasingly used for the research and treatment of intractable neurological disease. However, local neuronal loss and glial encapsulation are known to interfere with effective integration and communication between implanted devices and brain tissue, where these observations are typically based on assessments of broad neuronal and astroglial markers. However, both neurons and astrocytes comprise heterogeneous cellular populations that can be further divided into subclasses based on unique functional and morphological characteristics. In this study, we investigated whether or not device insertion causes alterations in specific subtypes of these cells. We assessed the expression of both excitatory and inhibitory markers of neurotransmission (vesicular glutamate and GABA transporters, VGLUT1 and VGAT, respectively) surrounding single-shank “Michigan”-style microelectrode arrays implanted in the motor cortex of adult rats using quantitative immunohistochemistry. We found a pronounced shift from significantly elevated VGLUT1 within the initial days following implantation to relatively heightened VGAT by the end of the 4-week observation period. Unexpectedly, we observed VGAT positivity in a subset of reactive glia during the first week of implantation, indicating heterogeneity in early-responding encapsulating glial cells. We coupled our VGLUT1 data with the evaluation of a second marker of excitatory neurons (CamKii α); the results closely paralleled each other and underscored a progression from initially heightened to subsequently weakened excitatory tone in the neural tissue proximal

to the implanted electrode interface (within 40 microns). Our results provide new evidence for subtype-specific remodeling surrounding brain implants which inform observations of suboptimal integration and performance.

Introduction

While changes in the densities of broad cellular classes surrounding devices have been described (i.e., neurons, astrocytes, and microglia), each of these cell types encompass multiple unique *subtypes* which may be differentially affected by injury. Neural circuitry in the brain is extraordinarily complex, where individual cells may receive thousands of connections from other cells, and neurons embody a remarkable diversity of form and function^{46,271}. In the cerebral neocortex, each of six functionally distinct lamina (layers I-VI) are populated by specific neuronal subtypes with unique morphologies and functional phenotypes. Cellular specification is driven by the expression of distinct transcription factors in concert with contextual cues during development^{167,272-275}. There are two major classes of neurons in the central nervous system (CNS), excitatory and inhibitory, which populate neocortex in a ~4:1 ratio²⁷⁶. Each of these classes can be delineated further into distinct subclasses of excitatory projection neurons and inhibitory interneurons based on physiological and anatomical criteria⁴⁶. Likewise, subtypes of astrocytes in the CNS are defined by differences in gene expression, function, and reactive states^{81,277}. Upon injury, astrocytes assume reactive phenotypes based on topographical gradients of extracellular signals, resulting in spatially patterned inflammatory and neuroprotective functions⁸³. Therefore, reactive heterogeneity is regulated as a function of distance and time from a source of injury⁸³. Since astroglial signaling is known to influence neuronal network dynamics in the uninjured brain^{168,278,279}, glial reactivity and remodeling of astrocyte-neuronal networks following device implantation have the potential to affect local signaling characteristics^{83,139,280,281}.

When neurons are lost and glia are gained surrounding devices, it is inevitable that the resulting local neuronal network is reorganized. Since it is increasingly appreciated that preferential activity of not only specific cellular types—but also subtypes—underlie certain behaviors, frequency bands of oscillation, pathophysiological states, and consequences of neurostimulation, a shift in cellular identity could influence the nature of recorded signals and/or the efficacy of neuromodulation^{282,283}. For example, heightened gamma band activity has been associated with sensory perception and can be driven by fast-spiking interneurons^{282,284}. While controversial, some observations suggest that glia are contributing cellular effectors of deep brain stimulation therapy^{93,100,158}. To overcome the tissue response to recording electrodes and more effectively harness the therapeutic potential of stimulating devices, it will be useful to understand remodeling surrounding electrodes on a cell type-specific basis.

Here, we investigated the remodeling of subtype-specific markers associated with either neuronal or glial cells surrounding microelectrode arrays implanted in the rat brain. We quantitatively analyzed excitatory (VGLUT1) and inhibitory (VGAT) synaptic markers to investigate preferential shifts in neuronal input at the neural interface. Unexpectedly, we identified a subpopulation of reactive glia expressing an inhibitory synaptic marker (VGAT+) proximal to the electrode surface. We quantitatively assessed a marker of excitatory somata surrounding devices (CamKii α), where progressive loss of CamKii α positivity paralleled the VGLUT1 result. Overall, our results reveal new observations of functional remodeling surrounding devices, where a shift toward reduced excitatory and increased inhibitory expression was evident.

Results

Shift in excitatory/inhibitory (VGLUT1/VGAT) expression surrounding devices over time

Our data demonstrated a progressive shift from VGLUT1 to VGAT predominance at the device interface over time (**Fig. 3.1**). VGLUT1 was significantly greater at 3 days than VGAT (** $p \leq 0.001$) (**Fig. 3.1A**), no significant difference was observed between the two markers at 7 days ($p > 0.05$) (**Fig. 3.1B**), and VGAT was significantly greater than VGLUT1 at 28 days (* $p \leq 0.05$) (**Fig. 3.1C**). The results indicate an overall “switching” of interfacial VGLUT1 to VGAT expression over time. These effects were based on comparisons of expression within the first 40 μ m of the device interface (the region in which unit activity is easily detected, 35,285).

Expression intensity was most elevated early on at the device interface, and decreased overall as a function of time. Both VGLUT1 and VGAT were significantly greater at 3 days compared to 7 days (** $p \leq 0.001$), and both VGLUT1 and VGAT were significantly greater at 7 days compared to 28 days (** $p \leq 0.001$).

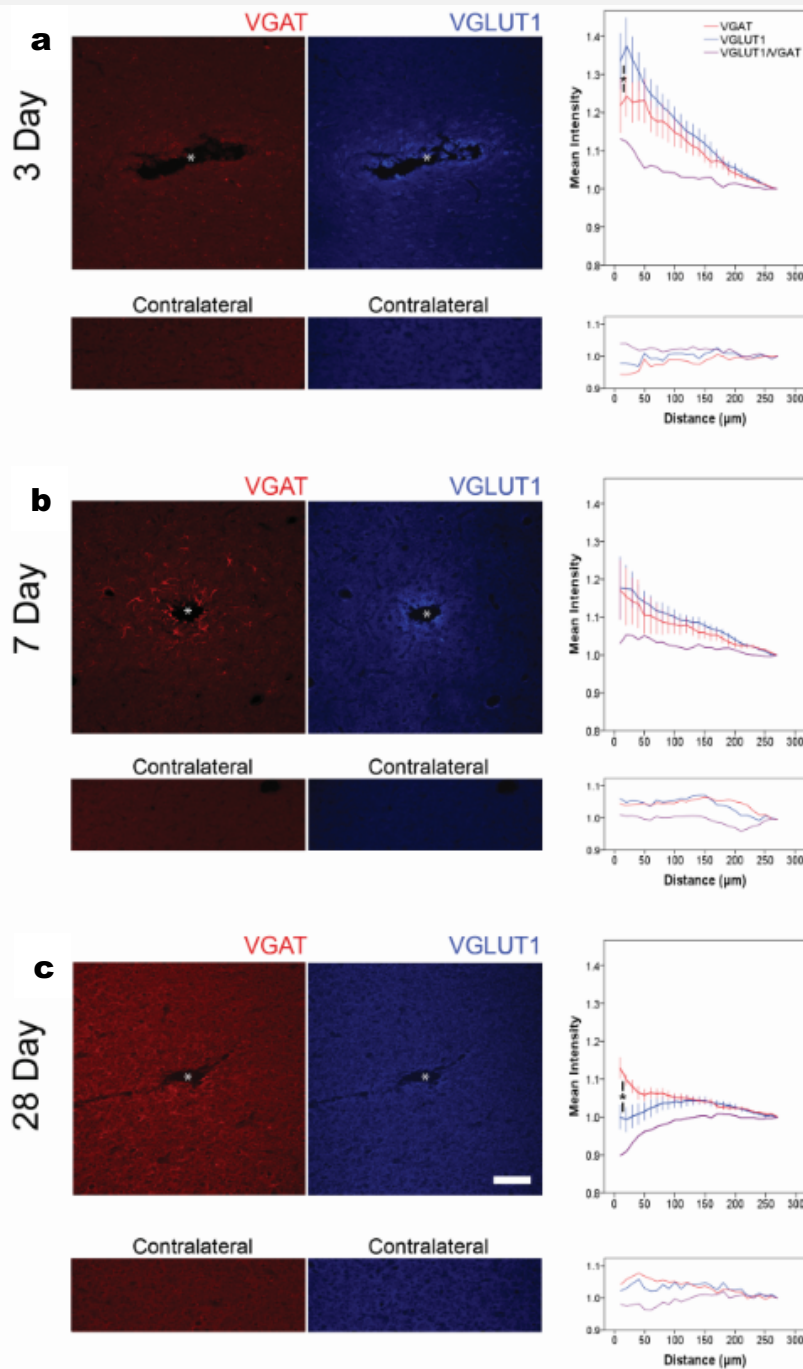


Figure 3.1 | Shift in VGLUT1/VGAT expression surrounding devices over time **A)** Within the first 40 μ m, VGLUT1 and VGAT are both significantly elevated (** $p \leq 0.001$) and VGLUT1 intensity is significantly greater than VGAT (** $p \leq 0.001$) ($n=12$ sections across 3 rats). **B)** VGLUT1 and VGAT are both significantly elevated within the first 40 μ m (** $p \leq 0.001$), with no significant difference between VGLUT1 and VGAT ($n=16$ sections across 4 rats). **C)** VGAT intensity is significantly elevated (* $p \leq 0.05$) and significantly greater than VGLUT1 (* $p \leq 0.05$) in the first 40 μ m ($n=19$ sections across 4 rats). Companion uninjured contralateral images are shown below each injury image for within-section visual comparison. White asterisks (*) denote injury sites. Scale bar = 100 μ m. Mean \pm standard error is shown. Figure reproduced¹⁴⁷.

A reactive glial subtype contributes to elevated VGAT positivity

Based on our quantified result of a shift toward decreasing excitatory and increasing inhibitory tone surrounding devices over time, we investigated the potential cellular source of these effects. Unexpectedly, VGAT expression was observed in a subpopulation of GFAP+ glia that appeared to migrate toward the device over time (**Fig. 3.2**). At 3 days, reactive VGAT+ glia were observed most distal to the interface, where only a subpopulation of GFAP+ cells were colocalized with VGAT (**Fig. 3.2A**). After 7 days, reactive VGAT+ glia were greatest in number, colocalized nearest the device interface, and distally scarce (**Fig. 3.2B**), suggesting a migratory pattern over time. VGAT+ glia were scarce but faintly observable at the device interface by 28 days (**Fig. 3.2C**). These observations suggest that reactive VGAT+ glia migrate to the device interface over the first 7 days following insertion, where their expression is mostly diminished/absent by 28 days.

Progressive loss of VGLUT1 is coupled to loss of CamKii α + neurons

To investigate a potential source of reduced excitatory synaptic transmission over time, we assessed the expression of a marker known to be preferentially expressed in excitatory somata in neocortex (CamKii α , ²⁸⁶). In parallel with the quantified VGLUT1 loss (**Fig. 3.1**), CamKii α density significantly declined from 3 days compared to both 7 and 28 days (* $p \leq 0.05$) (**Fig. 3.3**).

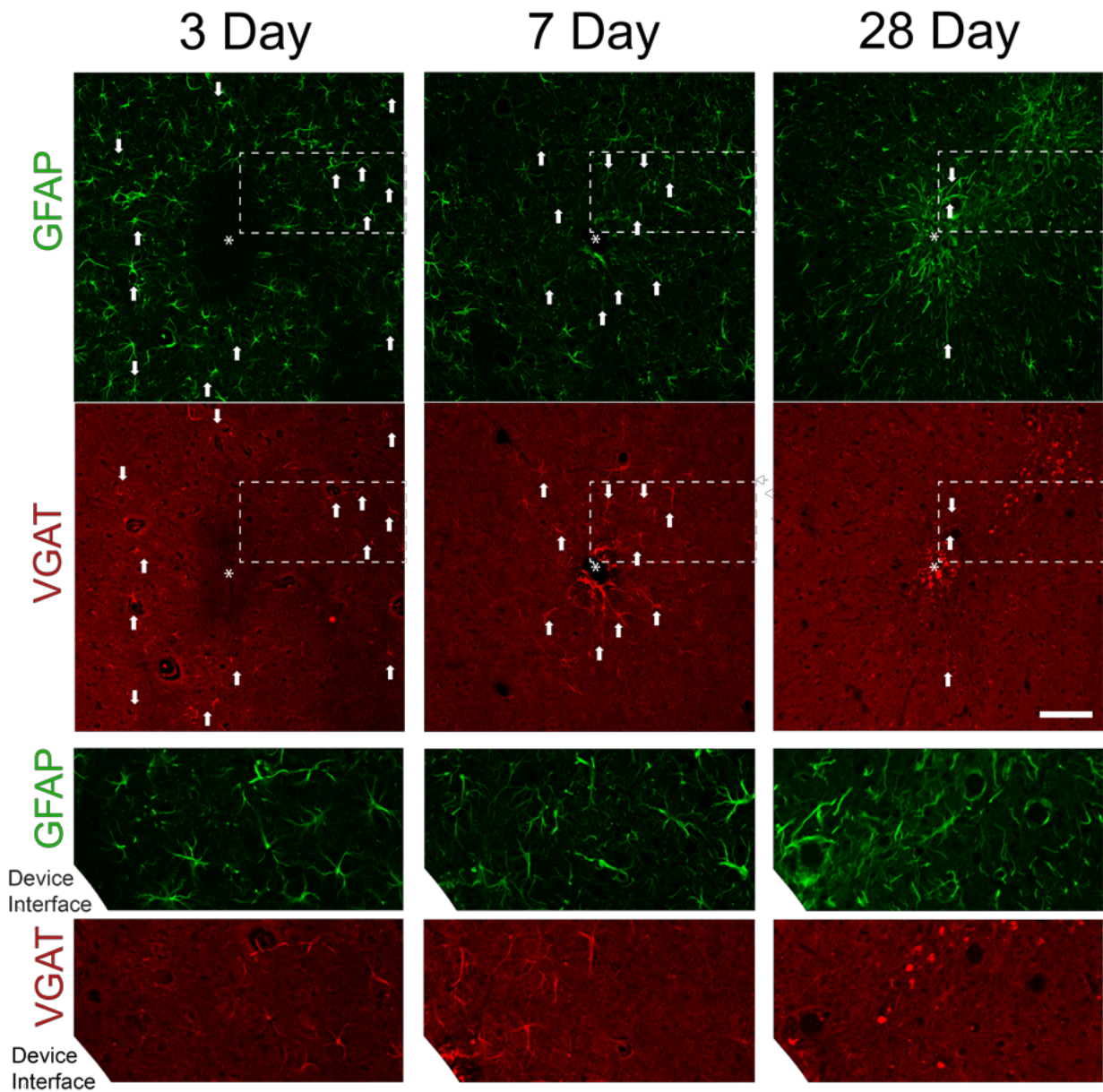


Figure 3.2 | Reactive glial subtype contributes to elevated VGAT over time **A)** At 3 days, VGAT+ glia first emerge distal to the device interface, where arrows indicate examples of GFAP+/VGAT+ cells, **B)** By 7 days, VGAT+ glia have encased the device interface, **C)** After 28 days, VGAT+ glia are scarce, with faint exceptions indicated by arrows. White asterisks (*) denote injury sites. Scale bar = 100 μ m. Figure reproduced¹⁴⁷.

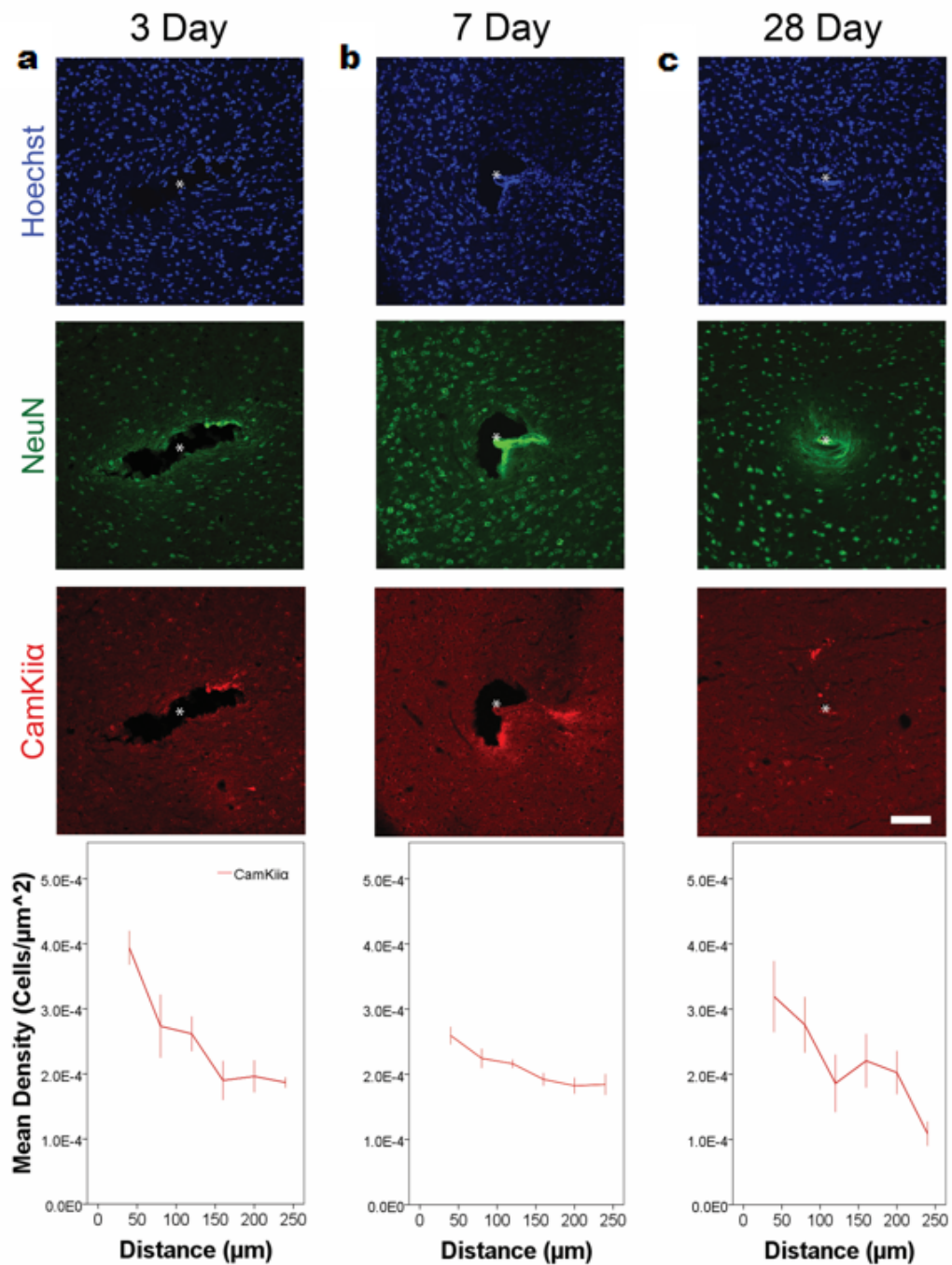


Figure 3.3 | Progressive loss of VGLUT1 is coupled to loss of CamKii α + neurons. CamKii α expression is significantly more robust at (A) 3 days (n=4 sections across 2 rats) compared to both (B) 7 days (**p \leq 0.001) (n=10 sections across 3 rats) and (C) 28 days (*p \leq 0.05) (n=9 sections across 2 rats). These results coincide with initial elevation in VGLUT1 at 3 days followed by a progressive decline over 28 days (Fig. 3.1). White asterisks (*) denote injury sites. Scale bar = 100 μ m. Mean \pm standard error is shown. Figure reproduced¹⁴⁷.

Discussion

Glial encapsulation and neuronal loss are commonly observed surrounding microelectrode arrays implanted in brain tissue (DBS leads, “Michigan” arrays, Utah arrays, etc.)^{34,76,287}. Many aspects of both the underlying mechanisms and consequences of this tissue response remain unclear, particularly regarding the cause-effect relationship between histological and electrophysiological outcomes^{30,121,287}. In this study, we investigated whether or not the tissue response differentially affects specific glial and neuronal *subclasses* in addition to known impacts on broader cellular classes (namely, neurons and astrocytes). Our data reveal new observations of a short-term elevation of excitatory markers followed by a sustained increase in inhibitory markers in the neuropil proximal to the device surface, indicating a shift in excitatory/inhibitory tone at the electrode interface over time. The results suggest a novel potential physiological contributor to the instability in recorded signal quality and stimulation thresholds which counteract effective long-term MEA function^{30,121,287}.

The injury caused by device insertion into brain tissue results in significant increases in glutamate in the extracellular environment²⁸⁸ where sources may include mechanically disrupted cellular membranes and reactive astrocytes^{83,98,158}. Our results demonstrate a transient increase in the predominant vesicular glutamate transporter expressed in the adult neocortex, VGLUT1²⁸⁹, within the first 40 microns of the device interface during the initial 3 days post-implantation (**Fig. 3.1**). Since increased VGLUT1 expression is associated with elevated extracellular glutamate²⁹⁰, the data suggest a novel vesicular source of excessive glutamate accumulation following the implantation of electrode arrays in the brain. A similar transient increase in glutamatergic transporter expression was reported previously in a

rodent stroke model, where an increase in cortical VGLUT1 expression 3 days after middle cerebral artery occlusion was followed by a decrease at the 1 week time point²⁹¹. The authors speculated that increased VGLUT1-associated glutamate release may be adaptive for recovery of network activity and/or promotion of neurogenesis following ischemic injury. Likewise, it is possible that elevated VGLUT1 could play similar compensatory role(s) to alleviate the trauma caused by device insertion. However, the stimulation of reactive gliosis is a known consequence of excessive glutamate release following brain injury^{83,98}; therefore, acute VGLUT1 elevation could act as an initial beacon for attracting encapsulating glia to devices following implantation.

The acute, localized increase in VGLUT1 relative to VGAT, followed by a reversal of these effects at chronic time points, suggests a shift from enhanced excitatory to inhibitory tone surrounding devices over time. When comparing expression within the first 40 microns of the device surface (the region in which unit activity is easily detected^{35,285}), a gradual switching from VGLUT1 to VGAT predominance is evident (3 days: VGLUT1>VGAT, 1 week: VGLUT1=VGAT, 4 weeks: VGAT>VGLUT1) (**Fig. 3.1**). The progressive increase in inhibitory neurotransmission would likely favor reduced excitability following an initial period of heightened activity within the recordable radius of an implanted electrode array (**Fig. 3.1**). We coupled our observations of VGLUT1 staining with the quantitative assessment of a marker associated with excitatory neuronal somata (**Fig. 3.3**)^{286,292}. The results indicated a transient elevation followed by a progressive decline in Camkii α positivity which paralleled the VGLUT1 result, further supporting a net loss of excitatory tone in the tissue surrounding

neuroprostheses over time and potentially suggesting a localized somatic, versus a long-range projection, source of the effect.

In comparison to VGLUT1 reactivity, the source of VGAT was unexpectedly complex, where we observed expression in a subset of GFAP+ astrocytes in addition to the expected observation of peri-somatic puncta in neurons (**Fig. 3.2**). Further, we observed an apparent migration of VGAT+ glia toward the device during the timeframe coinciding with peak reactivity³³ (**Fig. 3.2**). There is a growing body of evidence supporting vesicular neurotransmitter release from astrocytes²⁷⁹, although astrocytic vesicular GABA release remains more controversial^{279,293–297}. Whether or not the VGAT+/GFAP+ cells serve as an active GABA source is unknown, although it is tempting to speculate that the observation of a GABAergic marker in glia may allude to an inhibitory influence of reactive astrocytes on neuronal network activity, which has been shown elsewhere²⁹⁸. Nonetheless, it is clear that VGAT labels a distinct subpopulation of glia within surrounding brain tissue, delineating a reactive, apparently migratory phenotype from the broader GFAP+ population (**Fig. 3.2**). The identification of a new marker to distinguish reactive from non-reactive astrocytes in the early days following device implantation is of practical significance for identifying the origin of these cells, assessing their unique physiological characteristics, and developing treatments tailored to affect reactive cells specifically and improve tissue-device integration in a targeted manner.

Our study identified several novel effects of Michigan-style devices implanted in the brain on functional remodeling of surrounding brain tissue which provide opportunities for

further inquiry. Significant localized effects on markers of synaptic transmission were observed which indicated a gradual shift in excitatory to inhibitory tone over time. The potential impacts on effective tissue-electrode communication will be a subject of a future study, where we hypothesize that increased local inhibition will have a negative impact on the detection of recorded signals. The origin and physiological function of VGAT+ glia will be explored further, particularly in regard to long-term signal detection. Finally, it will be important to understand whether or not the effects observed here are generalizable to the broader array of electrode configurations, particularly considering the recent introduction of novel materials and architectures into devices designed to improve tissue integration. The success of next-generation brain implants will depend on the ability to access large numbers of neurons simultaneously with high spatiotemporal resolution, presenting significant challenges for device design and biocompatibility. Our work adds to the growing understanding of the mechanisms governing tissue-device interactions, unmasking effects on markers of synaptic transmission and glial subtypes and informing future strategies to improve long-term biointegration.

Methods

Surgery

Adult female Sprague-Dawley rats (SAS, 224-249g, Charles River, Wilmington, MA) were implanted with a single-shank probe using a surgical procedure similar to previous reports (Purcell et al. 2009b). Animals were anesthetized using isoflurane, with ~2.0% isoflurane maintained throughout surgery. A 2x2mm craniotomy was performed using a hand-drill to expose the primary motor cortex (+3.0 mm AP, 2.5 mm ML, -2.0 mm DV from Bregma), where the dura was resected and a non-functional, single-shank silicon microelectrode array (A1x16-3mm, NeuroNexus Technologies) was inserted using a stereotaxic arm. A dental acrylic head cap was anchored to three bone screws. Bupivacaine and Neosporin were topically applied around the head cap to minimize discomfort and prevent infection, and meloxicam was administered for pain management during the recovery period. Rats were free of infectious agents and parasites (Charles River VAF) and singly housed in a university animal facility with a 12-hour light/dark cycle and constant access to food and water. All surgical procedures were approved by the Michigan State University Animal Care and Use Committee.

Histology

At predetermined time points (3, 7, and 28 days), animals were deeply anesthetized using sodium pentobarbital and transcardially perfused with PBS followed by 4% PFA. Brains were explanted, postfixed in 4% PFA overnight at 4°C, and cryoembedded following sucrose protection. Immunohistochemistry followed previously reported methods³⁰, where 20µm-

thick cryosections were hydrated in PBS, blocked in 10% normal goat serum (NGS) in PBS and subsequently incubated with primary antibodies overnight at 4°C. The following day, sections were rinsed with PBS, incubated with secondary antibodies, and coverslipped with ProLong Gold antifade reagent (Molecular Probes by Life Technologies, Carlsbad, CA). Antibodies were diluted in a solution of 5% NGS and 0.3% Triton X-100 in PBS. Primary antibodies included guinea pig anti-vesicular glutamate transporter 1 (VGLUT1, 1:500, Millipore Corporation, Billerica, MA), mouse anti-Ca²⁺/calmodulin-dependent protein kinase II α (CaMKII α , 1:100, Santa Cruz Biotechnology, Inc., Santa Cruz, CA), rabbit anti-vesicular GABA transporter (VGAT, 1:400, Millipore Corporation, Billerica, MA), mouse anti-neurofilament heavy polypeptide (NF, 1:500, Abcam, Cambridge, MA), mouse anti-neuronal nuclei (NeuN, 1:500, Millipore Corporation, Billerica, MA), and mouse anti-gial fibrillary acidic protein (GFAP, 1:400, Millipore Corporation, Billerica, MA). Secondary antibodies included goat anti-mouse IgG (H+L) alexa fluor 488 conjugate (1:200, Thermo Fisher Scientific, Waltham, MA), goat anti-rabbit IgG (H+L) alexa fluor 594 conjugate (1:200, Thermo Fisher Scientific, Waltham, MA), and goat anti-guinea pig IgG (H+L) alexa fluor 405 (1:200, Abcam, Cambridge, MA). In selected sections, nuclei were counterstained with 1 μ g/mL Hoechst (Molecular Probes by Life Technologies, Carlsbad, CA). An Olympus Fluoview 1000 inverted confocal microscope was used to image samples with a 20x PlanFluor dry objective (0.5NA), where settings were optimized for individual images as previously described²³².

Image Analysis

Images were analyzed using a modified MATLAB script adapted from Kozai et. al (Kozai et al. 2014). Mean intensity was calculated for each individual image, and then averaged across all tissue sections for each time point. The imaged tissue section was divided into bins radiating from the center of the injury site. The fluorescence intensity within each bin was normalized using the corners of the image as a reference.

Holes in the tissue, such as from vasculature, can reduce the average intensity of the bin. To prevent this, a background noise intensity threshold was calculated and any bins that were dimmer than one standard deviation below this threshold were considered holes and removed from calculation. Originally, the script allowed only rectangular bins to be made; however, this resulted in either the tissue at the electrode-tissue interface being excluded from calculation or some of the injury site being included in calculation. We modified the script so that the bin outline could be a user-defined trace (See Supplementary Material). The subsequent concentric bins were then created by calculating a linear line from the center to each point on the bin outline and shifting those points 10 μ m along that line.

Cell counting was done manually within the MATLAB script (See Supplementary Material). The image would appear on the screen with an outline of the current bin area. If the majority of the cell was within the bin, that cell was considered to belong to that bin. Clicking on the cell would leave a marker to indicate which cells had already been counted. Additionally, the script would automatically keep track of how many times the mouse was clicked, giving us the number of cells in the bin. In the case of CamKii α , the cells were at times

not as discernible from the background as other stains. To help with identification, an image of CamKii α overlaid with NeuN was used as a reference. Because there is overlap between CamKii α and NeuN staining, if what is suspected to be a cell in the CamKii α image is also stained by NeuN in the reference image then it is more likely a cell is actually present.

Statistical Analysis

For VGLUT1/VGAT/NF expression, a total of 11 animals were used across 3 day (n=3), 7 day (n=4) and 28 day (n=4) time points. An average of four brain sections were assessed per animal. Mean intensity was obtained for each color channel as a function of distance from the device interface using 10 μ m bins.

For assessing shifts in neuronal density (NeuN+/Hoechst+) / non-neuronal density (NeuN-/Hoechst+) ratio (ND/NND) and CamKii α density over time, a total of 7 animals were used across 3 day (n=2), 7 day (n=3) and 28 day (n=2) time points. An average of four brain sections were assessed per animal. A single blinded user counted NeuN+, CamKii α + and Hoechst+ cells within 20 μ m bins from the device interface using an in-house generated MATLAB script.

Data were compiled and run through SPSS (IBM, Chicago, IL) using a linear mixed effects model to evaluate both distance and temporal effects (Purcell et al. 2009a). Results were assessed using a Fischer's Least Significance Difference method and defined as statistically significant at *p \leq 0.05 and **p \leq 0.001.

Acknowledgments

This work was supported by the National Institute of Neurological Disorders and Stroke (1R21NS094900), the Department of Biomedical Engineering, and the Department of Electrical and Computer Engineering at Michigan State University. The authors would like to thank Emily N. Smith for assistance with data analysis, Wenjuan Ma from CSTAT for assistance with statistical analysis, Melinda K. Frame from Center for Advanced Microscopy for confocal training, and Takashi D.Y. Kozai and Zhannetta Gugel for the intensity profiling MATLAB script. Co-authors included Bailey Winter and Matthew Drazin.

CHAPTER 4 | ALTERATIONS IN ION CHANNEL EXPRESSION SURROUNDING IMPLANTED MICROELECTRODE ARRAYS

Abstract

Microelectrode arrays designed to map and modulate neuronal circuitry have enabled greater understanding and treatment of neurological injury and disease. Reliable detection of neuronal activity over time is critical for the successful application of chronic recording devices. Here, we assess device-related plasticity by exploring local changes in ion channel expression and their relationship to device performance over time. We investigated four voltage-gated ion channels (Kv1.1, Kv4.3, Kv7.2, and Nav1.6) based on their roles in regulating action potential generation, firing patterns, and synaptic efficacy. We found that a progressive increase in potassium channel expression and reduction in sodium channel expression accompanies signal loss over 6 weeks (both LFP amplitude and number of units). This motivated further investigation into a mechanistic role of ion channel expression in recorded signal instability. We employed siRNA in neuronal culture to find that Kv7.2 knockdown (as a model for the transient downregulation observed at 1 day in vivo) mimics excitatory synaptic remodeling around devices. This work provides new insight into the mechanisms underlying signal loss over time.

Introduction

Charge movement across the cell membrane through ion channels enables the conduction and propagation of electrical signals that underlie neuronal communication and function¹³³. The remarkable diversity of ion channels in the mammalian brain (comprising more than 90 voltage-gated potassium channels alone) facilitates the rich repertoire of excitable properties that shape neuronal signaling to encode information along neuronal networks^{133,299}. The effective use of microelectrode arrays implanted in the brain relies on the ability to record electrical signals from single neurons and their populations over time^{27,29,300,301}. Neuronal loss and glial encapsulation are well-known consequences of implanting commonly used electrode designs^{30,34,302}, but impacts on the residual function of remaining neurons are unknown. Ion channel expression and function is highly dynamic and modulated by many factors¹³³, including changes to the surrounding environment caused by injury³⁰³⁻³⁰⁶ and inflammation^{211,307,308}. Channel modulation can impact not only the signal generation capabilities of single neurons, but also their frequencies, patterns, and waveform characteristics that underlie information encoding^{133,299}. Channel modulation can also contribute to neuronal network dysfunction (e.g., transcriptional and post-translational channel effects of cytokine exposure can result in cortical circuit hyperexcitability and epileptogenesis¹³⁹). Therefore, injury caused by device insertion could influence the signal detection of microelectrodes by modifying the firing properties and coordinated function of surrounding neurons over time.

Several lines of evidence support the notion that injury and inflammation associated with device insertion could result in changes to the structure and function of nearby neurons.

Cytokines and gliotransmitters released by reactive astrocytes have been shown to impact neuronal health (neurotoxic/protective effects^{43,47,98,309}) and function (ion channel/synaptic remodeling^{139,146,148,310}) to modify the composition, connectivity and excitability of local neuronal networks^{43,139,146,310}. Inflammatory cytokines possess neuromodulatory properties that alter ion channel expression and function in neuronal circuits that develops over acute and chronic periods of time^{139,308}. Although results vary⁴¹, general observations follow a trend from acute hyperexcitability to chronic hypoexcitability within affected neuronal networks¹³⁹. Similar trends have frequently been observed following traumatic brain and axonal injury models, where shifts in excitation/inhibition likewise occur^{39,40,311}. Interestingly, axonal damage produces transient changes in electrophysiological properties of both axotomized and surrounding intact neurons in the injured cortex³¹², where transient increases in membrane potentials ($\sim 10\text{mV}$) occurred within initial days that are of sufficient magnitude to impact the signal detection capabilities of implanted electrode arrays³⁵ (where a $\sim 10\text{mV}$ intracellular amplitude difference can equate to $\sim 70\text{uV}$ extracellular amplitude difference³⁵). The authors attributed these effects to changes in ion channel expression and function in axonal compartments (specifically, sodium channel and A-type potassium channel expression³¹²).

In this work, we have developed a platform for assessing local changes in ion channel expression surrounding implanted functional electrode arrays over time. While recognizing that neurons express a diverse repertoire of ion channels, we have chosen to initially explore four voltage-gated ion channels (Kv1.1, Kv4.3, Kv7.2, and Nav1.6) based on their roles in regulating action potential generation³¹³, firing patterns^{314–316}, and synaptic efficacy³¹⁵

(Table 1). Nav1.6 has been implicated in electrophysiological abnormalities following axonal injury³¹², where induced channel alterations have been demonstrated following axonal trauma³¹⁷, traumatic brain injury³⁰³, and exposure to inflammatory cytokines³¹⁸ that can evolve over time^{139,142,319}. Likewise, A-type potassium channels (e.g., Kv4.3/Kv4.2) have been proposed to contribute to the loss of intrinsic bursting activity surrounding axotomized neurons³¹², where expression is transiently downregulated following traumatic brain injury³⁰⁵. Upregulated Kv1.1 expression at 6-8 weeks following CNS injury³²⁰ has been shown to be a mechanism for axonal dysfunction in surviving axons, where increased K⁺ conductance was proposed to act as a shunt for blocking axonal conduction^{320,321}. Finally, Kv7.2 regulates vesicular glutamate transporter 1 (VGLUT1) expression and acts as a brake for repetitive firing³¹⁵, where our group observed changes in VGLUT1 expression surrounding implanted microelectrodes over time that motivated further investigation into a mechanistic role of this channel¹⁴⁷. Here, we report a progressive elevation in potassium channel expression coupled with a loss of sodium channel expression surrounding devices. These changes accompany a loss of signal over 6 weeks. Further, we provide insights into a mechanistic role of these ion channels in signal loss using siRNA in culture. Our study shows novel mechanisms of plasticity surrounding implanted devices that may affect their signal instability and long-term performance.

Ion Channel	Channel Type	Functional Role	Motivator
Nav1.6	Most abundant Na ⁺ channel / clustered at axon hillock	Initiating action potentials (depolarization)	Down-regulation shown to induce hypoexcitability ³²²
Kv1.1	Delayed rectifier	Setting action potential threshold / for AP down-stroke	Blocking/KO shown to induce hyperexcitability ³¹⁴
Kv4.3	A-type / inactivating	Setting inter-spike interval/firing rate	Blocking/KO shown to induce hyperexcitability ⁴²
Kv7.2	M-type	Regulating synaptic transmission / acts as a brake for repetitive firing	↓I _m (M-current) ↑excitatory synaptic density ³¹⁵

Table 4.1 | Motivation for ion channel selection.

Results

Ion channel expression evolves over time

Based on motivations described in **Table 1**, we chose to explore whether shifts in the expression of selected ion channels occurs at the interface of implanted single-shank microelectrode arrays over 6 weeks using quantitative immunohistochemistry (with time points at 1 day, 1 week and 6 weeks). Images obtained using confocal laser scanning microscopy (**Fig. 1**) were analyzed using a custom-modified MATLAB script as previously reported¹⁴⁷. Briefly, ion channel expression intensity was analyzed as a function of distance from the insertion site, where fluorescence intensity was calculated within 10um bins that were generated to extend radially from the user-defined insertion site (a total of 27 bins spanning a 270um radius). The same secondary antibody was used for all ion channels and distinct spatiotemporal patterns of expression were observed for each channel, mitigating the likelihood that non-specific background labeling contributed to our results.

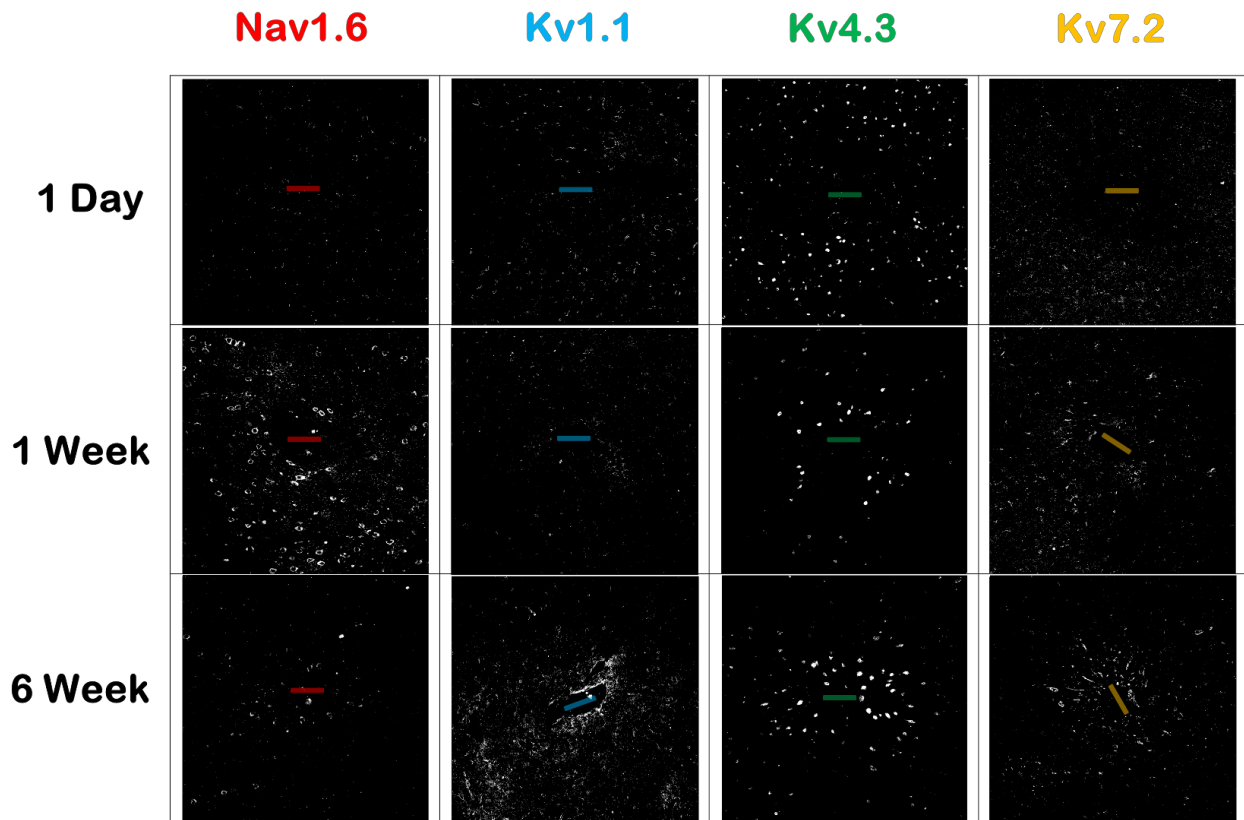


Figure 4.1 | Confocal laser scanning microscopy of ion channel expression surrounding the insertion site. Example images of ion channel expression surrounding the device tract. Immunohistochemistry reveals fluorescently stained ion channels on horizontal tissue sections taken from layer V of the primary motor cortex using the same secondary antibody. Electrodes illustrated for reference with dimensions to scale (100um x 15um).

Spatial differences in expression: To assess spatial differences between stains at each time point, we normalized intensity bins for each stain to their respective final bins as previously reported¹⁴⁷ and began with comparing the first 40um to the last 40um for statistical significance using a linear mixed effects model (**Fig. 2A**). At 1 day, we observed a significant reduction in both Kv7.2 (*) and Kv4.3 (***), followed by significant elevations in Kv7.2, Kv4.3, and Nav1.6 (***) at 1 week, and finally significant elevations in Kv7.2, Kv4.3, and Kv1.1 (***) at 6 weeks. Early local reductions in potassium channel expression at 1 day are followed by robust elevations at 1 and 6 weeks, and an elevation in Nav1.6 expression at 1 week is

subsequently reduced by 6 weeks. The results reveal a progressive increase in potassium channel expression coupled with a reduction in sodium channel expression surrounding devices over 6 weeks.

Next, we compared the first 40ums between channels at each time point for statistical significance, as depicted in **Fig. 2B**. Although represented with bar graphs for visual ease, these results still incorporated distance-related effects using the same mixed model in Fig. 2A (each bar represents the averaged value for the first 40um of the given stain). At 1 day, both Nav1.6 and Kv1.1 were statistically different from Kv7.2 (*) and Kv4.3 (***), followed by significant differences between all ion channels at 1 week (***). At 6 weeks, Nav1.6 was significantly different from all other ion channels (***) and Kv1.1 was significantly different from both Kv7.2 and Kv4.3 (***) (**Fig. 2B**). The results support a shift toward a decrease in sodium channel expression and an increase in potassium channel expression over the chronic 6-week time course.

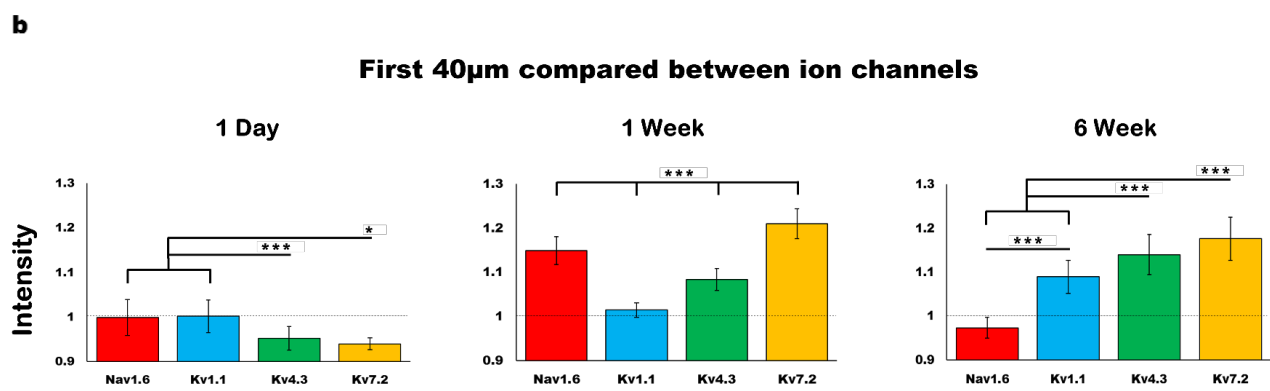
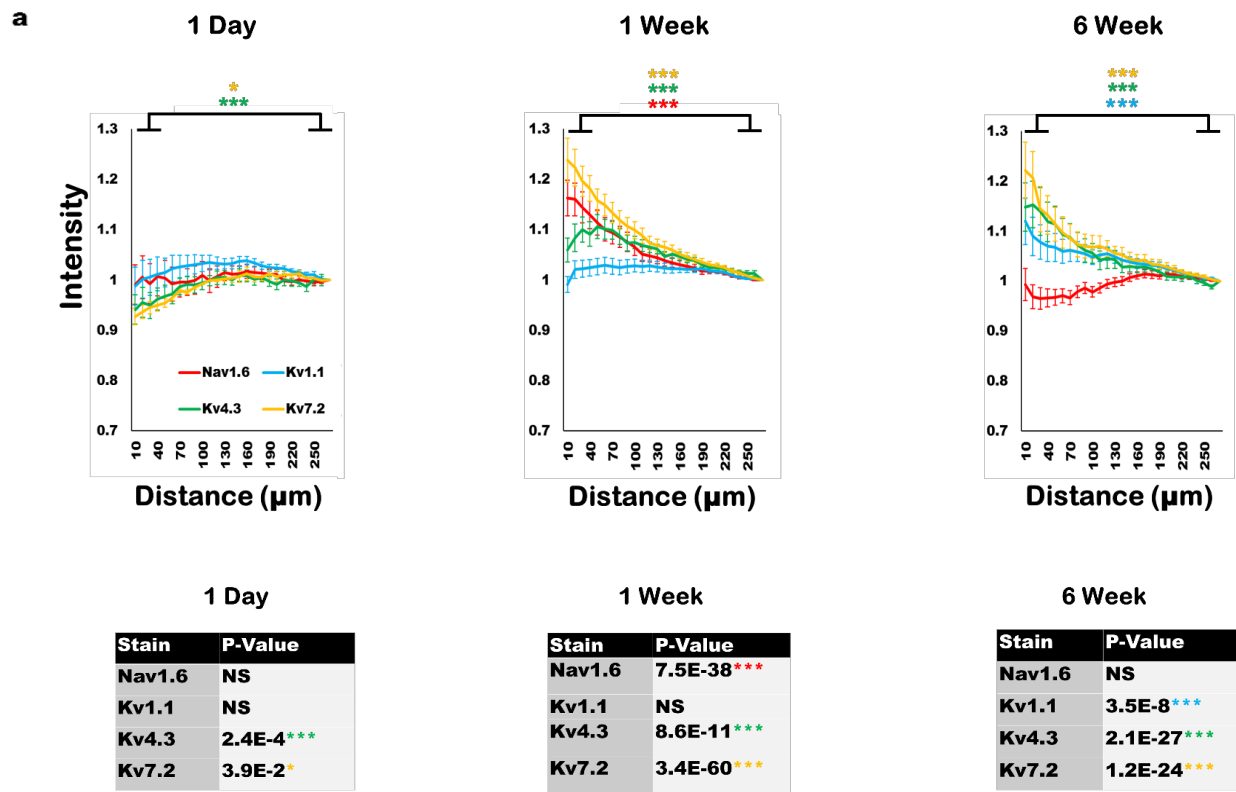


Figure 4.2 | Spatial differences in expression at each time point: Progressive increase in potassium channel expression is coupled with a reduction in sodium channel expression over 6 weeks. A) Averaged intensity from ion channel expression (normalized to final bin) revealed an increase in potassium channel expression and a loss of sodium channel expression over 6 weeks (p-values comparing 0-40µm and 230-270µm depicted). **B)** Significance compared between 0-40µm of each ion channel. Significance depicted as * $p < 0.05$ and *** $p < 0.001$. "NS" denotes non-significance. Standard error bars depicted in both panels. For each ion channel, there was an average of 7 devices and 21 tissue sections analyzed per time point.

Temporal differences in expression: To investigate temporal differences in expression levels, we normalized 1 and 6 week expression values to 1 day expression values (bin-for-bin) and displayed the results as a relative percentage change (**Fig. 3**). To quantify temporal shifts, we calculated the area under the curve to assess the relative percentage change for the total area for each ion channel (**Fig. 3B**). At 1 week, the total integrated area revealed a relative decrease in Nav1.6 (-12%), and a relative increase in Kv1.1, Kv4.3 and Kv7.2 (94%, 175%, and 255%, respectively). At 6 weeks, the total area showed a greater relative decrease in Nav1.6 (-154%), and a sustained relative increase in Kv1.1, Kv4.3 and Kv7.2 channels (98%, 97% and 180%, respectively).

Since these total values did not appear to represent the interfacial differences observed (**Fig. 3A**), we further segmented the surveyed distance into two distinct regions to assess temporal shifts in expression levels within the estimated radius generating detectable single unit (0-130um)³⁵ or LFP-only (140-270) activity (**Fig. 3A**). These distances were chosen based on the seminal work by Henze et. al, which determined the distances capable of producing sufficient amplitude for spike detection and clustering³⁵. The results indicate variability in the time course of ion channel expression surrounding devices. At 1 week, the integrated area for the “unit” region revealed a relative increase in Nav1.6 (+47% integrated area), Kv1.1 (+52%), Kv4.3 (+132%), and Kv7.2 (+208%), while the integrated area for the “LFP” region revealed a relative decrease in Nav1.6 (-56%) and increase in Kv1.1 (+39%), Kv4.3 (+38%), and Kv7.2 (+40%). At 6 weeks, the “unit” region showed a decrease in Nav1.6 (-81%), and increase in Kv1.1 (+73%), Kv4.3 (+110%), and Kv7.2 (+143%). The integrated area for the “LFP” region had a decrease for both Nav1.6 (-68%) and Kv4.3 (-14%), and an

increase in Kv1.1 (+22%) and Kv7.2 (+33%). Therefore, the relative shift in “unit” region Nav1.6 from elevation at 1 week to depression at 6 weeks, coupled with the sustained elevation in all Kv channels at both time points, indicates a temporal shift from hyper- to hypo-excitability within the recordable radius of the device relative to previous values.

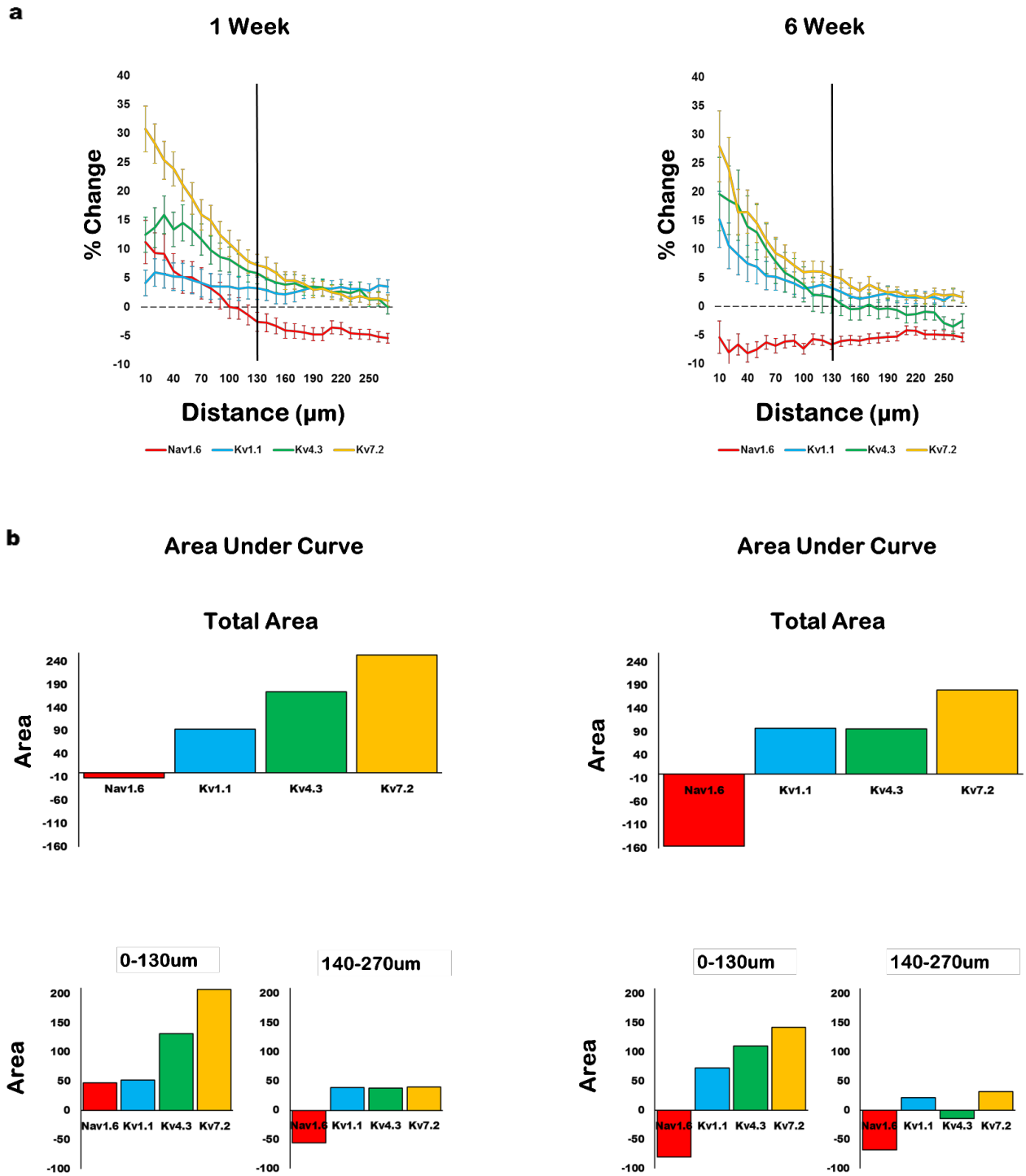


Figure 4.3 | Temporal differences in expression: Percentage change in expression relative to 1 day values corroborates progressive reduction in sodium channel expression and heightened potassium channel expression over time. A) Averaged percentage change for 1 and 6 week expression values relative to 1 day expression values with standard error bars. B) Area under the curve calculated for unit region (0-130um) and LFP region (140-270um) for both 1 and 6 week expression curves, as well as total integrated area calculated for the combined 270um radius.

Alterations in ion channel expression accompany signal loss

Bi-weekly recordings taken across subjects demonstrated a progressive decline in single unit detection over 6 weeks (**Fig. 4A**). A relatively stable LFP amplitude experienced a decline at ~3 weeks that remained at a steady state over the remaining time course (**Fig. 4A**). To further investigate the relationship between ion channel expression and signal loss, we plotted ratios to explore relative interactions (**Fig. 4B**). The results revealed that Nav1.6/Kv7.2 expression ratio may be most predictive of unit loss, as the two metrics decrease in accordance with one another over 6 weeks (**Fig. 4**), whereas Nav1.6/Kv4.3 may be most predictive of LFP amplitude (**Fig. 4**). Nav1.6/Kv1.1, however, does not appear to correspond to either of the signal metrics. These results may provide insight into novel metrics for guiding device-tissue integration.

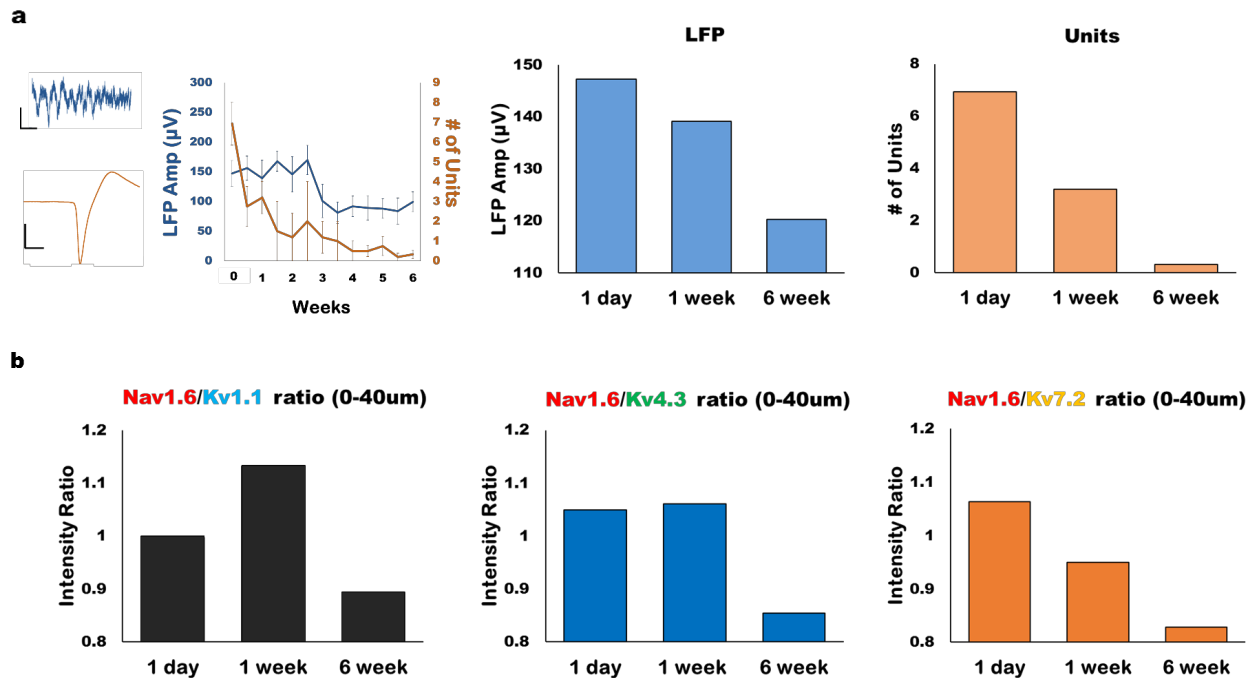


Figure 4.4 | Alterations in ion channel expression accompany decline in unit detection. A) Example of putative unit and LFP snippet from microelectrode arrays, accompanied by the quantified data (# of units and LFP amplitude) obtained from bi-weekly recording sessions across subjects (with standard error bars). Average LFP amplitude and # of units plotted on bar graphs for each time point. **B)** Averaged data within 0-40um for intensity ratios are plotted. Nav1.6/Kv7.2 intensity ratio appears to coincide closest with unit detection over the 6 week time course, whereas Nav1.6/Kv4.3 ratio appears to best correspond to LFP amplitude over 6 weeks. In contrast, Nav1.6/Kv1.1 does not appear to correspond to either signal metric.

Early observations suggest Kv7.2 expression modulates excitatory synaptic transporters

To explore whether ion channel expression may be a mechanism for shaping synaptic circuitry, we delivered siRNA in cultured rat cortical neurons to assess the consequences of Kv7.2 knockdown on excitatory synapses (to mimic transient reduction in Kv7.2 at 1 day, **Fig. 2A**). Neurons were transfected with either negative control siRNA (“scramble”) or siRNA against Kv7.2, and cells were harvested at either 3 or 7 days. RNA was collected to make cDNA, and primers for Kv7.2 (KCNQ2), VGLUT1, and PSD95 (post-synaptic density 95, an

excitatory postsynaptic marker) were used to perform qPCR. Detection levels were normalized to scramble control levels for the respective primer. We observed elevations in VGLUT1 at 3 and 7 days when comparing Kv7.2 siRNA with negative control siRNA (**Fig. 5**). We observed a robust elevation in PSD95 at 3 days that was drastically reduced by 7 days (**Fig. 5**). These results suggest that Kv7.2, in accordance with previous reports³¹⁵, regulates excitatory synaptic density (where previous reports demonstrated this relationship to VGLUT1 and PSD95 by pharmacological blockade of Kv7.2³¹⁵). While preliminary, these results correspond with the *in vivo* results of VGLUT1 upregulation at 3 and 7 days (**Fig. 5**), using data from a previous report¹⁴⁷. These results suggest that the transient reduction of Kv7.2 at 1 day *in vivo* (**Fig. 2A**) could contribute to the upregulation of VGLUT1 surrounding devices at 3 and 7 days (**Fig. 5A**)¹⁴⁷.

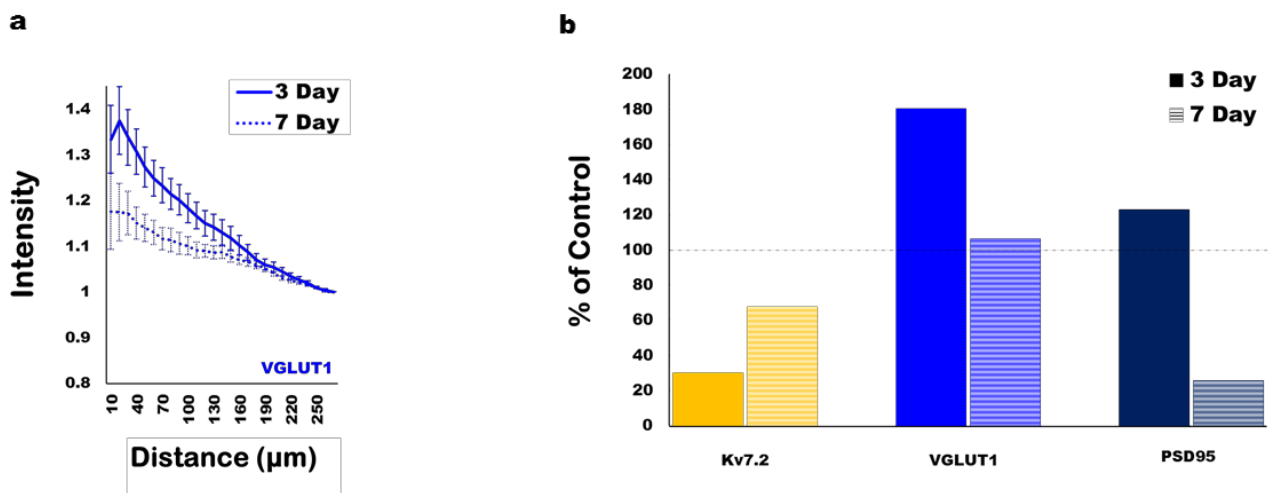


Figure 4.5 | Preliminary observations suggest Kv7.2 knockdown impacts excitatory synapses in culture. A) *In vivo* results of vesicular glutamate transporter 1 (VGLUT1), using data from a previous report¹⁴⁷, show an elevation in VGLUT1 at 3 and 7 days. **B)** *In vitro*, cortical neurons transfected with Kv7.2 siRNA show successful transient knockdown of Kv7.2, a similar trend in

Figure 4.5 (cont'd)

VGLUT elevation at 3 and 7 days compared to *in vivo* expression, and an impact on PSD95 in the form of a reduction at 7 days. Taken together, these data suggest that the transient downregulation of Kv7.2 at 1 day *in vivo* (**Fig. 2A**) may be a mechanism for the upregulation of VGLUT1 at 3 and 7 days *in vivo*. Two biological replicates were performed for the preliminary *in vitro* data.

Discussion

Neuronal loss and glial encapsulation are traditionally used as metrics to assess the biocompatibility of devices for chronic neural interfacing^{36,103,203,215,223,253,302,323-325}. However, recent work indicates that these conventional methods are insufficient to explain long-term signal quality³²⁶, where inter-day variability and progressive signal loss burden chronic recording arrays^{28,29,300,301,327}. Well-characterized alterations in ion channels and synapses following cortical injury^{41,146,148,303,305,310,317,328} and inflammation^{82,139,211,307,308,319} suggest that similar alterations may accompany implanted devices. In fact, recent studies using non-functional microelectrode arrays have revealed changes in network *connectivity* (synaptic circuitry¹⁴⁷) and *function* (calcium activity³²⁹) within the recordable radius of the device interface (~100um^{35,285}), providing evidence of local circuit remodeling that may contribute to chronic signal instability. Here, we reveal changes in the fundamental components that underlie neuronal signaling (ion channels) within the recordable radius of the device interface^{35,285}. The findings support our previously described trend from acute hyperexcitability to chronic hypoexcitability at the device interface¹⁴⁷ and expand upon it by providing a potential link between ion channel and synaptic transporter expression (**Figs. 2 & 5**)¹⁴⁷. Novel observations of ion channel expression surrounding devices revealed a progressive elevation in potassium and a reduction in sodium channel expression that temporally coincided with signal loss (**Figs. 2 & 4**). This work reveals insight into device-related mechanisms affecting the signal generation and firing properties (e.g., spike shape, firing rates, etc.) that underlie the characteristics of recorded signals.

The four ion channels were chosen based on their fundamental roles in regulating action potential generation³¹³, firing patterns³¹⁴⁻³¹⁶, and synaptic efficacy³¹⁵. Nav1.6, critical for action potential generation, has been implicated in electrophysiological abnormalities following axonal injury³¹⁷, TBI^{303,312}, and inflammation^{139,142,318,319}. In addition, electrophysiological abnormalities following axonal injury can persist in both axotomized and neighboring intact neurons³¹². The authors attributed these electrophysiological abnormalities to changes in the expression of sodium channels^{303,312,317}, where blocking sodium channel upregulation following TBI has been shown to improve outcomes by reducing excitability³⁰⁶. The authors additionally attributed abnormal activity to A-type potassium channels (with fast-activating/inactivating kinetics³³⁰), where reductions in channel expression has been shown to contribute to seizure susceptibility within initial days following TBI³⁰⁵ by increasing the excitability and firing rates of local neurons³⁰⁵. This is consistent with the transient downregulation of Kv4.3 observed at 1 day (**Fig. 2**), where the subsequent upregulation at 1 and 6 weeks may be a compensatory mechanism for counteracting hyperexcitability and epileptogenesis. Combined, these data suggest that the reduction in Nav1.6 and upregulation of Kv4.3 at 6 weeks could inhibit action potential generation and dampen excitability/firing rates within the immediate vicinity of the implant. Kv1.1 upregulation due to CNS injury³²⁰ has been shown to likewise underlie axonal dysfunction in surviving axons, where increased K⁺ conductance was proposed to act as an axonal conduction block by shunting Na⁺ current^{320,321}. This resulted in a reduction in the amplitude and area of compound action potentials for surviving axons at 6-8 weeks post-injury³²⁰. Therefore, the late upregulation of Kv1.1 observed at 6 weeks post-implantation may act as a shunt for preventing signal propagation within the recordable radius of the

device-interface. Kv7.2 produces slowly activating and inactivating subthreshold M-currents, which are responsible for regulating excitability, responsiveness to synaptic inputs, and neuronal discharge frequency³³¹⁻³³³. Kv7.2 channels located at pre- and post-synaptic terminals^{332,333} have been shown to be responsible for modulating neurotransmitter release, where M-current agonists prevent neurotransmitter release^{334,335}. Therefore, an upregulation of Kv7.2 as observed at 1 and 6 weeks can reduce excitability, firing frequency and neurotransmission. Taken together, Nav1.6 reduction and Kv4.3 upregulation can limit the probability of action potential generation and dampen excitability/firing rate, Kv1.1 upregulation can provide excess shunt current to block downstream axonal conductance, and Kv7.2 upregulation can reduce responsiveness to synaptic inputs, inhibit repetitive firing and reduce neurotransmitter release at the synapse. Therefore, the reduced excitability and propagation/transmission of signals by ion channel alterations indicates a novel source for impaired signal detection by implanted recording arrays.

Signal loss over the 6 week time course was accompanied by a progressive elevation in potassium and reduction in sodium channel expression surrounding devices (**Figs. 2, 3 & 4**). At 1 day, the local reductions in Kv7.2 and Kv4.3 in the absence of effects on Nav1.6 or Kv1.1 may reflect a hyperexcitable state, which accompanied optimal unit detection (**Figs. 2 & 4**). The shift at 1 week to elevated Nav1.6, Kv4.3 and Kv7.2 coincided with a modest reduction in unit detection (**Figs. 2, 3 & 4**), which could be more heavily affected by the dual Kv4.3/Kv7.2 upregulations. The final shift at 6 weeks to a relative loss of Nav1.6 and gain in Kv1.1 indicates a more hypoexcitable state, which coincided with the poorest unit detection (**Fig. 4**). To further investigate this relationship, ion channel intensity ratios were plotted to

compare with signal decline (**Fig. 4**). Nav1.6/Kv7.2 intensity ratio appears to temporally coincide best with unit detection. The decreased Nav1.6/Kv7.2 ratio indicates lower action potential probability from reduced sodium currents and increased sub-threshold K⁺ currents. Thus, the Nav1.6/Kv7.2 ratio could provide insight into neuronal excitability and firing rates that may contribute to unit loss. While the origin of the LFP was historically considered to largely emerge from postsynaptic potentials^{336,337}, recent work indicates that it is instead mostly composed of non-synaptic currents³³⁸. Here, the Nav1.6/Kv4.3 ratio appears to correspond best with the LFP (**Fig. 4**), which coincides with modeling data showing that the LFP is dominated by active membrane currents rather than postsynaptic conductance changes³³⁸. Kv4.3 channels are critical for producing high-frequency activity (which is achieved by their fast inactivation recovery³³⁰). Enhanced activity from Kv4.3 upregulation could increase active membrane conductances, which could in turn attenuate LFP amplitude³³⁸. Moreover, the combined upregulation with Kv1.1 and Kv7.2 channels could also contribute to increased membrane leakiness that may underlie LFP attenuation by 6 weeks³³⁸ (**Fig. 4**). Finally, these results could potentially explain electrophysiological mechanisms that underlie inter-day variability of unit detection and amplitude^{28,29,300,301,327}. For example, modeling data for ionic current contributions to extracellular action potentials demonstrate that conductance densities for heterogeneous subtypes of K⁺ currents largely underlie variability in recorded waveforms³³⁹. Thus, the fluctuations seen in Kv1.1, Kv4.3, and Kv7.2 across the 6 week time course could explain unit variability observed by chronic neural interfaces^{28,29,300,301,327}. In addition, the fluctuations in Nav1.6 could likewise explain inter-day variability in amplitude^{28,29,301,339}. Taken together, these results may provide novel metrics to assess the biocompatibility of devices for improved long-term function.

Our results must be interpreted relative to the well-known changes in cellular densities that are associated with chronically implanted electrodes, including neuronal loss and glial encapsulation^{34,36,103,203,223,302,324}. However, density changes do not fully explain inadequate performance, day-to-day variability, and signal loss accompanied by ideal histology and device integrity³²⁶. Another important consideration is the potential for expression of ion channels to occur in non-neuronal cell types. Of the four ion channels assessed, the only channel expressed in non-neuronal cells (to the best of our knowledge) is Kv1.1, which is also expressed in microglia³⁴⁰. However, because the elevation in Kv1.1 did not occur until 6 weeks, this indicates that it is unlikely that microglia are the source of Kv1.1 expression, as a stark microglial layer forms around the device within initial hours and days⁷⁵. The fact that Kv1.1 expression is stable at 1 day and 1 week across the observed 270um (**Figs. 2 & 3**), therefore, supports non-microglial labeling. In general, we observed subcellular expression patterns which were consistent with neuronal labeling. Kv1.1 appeared to be localized to axons and terminals as previously described^{314,320} (also validated with the vendor antibody³⁴¹). Nav1.6 labeling appears consistent with somatic and axonal initial segment localization^{317,322}, which aligns with previous reports using the same antibody^{342,343}. Kv4.3 labeling is consistent with somatic localization in layer V pyramidal neurons³⁴⁴, and corresponds with validated labeling in hippocampal CA3 neurons using the vendor antibody³⁴⁵. Finally, Kv7.2 labeling appears to be expressed in axons and synaptic terminals^{332,333}, where our specific antibody has been confirmed with heavy colocalization in the Nodes of Ranvier³⁴⁶. While these results will be further validated in future work, the staining appears to be consistent with neuronal localization.

Since Kv7.2 activity is known to regulate excitatory synaptic density (specifically VGLUT1 and PSD95³¹⁵), we chose to explore the impact of Kv7.2 knockdown on excitatory synapses *in vitro*. Our preliminary results revealed upregulated VGLUT1 expression at both 3 and 7 days following Kv7.2 knockdown. These outcomes suggest that the reduced Kv7.2 expression observed at 1 day *in vivo* may be a mechanism for upregulating VGLUT1 expression at 3 and 7 days *in vivo* (**Figs. 2 & 5**) as previously reported¹⁴⁷. The subsequent reduction in PSD95 at 7 days may be initiated by excitotoxicity at earlier time points. Since glutamate release scales with VGLUT1 expression²⁹⁰, excessive glutamate release (coupled with hyperexcitability) could explain the loss of PSD95 (where dramatic decreases in PSD95 have been shown in excitotoxic models³⁴⁷). Therefore, the observed trend toward hypoexcitability (**Fig. 2**) could be a reparative effort to promote neuroprotection and prevent further excitotoxicity. While acute alterations in potassium channel expression may be responsible for the shift in synaptic circuitry *in vivo*, the underpinnings responsible for the shift in ion channel expression will need to be identified in future work. Sources may include reactive signaling cascades initiated by insertion (such as the release of inflammatory cytokines that alter ion channel expression and function)^{139,302}, and strategies to modify inflammatory mechanisms have improved long-term recording quality in previous reports^{138,348}. This work may provide new insight into mechanisms of tissue reactivity surrounding devices that may contribute to signal loss.

Next-generation device designs are emerging to tune the tissue response to mitigate gliosis and neuronal loss^{36,103,203,223,323,324} in an effort to develop recording arrays with improved long-term function. However, ideal histology and device integrity based on these

traditional methods have still not guaranteed adequate recording quality³²⁶, suggesting that the principles guiding the design of improved devices may require further consideration. By assessing the fundamental components that underlie neuronal signaling (ion channels and synaptic circuitry), the innovative methods described herein may provide a more reliable indication of recorded signal quality based on their inherent contributions to neuronal signaling events. We have provided four (4) fundamental ion channels that appear to be especially informative of recording quality based on their corresponding relationships (**Figs. 2, 3 & 4**). Specifically, the number of units detected over 6 weeks appears to correspond best with the Nav1.6/Kv7.2 ratio (**Fig. 4**), and LFP amplitude appears to correspond most closely with the Nav1.6/Kv4.3 ratio (**Fig. 4**). This technique can be implemented to not only guide next-generation device designs (e.g., architecture, size, flexibility, surface chemistry/topography^{36,103,203,302,323}), but also intervention strategies (e.g., coatings, microfluidic delivery, etc.^{85,349-351}) aimed at improving long-term recording quality.

Methods

Surgery

Adult male Sprague-Dawley rats (SAS, 250-400g, Charles River, Wilmington, MA) were bilaterally implanted in the primary motor cortex with 16-channel single-shank microelectrode arrays (A1x16-3mm, 703um² site sizes, NeuroNexus, Ann Arbor, MI) using a surgical procedure similar to that previously described¹⁴⁷. Briefly, animals were anesthetized and maintained at ~2.0% isoflurane throughout surgery, whereby a 2x2mm craniotomy was performed over the primary motor cortex (+3.0mm AP, 2.5 ML), the dura was resected, and a single-shank probe was stereotaxically inserted 2mm from the cortical surface. Dental acrylic was used to secure the bilateral implants, where a bone screw was placed posterior of each device to anchor the headcap. Bupivacaine and Neosporin were topically applied around the wound to minimize discomfort and risk of infection, and meloxicam was administered for pain management. All surgical procedures were approved by the Michigan State University Animal Care and Use Committee.

Extracellular electrophysiology

Bi-weekly recording sessions were performed with isoflurane (~1-1.5%) using TDT software (Tucker Davis Technologies, TDT, Alachua, FL) by connecting a ZIF-clip headstage to a Z25 pre-amplifier (TDT) and PZ2 amplifier (TDT), to obtain 5 minute recording blocks per device per recording session. Low-pass filter for local field potential (LFP, 300Hz) and high bandpass filter for unit activity (500Hz-5KHz), yielded recording blocks that were then analyzed using a previously reported MATLAB script^{30,103} to determine the LFP amplitude

and number of units. Single units were detected based on threshold crossings (3.5 standard deviations from noise floor), where principal component analysis and fuzzy c-means clustering were then used to isolate putative units (in combination with visual inspection of mean waveforms).

Histology

Animals were deeply anesthetized using sodium pentobarbital at predetermined time points (24hrs, 1wk, 6wks) and transcardially perfused with PBS followed by 4% PFA. Explanted brains were postfixed overnight in 4% PFA at 4°C, and then sucrose protected for cryoembedding. Immunohistochemistry was performed according to previously reported methods¹⁴⁷, where 20µm-thick horizontal cryosections from depths estimated in layer V of primary motor cortex were hydrated in PBS, blocked in 10% normal goat serum (NGS) in PBS and subsequently incubated in primary antibodies overnight at 4°C. The sections were rinsed the following day with PBS, incubated with secondary antibodies, and coverslipped with ProLong Gold antifade reagent (Molecular Probes by Life Technologies, Carlsbad, CA). Antibodies were diluted in carrier solution consisting of 5% NGS and 0.3% Triton X-100 in PBS. Primary antibodies included rabbit anti-Nav1.6, -Kv1.1, -Kv4.3, and -Kv7.2 (1:200, Alomone Labs, Jerusalem, Israel). Secondary antibodies included goat anti-rabbit IgG (H+L) alexa fluor 594 conjugate (1:200, Thermo Fisher Scientific, Waltham, MA). An Olympus Fluoview 1000 inverted confocal microscope was used to image samples with a 20x PlanFluor dry objective (0.5NA), where settings were optimized for individual images as previously described²³². Images were then analyzed with a previously reported MATLAB script¹⁴⁷ adapted from Kozai et. al²³². Briefly, 10µm concentric bins were generated to

radiate concentrically from a user-drawn injury outline (a total of 27 bins spanning a 270um radius), where the pixel intensity was averaged within each bin. In this way, image intensity was analyzed as a function of distance to quantify interfacial patterns of protein expression over distance and time. Area under the curve was calculated using the *trapz* function in MATLAB to perform discrete integration on the averaged intensity data points.

Cell culture and transfection

Rat primary cortical neurons (E18, Life Technologies, Carlsbad, CA) were cultured in neurobasal medium (1mL B27, 125 uL GlutaMax in 50mL Neurobasal Media) for one week prior to transfection. For transient transfections, siRNA (Kv7.2 or negative control stealth, Life Technologies, Carlsbad, CA) was mixed with Optimem and Lipofectamine RNAiMax (according to manufacturer's instructions) and incubated overnight, followed by a complete exchange with fresh neurobasal media. Cells were harvested after 3 or 7 days post-transfection (RNEasy mini kit, Qiagen), whereby cDNA was made and amplified via qPCR with primers for GAPDH, KCNQ2 (Kv7.2), VGLUT1, and PSD95. All primer levels were normalized to GAPDH levels, and then normalized to the scramble siRNA control levels for each primer.

Statistical analysis

A linear mixed effects model was performed with SPSS (IBM, Chicago, IL) and incorporated both distance and temporal effects. Results were assessed using a Fischer's Least Significance Difference test and defined as significant at * $p < 0.05$ and *** $p < 0.001$. For each

ion channel, there was an average of 7 devices and 21 tissue sections analyzed per time point. At 1 day, there was an average of 5 devices and 12 tissue sections analyzed per ion channel stain; at 1 week, an average of 9 devices and 30 tissue sections; and at 6 weeks, an average of 7 devices and 21 tissue sections.

Acknowledgments

This work was supported by NIH grant 1R21NS094900 (NINDS), and the Departments of Biomedical Engineering and Electrical and Computer Engineering at Michigan State University. Thanks to Steven Suhr of Biomilab, LLC for *in vitro* knockdown training, Melinda Frame from Center for Advanced Microscopy for confocal training, Stefanos Palestis for assistance with signal processing, Matthew Drazin for assistance with cyrosectioning, and TK Kozai and Bailey Winter for the intensity profiling MATLAB script. Thanks to TK Kozai and Ali Mohebi for valuable feedback. Co-authors and contributors to this work include Arya Kale, Stefanos Palestis, and Steven Suhr.

CHAPTER 5 | ONGOING WORK AND FUTURE DIRECTIONS: NEW APPROACHES AND OPPORTUNITIES TO EXPLORE THE INTERFACE

Abstract

The previous chapters provide fundamental insight into major circuit changes at the interface that inform both basic-science knowledge and new strategies for improving the biointegration of brain implants. We are developing new approaches to reveal the mechanistic role of these factors in affecting recorded signals over time. These include the development and validation of innovative strategies to deliver genetic material at the interface *in vivo* to yield entirely new avenues of research with opportunities to regulate gene expression and/or introduce new genetic material to reprogram cellular identity and rewire the interfacial network. These approaches offer the unique opportunity to unmask key circuit-remodeling effects that impair device performance as well as inform the seamless integration of brain implants.

Unpacking mechanisms of plasticity: new approaches to explore the interface

In this section, we describe the development of methods to unpack mechanisms of plasticity at the device interface. This includes a brain slice preparation to reveal plasticity in the excitability and connectivity of interfacial neurons (spearheaded by Bronson Gregory with the Lee Cox Group), as well as unique strategies to deliver genetic material for perturbing the interfacial network (such as knocking down ion channels, etc.). These perturbation strategies include methods by which *in vitro* cell culture can be a useful tool to initially validate and optimize the delivery of genetic material to neural cells prior to *in vivo*

administration around devices, as well as methods to deliver genetic material to unmask plasticity *in vivo* given different requirements (single acute delivery during implantation surgery, chronic delivery packages for repeated infusions over time, etc.).

Approaches to unmask plasticity at the interface: brain slice electrophysiology

Our lab has pioneered an innovative approach to assess the electrical properties of individual neurons at the device interface in a relatively high-throughput manner (compared to traditional *blind* patching around microelectrode arrays *in vivo*³⁵) (**Fig. 5.1**).

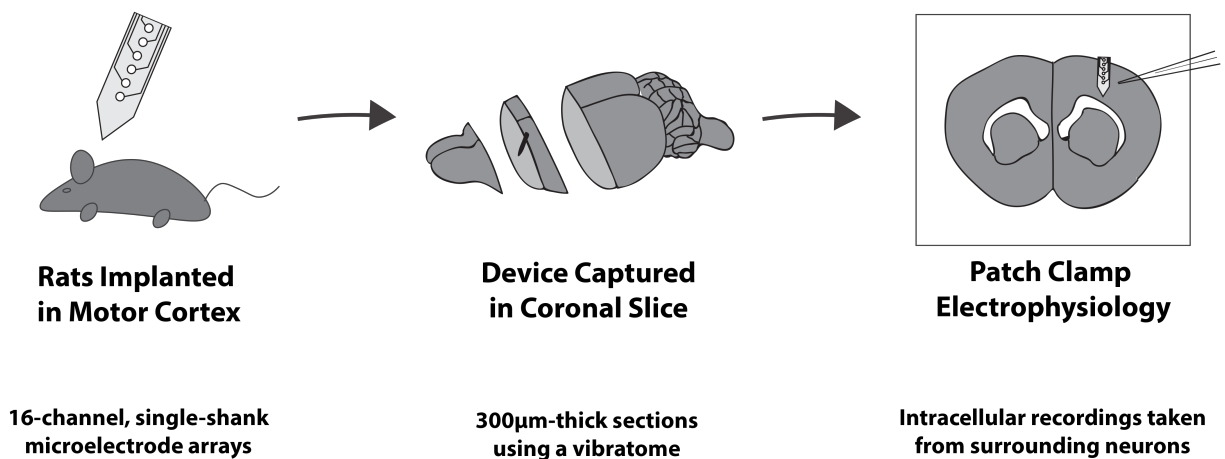


Figure 5.1 | Schematic of methods for capturing devices in a brain slice preparation. 16-channel, single-shank microelectrode arrays are implanted in the primary motor cortex of adult Sprague Dawley rats for predetermined time points, whereby the brain is rapidly extracted and a vibratome is used to take 300µm-thick coronal sections to capture the device in a single slice, whereby that slice is then used to perform patch clamp electrophysiology on interfacial neurons within the recordable radius of the device interface (<100µm). These neurons can additionally be filled with Alexa Fluor dyes for performing dendritic spine imaging, as well as perturbed with molecule uncaging to investigate nuanced changes in synaptic transmission and excitability.

This brain slice preparation provides an opportunity to probe individual neurons at the device interface, which can be coupled with two-photon imaging techniques to image and quantify dendritic spine density by filling patched cells with Alexa Fluor dye (**Fig. 5.2**). Ample opportunities exist for further exploration of connectivity and function of those same circuits via caged molecule photolysis, electrical/optogenetic stimulation, etc. during electrophysiological recordings. This includes investigating nuanced changes in synaptic transmission or excitability via neurotransmitter uncaging at individual synapses during a recording session to uncover receptiveness to neurotransmission, electrical stimulation of adjacent cells to uncover responsiveness to synaptic inputs, etc. This is a novel approach to systematically unpack functional circuit remodeling that can be translated to explain changes in device performance.

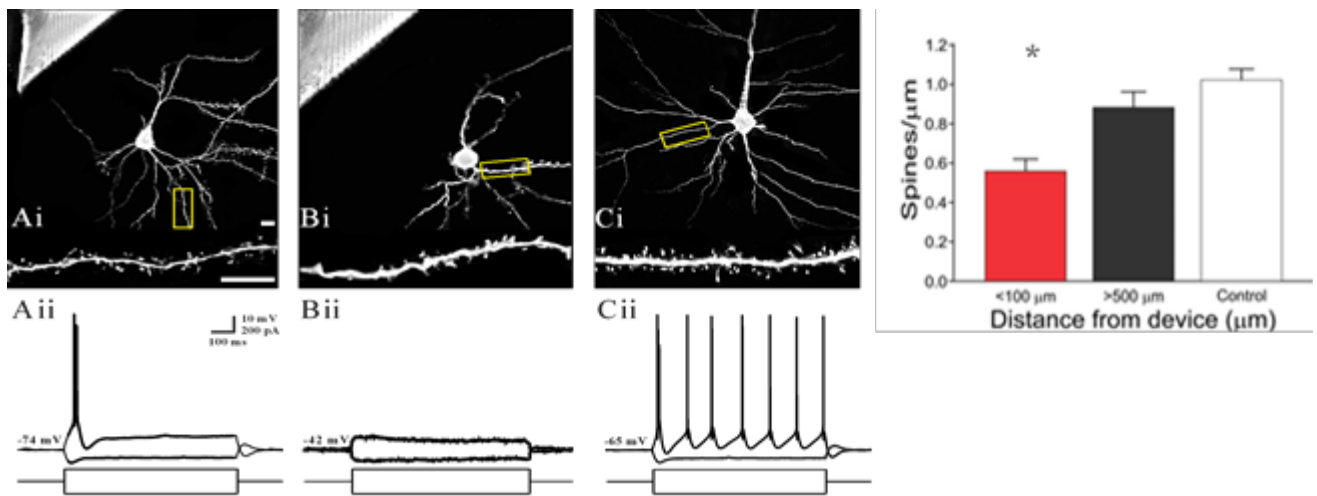


Figure 5.2 | Combining whole-cell brain slice electrophysiology with two-photon dendritic spine imaging: new opportunities for exploring plasticity at the interface. Preliminary work from the Regenerative Electrode Interface Lab (spearheaded by Bronson Gregory with the Lee Cox Group) characterizing both electrophysiology and dendritic spine density in single neurons near the device interface (<100μm, A and B, device edge in top left corners) and >500μm away (C) at 1 week. Results indicate that near-device neurons have reduced firing properties (A and B) and reduced dendritic spine density (D) compared to both >500μm and naïve controls.

Approaches to validate the delivery of genetic material to neural cells: in vitro optimization

A future area of interest for the lab is to genetically modify cells to reveal their role in tissue device integration. As a first step, we decided to reprogram astrocytes into neurons, with the idea of changing the scar forming astrocytic barrier into signal generating neurons. We have successfully validated the delivery of genetic material *in vitro* to reprogram rat cortical astrocytes into functional neurons. After a battery of pro-neural factors (Fig. 5.3), we identified ASCL1 in isolation as the single most robust approach to produce both morphologically and electrophysiologically mature neurons based on our characterizations performed using whole-cell patch clamp electrophysiology and immunohistochemistry (Fig. 5.3).

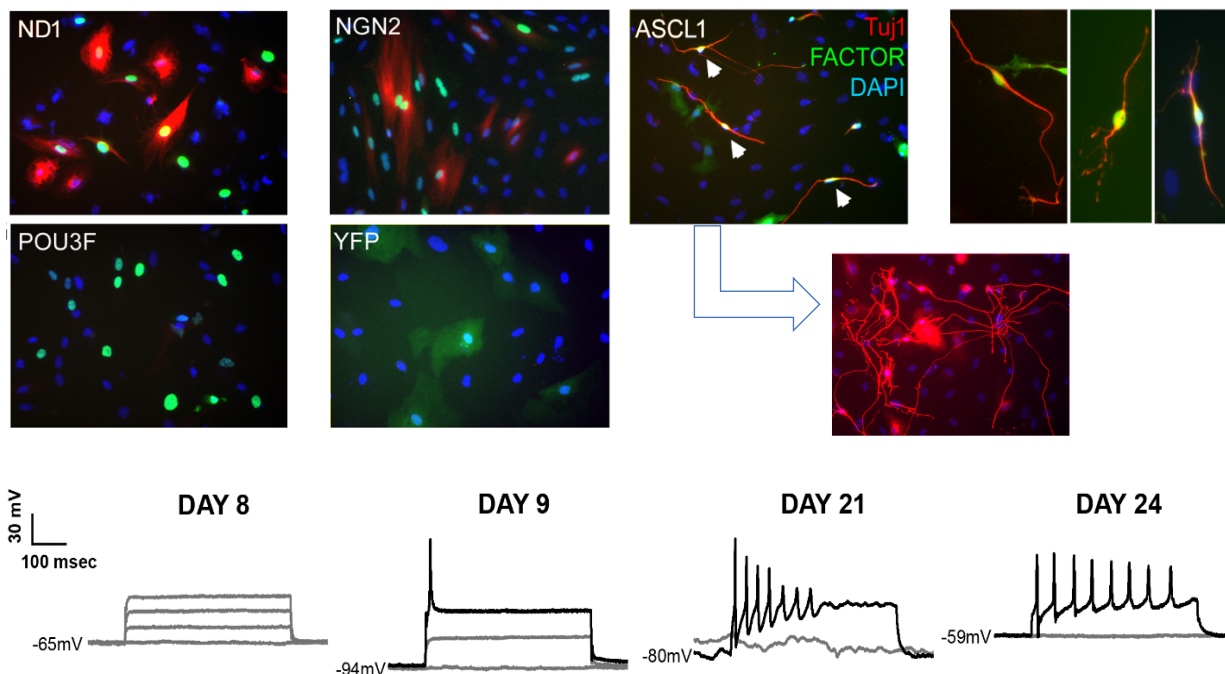


Figure 5.3 | Reprogramming glia into neurons: histological and electrophysiological evidence of neuronal conversion *in vitro*. Early observations indicate that the ASCL1 transgene is capable of

Figure 5.3 (cont'd)

producing cells with neuronal morphology and marker expression (TUJ1, SYN) from astrocyte cultures. Delivery of NeuroD1 (ND1) or Neurogenin-2 (NGN2) produced TUJ1 positivity (red) without accompanying morphological changes. POU3F and control YFP-infected cultures exhibited no observable conversion to neuronal fate. Scales = 5 μ m. Reprogrammed astrocytes were capable of eliciting a single spike in response to injected current by Day 9 post-infection, repetitive spiking by Day 21, and mature spike trains by Day 24 (representative traces). Earlier time points were consistently devoid of spiking activity. Control cultures displayed typical glial morphology and were likewise non-responsive to stimulation (not shown). Figure modified from³⁵².

This *in vitro* approach, which can combine histology, patch clamp electrophysiology and qPCR, provides a unique platform to validate and optimize the delivery of genetic material to neural tissue before implementation *in vivo*. This can be extended to knockdown of ion channels, as reported in Chapter 4 with qPCR (**Fig. 4.5**), and the knockdown of synaptic transporters currently being explored by our lab (data not shown), where the ability to systematically assess the electrophysiological impacts via patch clamp can prove especially useful for translating potential impacts on recorded signals *in vivo*.

Approaches to perturb plasticity at the interface: delivering genetic material in vivo

We have developed several techniques to deliver genetic material *in vivo* at both acute and chronic time points surrounding microelectrode arrays. For navigating the chronic setting, we began with the implantation of a cannula positioned adjacent to the electrode array, such that the delivery of the material was most concentrated at the tip of the electrode shank (**Fig. 5.2a**). Due to the invasiveness of the cannula, we explored the fabrication of a custom NeuroNexus probe with a microfluidic channel positioned along the shank of the electrode array for more precise delivery at the tip and with less damage (**Fig. 5.4c**). We have validated successful delivery of genetic material, with considerably less damage, using the microfluidic

device in comparison to the cannula (**Fig. 5.4d**, work spearheaded by Bailey Winter and published in *Micromachines*³⁵¹). Finally, we implemented a micropipette injection method to deliver material prior to the implantation of the device, which is suitable for intervention strategies that only require acute administration (without need for the added invasiveness of the chronic delivery packages) (**Fig. 5.4b**).

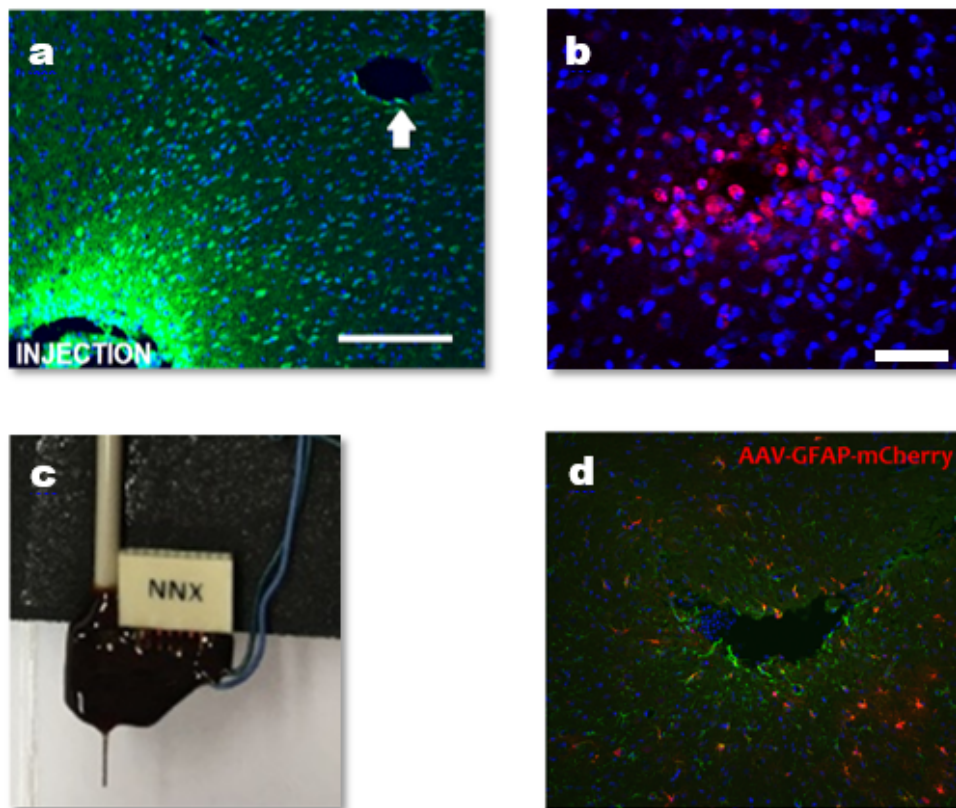


Figure 5.4 | Methods to deliver genetic material in vivo. A) Delivery of an AAV-CMV-GFP vector from a cannula (“INJECTION”) to the electrode array (“↑”). B) Acute delivery of BLOCK-iT siRNA reporter using a pulled glass capillary micropipette (alexafluor 555, counterstained with Hoechst). C) Custom-made NeuroNexus probe with a microfluidic channel affixed to the microelectrode shank for chronic delivery. D) Delivery of AAV-GFAP-mCherry at the tip of the electrode array using the custom NeuroNexus device (counterstained with GFAP using alexafluor 488). A and B not published, C and D reproduced from³⁵¹.

Building off of this foundation and expanding upon the work reported in Chapter 4, we have utilized the *in vitro* protocol to systematically identify an ideal ion channel for knockdown as determined by the resulting impacts on excitatory synaptic circuitry with a preliminary data set (Fig. 5.5). By systematically knocking down each ion channel investigated in Chapter 4 and assessing the relative expression levels of ion channels and excitatory synapses, we identified Kv7.2 as the most likely to heighten excitatory synapse formation and, potentially, overall excitability from increased Nav1.6 and reduced Kv channels at 1 week (Fig. 5.5).

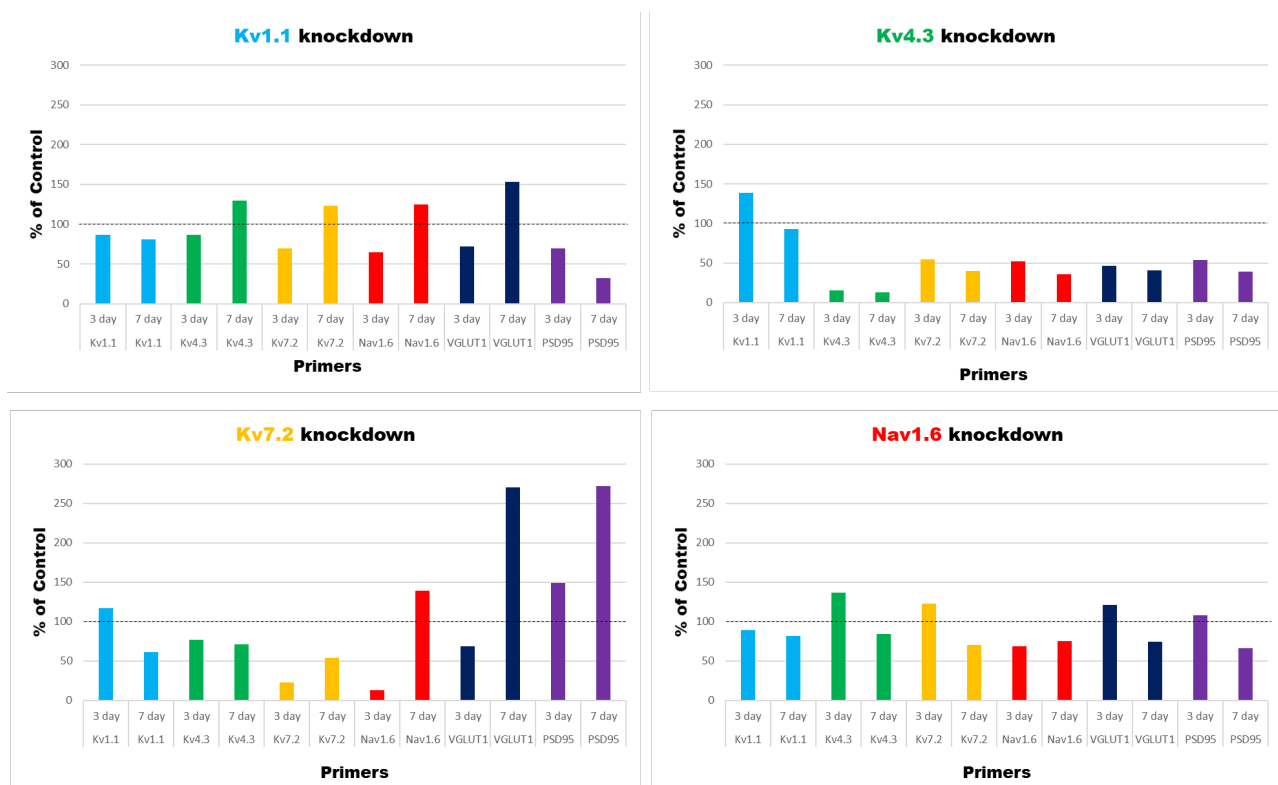


Figure 5.5 | Preliminary ion channel knockdown *in vitro* to systematically screen for impacts on excitatory synapses. Ion channels were knocked down in rat cortical neurons with siRNA for the respective channels. After harvesting the RNA, cDNA was made using an RNEasy kit and Taqman probes were used to quantify RNA for the respective sequences. Results indicate that Kv7.2 most robustly impacts excitatory synapses (VGLUT and PSD95 upregulation) and hyperexcitability (Nav1.6 upregulated, and Kv7.2/Kv4.3/Kv1.1 downregulated) at 1 week. N=3 biological repeats for each condition.

We hypothesized that this impact on excitatory synapses would most robustly improve signal retrieval by implanted devices. From this, we generated new methods for knocking-down ion channel expression and assessing its direct relationship to recorded signal quality. Here, we have generated preliminary data of bilateral siRNA delivery and device implantation (with Kv7.2 siRNA infused in left hemisphere and SCR siRNA infused in right hemisphere of each subject using the “acute” micropipette method prior to electrode implantation) (**Fig. 5.4**). The results indicate successful knockdown of Kv7.2 at 1 week post-implantation, where accompanied VGLUT1 expression is downregulated relative to scramble control (**Fig. 5.6**). While blocking Kv7.2 channels *in vitro* has been shown to increase neuronal firing rate and induce excitatory synapse formation³¹⁵, which coincided with our *in vitro* results (**Fig. 5.5**), the *in vivo* environment following injury is inherently prone to excitotoxic sequelae^{43,139,140}, where the reduced units and excitatory synaptic density at 7 days could potentially be explained by hyperexcitability and excitotoxicity that followed Kv7.2 knockdown with concomitant inflammation and reactive signaling (**Fig. 5.6**). This gives insight into mechanisms that exacerbate signal loss and supports a neuroprotective role of early Kv7.2 upregulation.

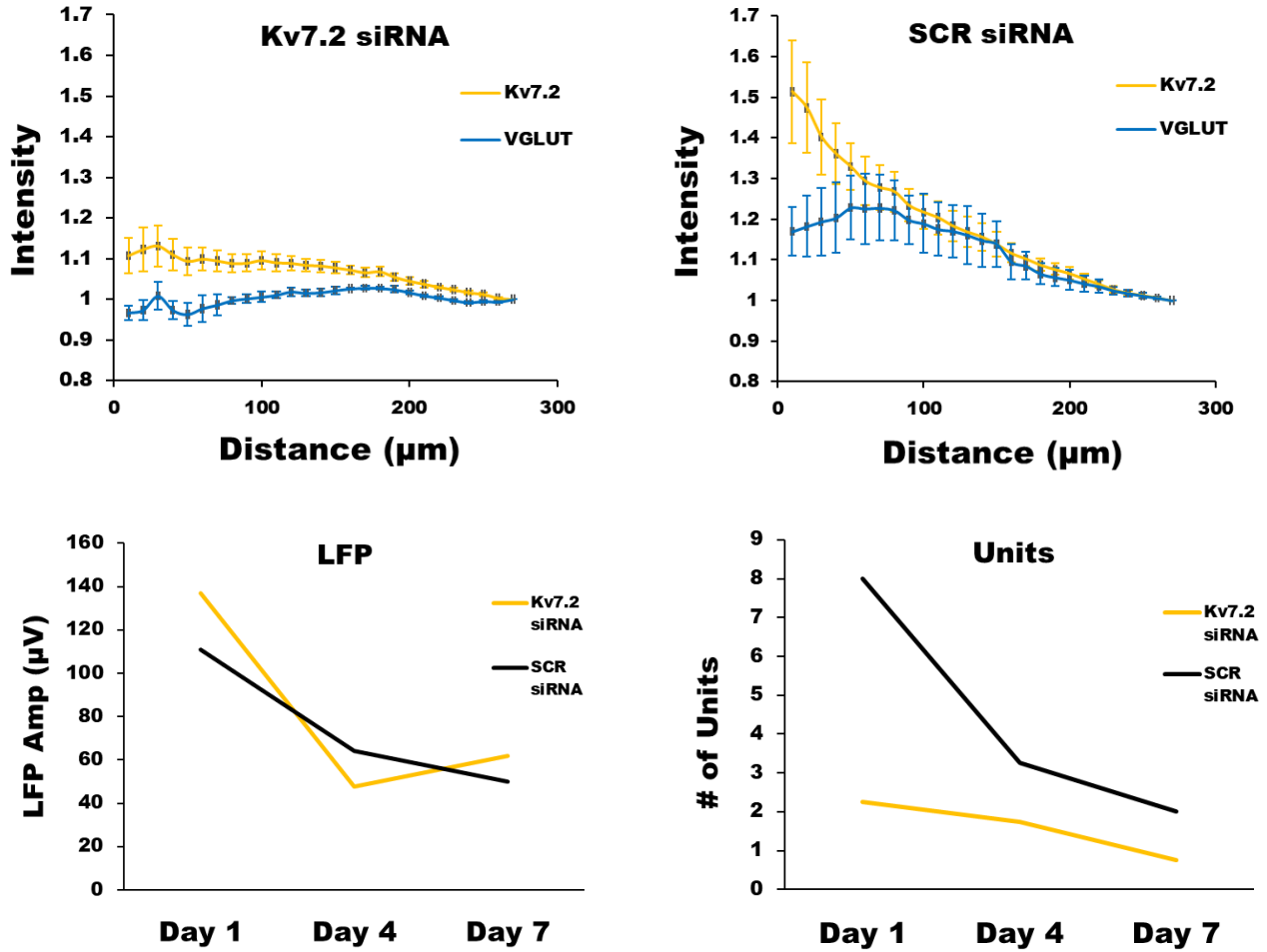


Figure 5.6 | Preliminary knockdown of Kv7.2 *in vivo* with accompanied recordings over 1 week. Preliminary data shows successful knockdown of Kv7.2 *in vivo* relative to scramble (SCR) siRNA control as determined by quantitative immunohistochemistry (n=3 devices per condition). Additionally, accompanied recordings (n=4 devices per condition) indicate reduced unit detection from the Kv7.2 knockdown condition relative to SCR control.

These results provide a novel method for perturbing mechanisms of neural circuit remodeling surrounding devices to identify those which impact recording quality.

Synthesizing approaches for investigation

Combined, these approaches provide a novel toolset for exploring the impact of device implantation on neural circuit function by perturbing relevant biological mechanisms and assessing changes in individual circuit elements and device performance. *In vivo* perturbation of interfacial circuitry (**Figs. 5.4, 5.6**) allows for investigation of changes in extracellular electrophysiology over the implantation period via the microelectrode arrays, which can be combined with a brain slice preparation (**Fig. 5.2**) at terminal time points to assess impacts on interfacial neurons that can be translated to device performance.

Unpacking gliotransmission at the interface: exploring impacts on synaptic transmission and neural circuit function

It has become increasingly appreciated that astrocytes comprise critical components of the traditional synapse (now termed the “tripartite synapse”³⁵³⁻³⁵⁶), where they integrate information along neuronal networks and actively regulate the function, strength, and wiring of synapses in a circuit-specific manner^{278,279,353-355}. By sensing neurotransmitters during synaptic transmission, astrocytes actively respond by releasing gliotransmitters back onto the synaptic terminals to impact the immediate efficacy of transmission, the subsequent plasticity of the synapse by modulating presynaptic release probability and post-synaptic sensitivity, and the formation or pruning of synapses by actively regulating the organization and function of specific circuits under their influence. Recent work has further demonstrated a pivotal role of astrocytes in remodeling the structure and function of neuronal networks following injury, where their gliotransmission is modified by inflammatory- and damage-associated cues in the local environment. This “reactive” gliotransmission impacts

remodeling of vesicular transporters and ion channels in synapses and soma to impact neuronal connectivity and function, such as excitotoxic or neuroprotective/silencing changes to restore lost connections or preserve cell health, respectively. It will therefore be important to understand the impacts of interfacial gliotransmission on local neural circuit function and, in turn, device performance, which remains to be investigated surrounding electrodes implanted in the brain.

Exploring inflammatory pathways that impact gliotransmission

Inflammatory signals initiate key pathways to directly modify the nature and extent of gliotransmission in the CNS. Inflammation can act as a beacon to incite gliosis and, in turn, modify neurotransmission and excitability in the immediate environment, which can have both excitotoxic and neuroprotective effects depending upon inflammatory-mediators and context^{139,145,211,357}. It will therefore be important to develop an understanding of the inflammatory mechanisms that influence gliotransmission following implantation and, in turn, how that resulting gliotransmission influences device performance. As an example, the Toll-like receptor (TLR) pathway is connected to the induction of hyperexcitability, seizures and epileptogenesis in a plethora of neurological conditions and injuries^{307,358-360}. This TLR pathway can be activated in response to IL-1 signaling (both of which are upregulated around implanted arrays^{361,362}) and can in turn activate and upregulate microglial inflammation, downstream astroglial activation, and subsequent astroglial signaling to promote excitatory synapse formation, hyperexcitability, seizures, and epileptogenesis^{358,359}. In fact, recent work from the Capadona Lab has revealed that microelectrode performance over 16 weeks improved when inhibiting the cluster of

differentiation 14(CD14) (a co-receptor to TLRs)³⁶³, providing evidence for impacts of gliotransmission on device performance. Here, recent work by Tzour et. al has connected inflammation (via TLR activation) to neuronal hyperexcitability through downstream inhibition of Kv7.2 channels³⁶⁴ (**Fig. 5.7**), where Kv7.2 inhibition was mediated by astrocytes. This effect required initial purinergic activation of astrocytes via P2Y1Rs, subsequent activation of neuronal mGluRs via astroglial glutamate release, and the resulting release of Ca²⁺ from neuronal intracellular stores that inhibited Kv7.2 (likely via the M-channel auxiliary calmodulin subunit, which has been shown elsewhere to directly inhibit Kv7.2 activity upon Ca²⁺ release^{365,366}) (**Fig. 5.7**).

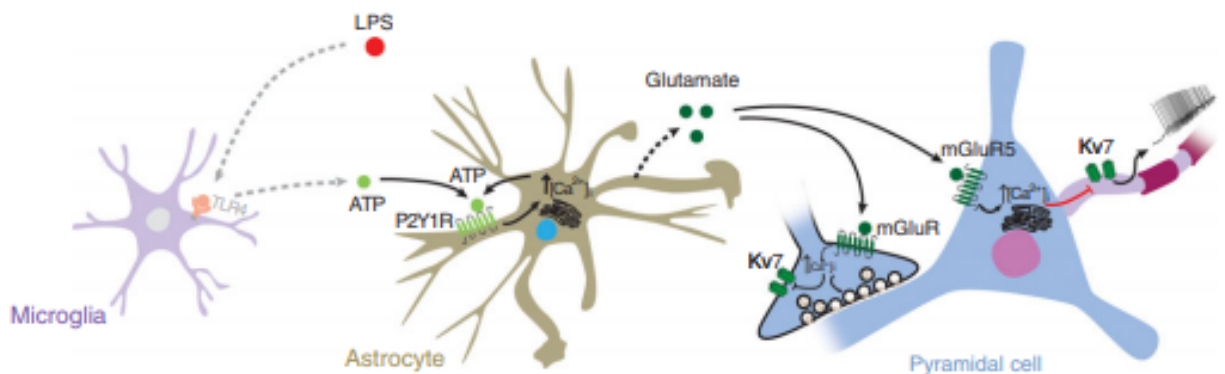


Figure 13. Key steps in the LPS-induced neuroinflammation-hyperexcitability cascade

In the scheme, LPS activates TLR-4 on microglia, leading to ATP release. ATP, in turn, acts on astrocytic P2Y1 receptors, increasing astrocytic [Ca²⁺]_i. This signal may be further amplified by ATP release from astrocytes and activation of autocrine P2Y1 receptors. Consequently, activated astrocytes release glutamate, which acts postsynaptically on mGlu5 receptors (mGluR5) to block neuronal Kv7/M channels by releasing Ca²⁺ from internal stores. The resultant inhibition of *I_M* leads to an increase in intrinsic neuronal excitability. The scheme also depicts LPS-induced inhibition of putative presynaptic Kv7/M channels, leading to enhanced excitatory neurotransmission. [Colour figure can be viewed at wileyonlinelibrary.com]

Figure 5.7 | TLR activation produces hyperexcitability in neighboring neurons via astrocytes. The following depicts mechanisms by which TLR activation and resulting glial signaling induces neuronal hyperexcitability. Figure reproduced from³⁶⁴.

Inhibition of Kv7.2 not only depolarizes neurons and increases firing frequency, but it also induces excitatory synapse formation over subsequent days³¹⁵. Therefore, this TLR activation could potentially be a mechanism responsible for excitotoxicity following device implantation, which could lead to a long-term compensatory mechanism favoring inhibition, as we observed in Chapters 3 and 4. Specifically, early TLR signaling could explain the downregulation of Kv7.2 at 24hrs (**Fig. 4.2**), and this downregulation of Kv7.2 at 24hrs could explain the subsequent upregulation of VGLUT1 at 3 days (**Fig. 3.1**). The chronic shift to inhibitory tone observed, with both elevated VGAT at 28 days (**Fig. 3.1**) and elevated Kv channels at 6 weeks (**Fig. 4.2**), could be a compensatory mechanism to counteract excitotoxicity and neuronal loss. Thus, improved chronic recording quality observed with TLR inhibition could potentially be explained by mitigating these early hyperexcitability mechanisms caused by gliotransmission. Therefore, investigation of similar inflammatory pathways and their resulting changes in gliotransmission may be critical for understanding mechanisms that diminish neural circuit function and device performance.

Additional inflammatory pathways initiated following CNS injury include interleukins (e.g., IL-1A, IL-1 β , IL-6), tumor necrosis factors (TNF α), damage-associated molecular pathways (DAMPS, e.g., HMGB1), complement pathways (C1q, C3), cyclooxygenase (COX2), chemokines, rage receptor pathways, etc., many of which act upstream of the nuclear factor kappa B (NF κ B) transcription factor and all of which impact neuronal function^{139,140}. In fact, several of these inflammatory pathways have been recently observed around implanted electrodes³⁶⁰⁻³⁶². Here, a unique approach to uncover potential involvement of these pathway in remodeling interfacial circuitry would consist of utilizing

the methods outlined above (**Figs 5.2, 5.3, and 5.4**). Specifically, knocking down an inflammatory pathway (e.g., TLR4) at the time of implantation, monitoring recording quality over the implantation window, and performing brain slice electrophysiology at terminal time points would prove useful in identifying the functional impacts of the inflammatory pathway over chronic periods of implantation. For the brain slice approach, evidence of excitotoxicity can be probed by investigating changes in dendritic spine density, electrophysiological sensitivity to glutamate uncaging, and the ratio of inhibitory/excitatory post-synaptic currents with passive recordings would prove especially useful, where a hypothesized loss of dendritic spine density, reduced glutamate sensitivity, and reduced EPSPs at chronic time points would indicate the presence of excitotoxic phenomena. Per this hypothesis, the TLR4 knockdown condition would reduce this excitotoxic sequelae in comparison to a scramble siRNA control.

Taken together, inflammatory-mediated gliotransmission pathways may be critical drivers by which neuronal signaling is altered at the device interface, and therefore could be molecular determinants that ultimately shape device performance. Given the role of glia in regulating these pathways, the impacts of glial signaling on circuit-specific functions will be important to investigate as they relate to device function.

Exploring the impacts of gliotransmission on neural circuit function

After identifying inflammation- and damage-related signals that modulate gliotransmission following injury, it will be vital to understand the subsequent impacts of that gliotransmission on neural circuit function and device performance.

In Chapter 3, we identified a unique subtype of glia that was restricted to the device-interface (“GFAP+/VGAT+” cells). Whether this antibody is actually labeling VGAT on these glia and, if so, whether VGAT plays a functional role in these cells, such as facilitating vesicular release of GABA as suggested, holds significant implications for local circuit function and will need to be further investigated to understand its impacts on device function. Initial validation of the presence of VGAT will need to be achieved, which could be done using several methods. Recent work in the field has reported the precise excision of tissue following electrode removal at terminal time points for the purpose of performing qPCR^{361,362} (using a Ted Pella Brain Matrix). Here, fluorescence activated cell sorting (FACS) would be ideal for sorting out VGAT+/GFAP+ cells from the excised tissue, which could then be prepared for either qPCR or RNAseq. Using qPCR would be sufficient for determining VGAT RNA presence, while RNAseq would be vastly more informative by providing the entire genomic profile of this phenotype. If using qPCR, it would be important to ensure that the VGAT antibody used for histology is not labeling, for example, GAT (GABA Transporter). If the results indicate the presence of VGAT RNA, then for additional rigor gold-particle immunohistochemistry and transmission electron microscopy (TEM) could be used to visualize VGAT-positivity on synaptic vesicles in glia. If all results point to the presence of VGAT, then further investigation into a functional role of this protein could be warranted.

Previous work has reported the release of GABA from astrocytes^{295,367,368}, including under pathological conditions²⁹⁸. However, to the best of our knowledge, astrocytic GABA release via vesicular machinery has not been reported. Astrocytes have been shown to contain SNARE (soluble NSF attachment protein receptor) machinery necessary for vesicle

fusion as well as contain vesicular transporters, where both glutamate and ATP have been shown to be released via vesicular machinery³⁶⁹⁻³⁷¹, and astroglial glutamate release has been stifled by administering Bafilomycin A₁ to inhibit V-ATPase (preventing vesicular transporter filling) and Botulinum B to cleave the SNARE protein synaptobrevin³⁷². Therefore, it appears reasonable to postulate the existence of a functional VGAT protein in these glia labeled by the VGAT antibody. To investigate VGAT function, a brain slice model similar to that described in this section could be implemented (**Fig. 5.2**), where it would be interesting to label these cells specifically using an injection package (**Fig. 5.4**) to identify whether or not they perform vesicular release. This could potentially be identified with a synaptopHluorin gene³⁷³, which is a pH-sensitive fluorescent protein in synaptic vesicles that fluoresces when the vesicle fuses with the synaptic membrane and is exposed to the more basic pH of the extracellular space. This cell-specific labeling could potentially be achieved with a cre-lox recombinase model driven by a GFAP promoter, where the synaptopHluorin gene could be encoded downstream of VGAT so that only GFAP+ cells that express VGAT will also express synaptopHluorin once recombinase expression/recombination occurs. This fluorescence could be imaged in real time around a device in a brain slice preparation. If vesicular release is observed, a 'sniffer-patch' approach³⁷⁴ would prove especially useful to identify whether the vesicular release is of GABA, where an outside-out patch of membrane from a GABA receptive cell would be positioned at the site of gliotransmission to sense GABA release in this same brain slice while imaging synaptopHluorin. In fact, a recent sniffer-patch technique has been developed for higher-throughput using HEK cells expressing GABAA receptors³⁶⁷ (an engineered "GABA sensor"), where this technique was used to identify that astrocytes in the dorsal horn of the

spinal cord release GABA in response to glutamate puff application³⁶⁷. Therefore, this sniffer patch application could prove especially useful for identifying whether synaptofluorin-visualized vesicular release, if observed, is of GABA. Finally, for additional rigor, application of botulinum toxin light chains and/or bafilomycin³⁷² to the intracellular compartment of the same glia would further validate vesicular mechanisms of release.

If identified that GABAergic vesicular release occurs by this subpopulation of interfacial glia, then further investigations into the functional consequences on interfacial neurons will be warranted for translating impacts on device function. Within this brain slice, it would be especially useful to uncage molecules (e.g., glutamate or ATP) to stimulate AAV transfected VGAT+/GFAP+ glia with the synaptofluorin gene to image synaptic transmission in real time at the interface via 2P. This could be done with uncaging of multiple neurotransmitters to identify whether, say, glutamate selectively or preferentially stimulates these cells to release GABA. Additionally, intracellular filling of the glia with NP-EGTA-bound Ca²⁺ and photostimulated uncaging could be investigated to selectively trigger vesicular release. This approach would be especially useful to study while recording from neighboring neurons to identify the functional consequences of GABAergic transmission from these glia on local circuitry. In addition, the direct impacts of this signaling on device function could then be unpacked by optogenetically stimulating the VGAT+ glia at the device interface *in vivo* via ChR2 virus using a similar targeting mechanism for this cell type as above. This could uncover whether these glia are a source of GABAergic inhibition at the interface that impairs signal detection by implanted electrodes.

Together, it will be valuable to knockdown these and other glial pathways to identify those which influence neuronal function at the interface and device performance. Specifically, it will be important to uncover glial mechanisms that impact the both *structure* and *function* of neural circuitry as they relate to device performance.

Synthesizing mechanisms: new targets for intervention strategies

Previous work in the field has investigated the extent of gliosis and neuronal loss as they relate to electrode design for informing next-generation devices, or as they relate to the delivery of bioactive molecules for informing intervention strategies³⁶. However, ideal histology and device integrity based on these traditional methods have still not guaranteed adequate recording quality³⁷⁵, and there have yet to be reports of any guiding principles that connect signal loss to changes in neuronal function. Here, this work provides fundamental insight into major circuit changes at the device interface that correspond with signal decline, where a trend from hyper- to hypoexcitability is observed across multiple structural and functional metrics. This work also provides a platform to directly unpack circuit-specific elements that impair device performance. These elements can then be synthesized to deliver unique and effective intervention strategies that target the *biological mechanisms* by which devices fail over time. Therefore, this approach could eliminate the need to broadly modify inflammation (which still offers countless neuroprotective/reparative benefits following TBI³⁷⁶) by instead targeting the exact mechanisms responsible for impairing neural circuit function and device performance.

Here, it will be important to explore glial mechanisms as they relate to two major remodeling events: those that impact the *structure* and the *function* of interfacial neuronal circuitry (**Fig. 5.8**). Structural components can be broken down into those comprising the connectivity of synaptic circuitry (with respect to density and organization, such as those initiating synaptic pruning or sprouting) (**Fig. 5.8**), whereas functional components can be broken down into ion channels and synaptic machinery that influence the intrinsic excitability and synaptic transmission of interfacial circuitry (**Fig. 5.8**). These remodeling events can be broadly categorized by those contributing to the hyper- to hypo-excitability shift observed with chronic devices in this work that corresponded with signal loss.

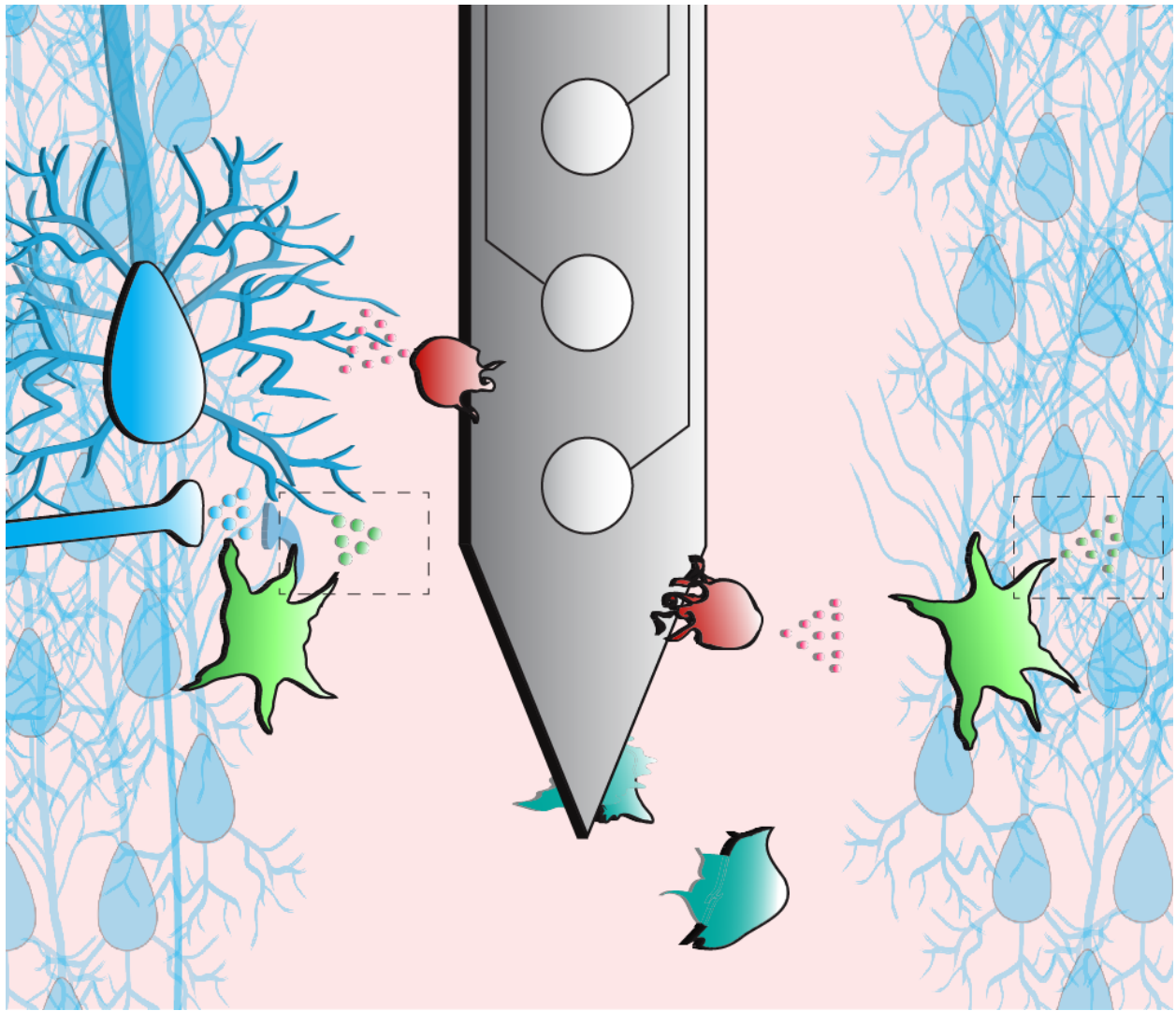
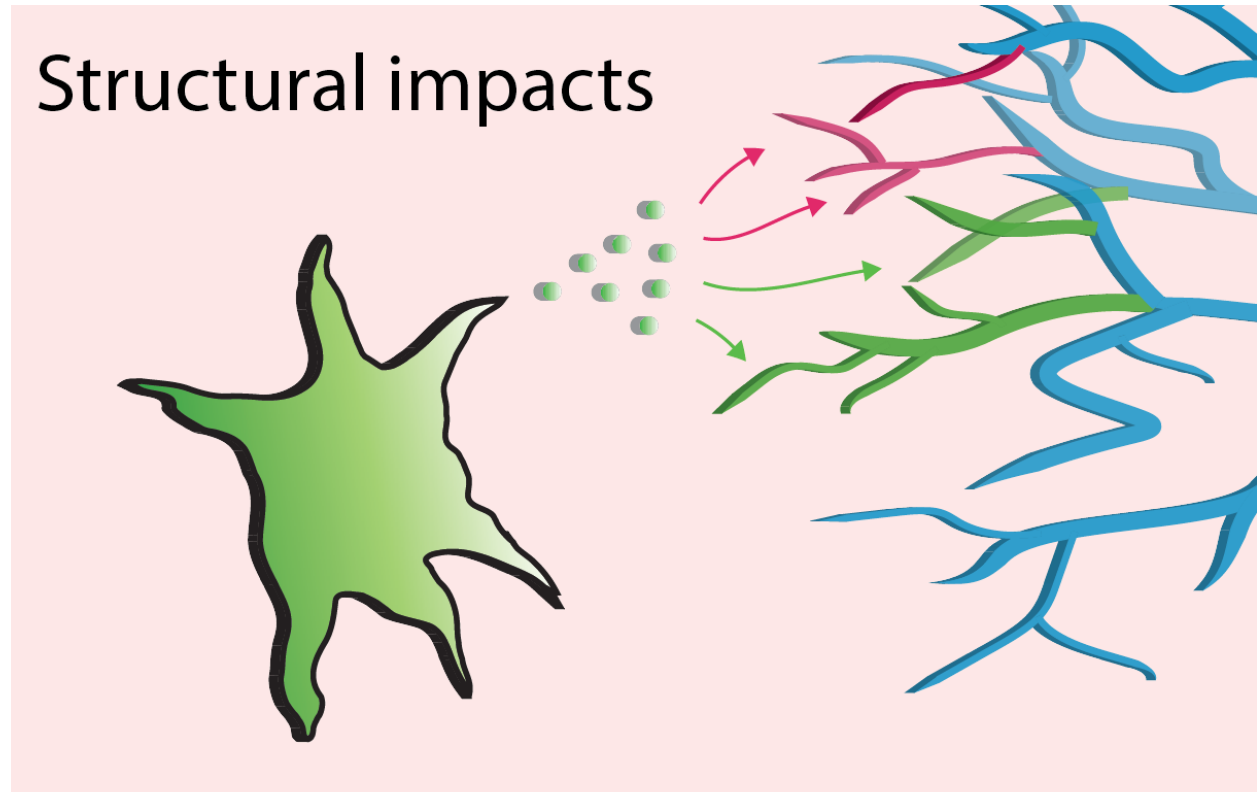


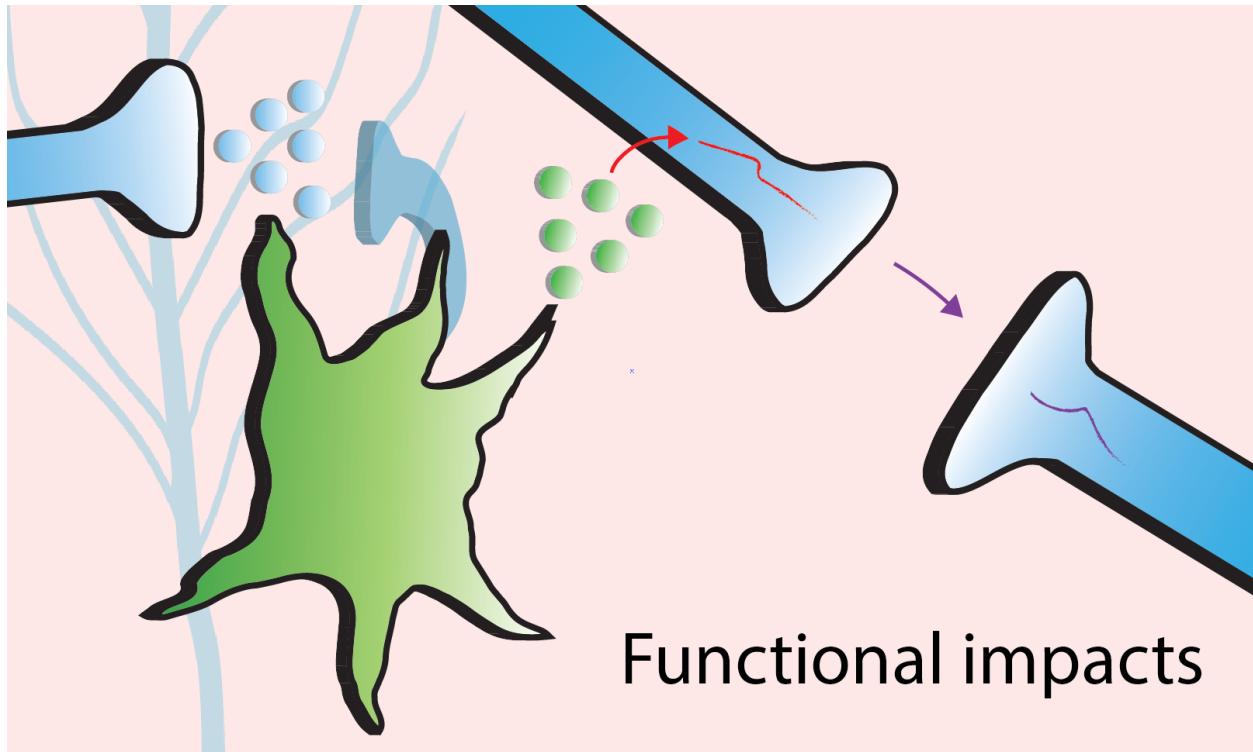
Figure 5.8 | Structural and functional remodeling of neuronal circuitry by glia: mechanisms to inform electrode injury models. Depiction of device-related mechanisms of neural circuit remodeling. For both structural and functional impacts, a corresponding table depicts potential glial mechanisms that may drive the remodeling observed around implanted electrode arrays in this work (continued on next pages).

Figure 5.8 (cont'd)



Synaptogenesis		Synaptic pruning	
Glial mechanisms that can induce excitatory synapse formation	TGFβ ³¹⁰ , TSPs ³⁷⁷ , TLR4 ³⁵⁸ , Gpc4 & 6 ³⁷⁸ γ-protocadherins ³⁷⁹ , D-Serine ³⁸⁰ , NP2/Narp ^{381,382} .	Glial mechanisms that can initiate excitatory synapse stripping	Neuronal pentraxin NP1 ³¹⁵ , complement C1q pathway ³⁸³ , class I MHC ³⁸⁴ , C3 pathway ³⁸⁵ .
Glial mechanisms that can initiate inhibitory synapse formation	TGFβ+glutamatergic neurotransmission ¹⁴⁹ , Trk ³⁸⁶ , BDNF ^{386,387} .	Glial mechanisms that can initiate inhibitory synapse stripping	Complements C1q and C3 ³⁸⁵ , pCamKIV/ pCREB/ pERK1/2 ³⁸⁸ .

Figure 5.8 (cont'd)



Intrinsic excitability		Synaptic transmission	
<p>Glial mechanisms that can induce hyper-excitability</p>	<p>HMGB1/TLR4³⁸⁹, IL1β³⁸⁹⁻³⁹¹, RAGE³⁹², ADK³⁹³, TLR/ P2Y1R/mGluR³⁶⁴, PGE2 and COX2³⁹⁴.</p>	<p>Glial mechanisms that can impact excitatory synaptic transmission</p>	<p>IL-1β^{391,395}, COX2³⁹⁴, MyD88³⁹⁶, TNFα^{155,397}, Gpc4&6³⁷⁸, ADK³⁹³, NP2/Narp^{381,382}, Gln synthetase^{281,398}.</p>
<p>Glial mechanisms that can induce hypo-excitability</p>	<p>IL1β^{141,143,318,399,400}, IL-6¹⁴², TNF/p75³⁵⁷, NP1³¹⁵, adenosine⁴⁰¹.</p>	<p>Glial mechanisms that can impact inhibitory synaptic transmission</p>	<p>IL-6¹⁴⁵, TNFα^{402,403}, BDNF³⁸⁷, IL1β^{402,403}, IL-1⁴⁰⁴, A1R^{369,405-407}.</p>

By implementing a multi-modal approach described in this chapter (e.g., delivering genetic material to perturb mechanisms and performing histology/brain slice electrophysiology to assess the impacts on individual circuits), direct biological mechanisms and their specific impacts on neural circuit function can be systematically uncovered as they relate to device function. In order to develop intervention strategies with high efficacy for improving device function, it will be critical to unpack and target the gliotransmission mechanisms that act as a final step in remodeling neural circuits (**Fig. 5.9**).

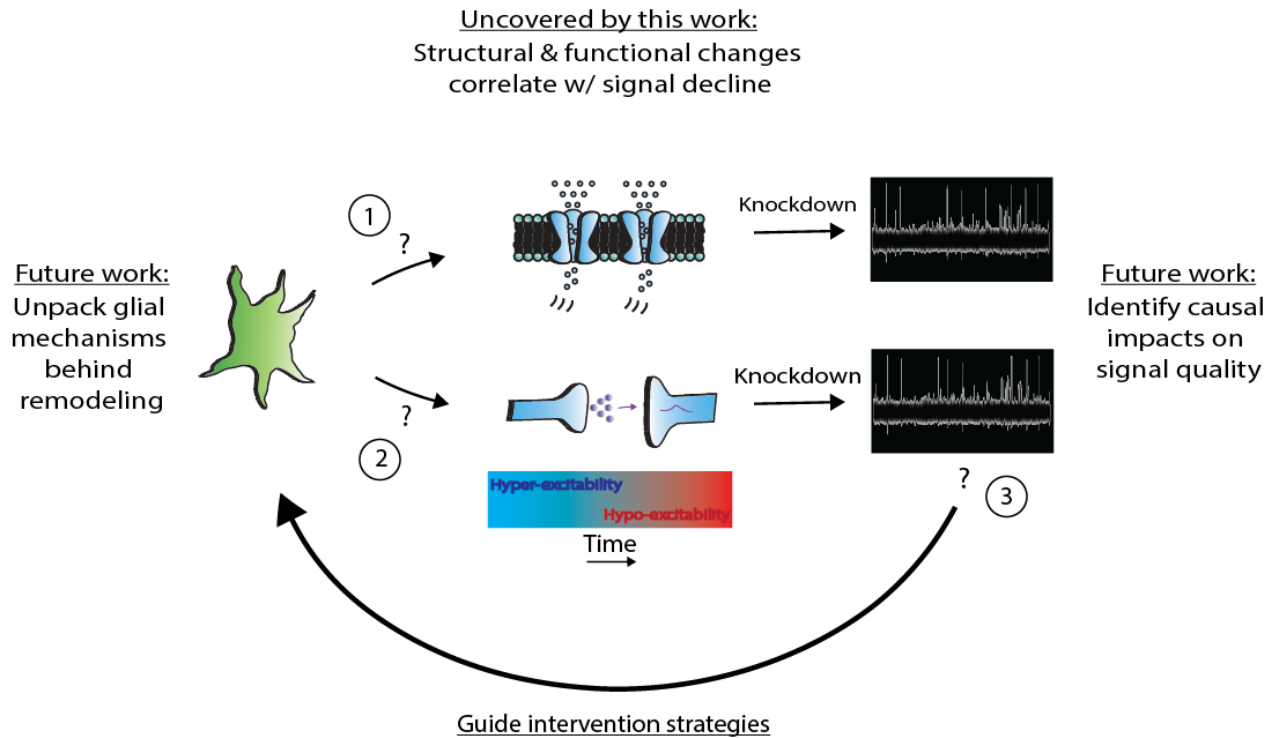


Figure 5.9 | Future outlook: designing intervention strategies to improve device performance by targeting glial mechanisms. Based on the data and methods reported in this dissertation, it will be possible to design intervention strategies aimed at improving device function by modulating glial mechanisms that impact neural circuit remodeling and, in turn, device performance. Several steps will be necessary to this end: (1) It will be important to investigate glial mechanisms that contribute to remodeling of ion channels around implanted electrodes (by modulating them via siRNA, etc. with methods described in this chapter), and to identify causal relationships to recording quality (with potential candidates for glial mechanisms outlined in Fig. 5.7, and methods to assess impacts on neural circuit remodeling and device performance in Figs. 5.1-5.5); (2) It will be important to investigate glial mechanisms that contribute to the remodeling of synaptic circuitry around devices, and to identify causal relationships to signal quality; (3) Finally, any mechanisms identified that causally impact signal quality can then be used to guide intervention strategies aimed at modulating the specific glial mechanisms responsible.

Outlook

This work is pioneering innovative strategies for the precise delivery of genetic materials to engineer neural circuitry at the brain-electrode interface. These developments open up a new design space for 1) unpacking circuit-specific elements that impair device performance, 2) designing (neuroengineered) intervention strategies to improve device integration and longevity, and 3) advancing current capabilities of interfacing with the nervous system by creating cell type- and circuit-specific pathways for transmitting information with unparalleled specificity.

REFERENCES

REFERENCES

1. Fritsch, G. & Hitzig, E. Electric excitability of the cerebrum (Über die elektrische Erregbarkeit des Grosshirns). *Epilepsy Behav.* **15**, 123–130 (2009).
2. Ferrier, D. Experimental researches in cerebral physiology and pathology. *Br. Med. J.* 457 (1873).
3. Grunvaum, A. & Sherrington, C. Observations on the Physiology of the Cerebral Cortex of some of the Higher Apes. *Proc. Roy. Soc. Lond.* **69**, (1901).
4. Penfield, W. & Boldrey, E. Somatic motor and sensory representation in the cerebral cortex of man studied by electrical stimulation. *Brain* **60**, 389–443 (1937).
5. Fetz, E. E., Finocchio, D. V, Baker, M. A. & Soso, M. J. Sensory and motor responses of precentral cortex cells during comparable passive and active joint movements. *J. Neurophysiol.* **43**, 1070–89 (1980).
6. Albe-Fessard, D. & Liebeskind, J. Origine des messages somato-sensitifs activant les cellules du cortex moteur chez le singe. *Exp. Brain Res.* **1**, (1966).
7. Lemon, R., Hanby, J. & Porter, R. Relationship between the activity of precentral neurones during active and passive movements in conscious monkeys. *Proc. R. Soc. London. Ser. B. Biol. Sci.* **194**, 341–373 (1976).
8. Hodgkin, A. & Katz, B. The effect of sodium ions on the electrical activity of the giant axon of the squid. *J. Physiol.* **8**, (1949).
9. Hodgkin, A. L., Huxley, A. F. & Katz, B. Measurement of current-voltage relations in the membrane of the giant axon of *Loligo*. *J. Physiol.* **116**, 424–448 (1952).
10. Neher, E. & Sakmann, B. Single-channel currents recorded from membrane of denervated frog muscle fibres. *Nature* **260**, 799–802 (1976).
11. Neher, E., Sakmann, B. & Steinbach, J. H. The extracellular patch clamp: A method for resolving currents through individual open channels in biological membranes. *Pflügers Arch. Eur. J. Physiol.* **375**, 219–228 (1978).
12. Sakmann, B. Patch Clamp Techniques for Studying Ionic Channels in Excitable Membranes. *Annu. Rev. Physiol.* **46**, 455–472 (2002).
13. Fetz, E. E. Operant Conditioning of Cortical Unit Activity. *Adv. Sci.* **163**, 955–958 (1969).

14. BeMent, S. L., Wise, K. D., Anderson, D. J., Najafi, K. & Drake, K. L. Solid-State Electrodes for Multichannel Multiplexed Intracortical Neuronal Recording. *IEEE Trans. Biomed. Eng.* **BME-33**, 230–241 (1986).
15. Drake, K. L., Wise, K. D., Farraye, J., Anderson, D. J. & BeMent, S. L. Performance of Planar Multisite Microprobes in Recording Extracellular Single-Unit Intracortical Activity. *IEEE Trans. Biomed. Eng.* **35**, 719–732 (1988).
16. Anderson, D. J. *et al.* Batch-Fabricated Thin-Film Electrodes for Stimulation of the Central Auditory System. *IEEE Trans. Biomed. Eng.* **36**, 693–704 (1989).
17. Georgopoulos, A., Schwartz, A. & Kettner, R. Neuronal population coding of movement direction. *Science (80-.)*. **233**, 1416–1419 (1986).
18. Churchland, M. M. & Shenoy, K. V. Temporal Complexity and Heterogeneity of Single-Neuron Activity in Premotor and Motor Cortex. *J. Neurophysiol.* **97**, 4235–4257 (2007).
19. Suminski, A. J., Tkach, D. C., Fagg, A. H. & Hatsopoulos, N. G. Incorporating Feedback from Multiple Sensory Modalities Enhances Brain-Machine Interface Control. *J. Neurosci.* **30**, 16777–16787 (2010).
20. Hatsopoulos, N. G. & Suminski, A. J. Sensing with the Motor Cortex. *Neuron* **72**, 477–487 (2011).
21. Suminski, A. J., Tkach, D. C. & Hatsopoulos, N. G. Exploiting multiple sensory modalities in brain-machine interfaces. *Neural Networks* **22**, 1224–1234 (2009).
22. Hochberg, L. R. *et al.* Neuronal ensemble control of prosthetic devices by a human with tetraplegia. *Nature* **442**, 164–171 (2006).
23. Hochberg, L. R. *et al.* Reach and grasp by people with tetraplegia using a neurally controlled robotic arm. *Nature* **485**, 372–5 (2012).
24. Bouton, C. E. *et al.* Restoring cortical control of functional movement in a human with quadriplegia. *Nature* **533**, 247–250 (2016).
25. Rosin, B. *et al.* Closed-loop deep brain stimulation is superior in ameliorating parkinsonism. *Neuron* **72**, 370–384 (2011).
26. Perge, J. A. *et al.* Intra-day signal instabilities affect decoding performance in an intracortical neural interface system. *J. Neural Eng.* **10**, 036004 (2013).
27. Jackson, A. & Fetz, E. E. Compact movable microwire array for long-term chronic unit recording in cerebral cortex of primates. *J. Neurophysiol.* **98**, 3109–18 (2007).
28. Chestek, C. A. *et al.* Neural prosthetic systems: Current problems and future directions.

in *2009 Annual International Conference of the IEEE Engineering in Medicine and Biology Society* 3369–3375 (IEEE, 2009). doi:10.1109/IEMBS.2009.5332822

29. Chestek, C. A. *et al.* Long-term stability of neural prosthetic control signals from silicon cortical arrays in rhesus macaque motor cortex. *J. Neural Eng.* **8**, 045005 (2011).
30. Purcell, E. K., Thompson, D. E., Ludwig, K. A. & Kipke, D. R. Flavopiridol reduces the impedance of neural prostheses in vivo without affecting recording quality. *J. Neurosci. Methods* **183**, 149–157 (2009).
31. Liu, X. *et al.* Stability of the interface between neural tissue and chronically implanted intracortical microelectrodes. *IEEE Trans. Rehabil. Eng.* **7**, 315–326 (1999).
32. Turner, J. N. *et al.* Cerebral Astrocyte Response to Micromachined Silicon Implants. *Exp. Neurol.* **156**, 33–49 (1999).
33. Szarowski, D. H. *et al.* Brain responses to micro-machined silicon devices. *Brain Res.* **983**, 23–35 (2003).
34. Biran, R., Martin, D. C. & Tresco, P. A. Neuronal cell loss accompanies the brain tissue response to chronically implanted silicon microelectrode arrays. *Exp. Neurol.* (2005). doi:10.1016/j.expneurol.2005.04.020
35. Henze, D. A. *et al.* Intracellular features predicted by extracellular recordings in the hippocampus in vivo. *J. Neurophysiol.* **84**, 390–400 (2000).
36. Wellman, S. M. *et al.* A Materials Roadmap to Functional Neural Interface Design. *Adv. Funct. Mater.* 1701269 (2017). doi:10.1002/adfm.201701269
37. Hong, G. & Lieber, C. M. Novel electrode technologies for neural recordings. *Nat. Rev. Neurosci.* (2019). doi:10.1038/s41583-019-0140-6
38. Lacour, S. P., Courtine, G. & Guck, J. Materials and technologies for soft implantable neuroprostheses. *Nat. Rev. Mater.* **1**, 16063 (2016).
39. Prince, D. A., Parada, I. & Graber, K. *Traumatic Brain Injury and Posttraumatic Epilepsy. Jasper's Basic Mechanisms of the Epilepsies* (National Center for Biotechnology Information (US), 2012).
40. Prince, D. A., Parada, I., Scalise, K., Graber, K. & Shen, F. Epilepsy following cortical injury: cellular and molecular mechanisms as targets for potential prophylaxis. **50**, 30–40 (2010).
41. Ding, M.-C., Wang, Q., Lo, E. H. & Stanley, G. B. Cortical Excitation and Inhibition following Focal Traumatic Brain Injury. *J. Neurosci.* **31**, 14085–14094 (2011).

42. Lei, Z., Deng, P., Li, J. & Xu, Z. C. Alterations of A-Type Potassium Channels in Hippocampal Neurons after Traumatic Brain Injury. *J. Neurotrauma* **29**, 235–245 (2012).
43. Burda, J. E., Bernstein, A. M. & Sofroniew, M. V. Astrocyte roles in traumatic brain injury. *Exp. Neurol.* **275**, 305–315 (2016).
44. Kasthuri, N. & Lichtman, J. W. Neurocartography. *Neuropsychopharmacology* **35**, (2010).
45. Oberlaender, M. *et al.* Three-dimensional axon morphologies of individual layer 5 neurons indicate cell type-specific intracortical pathways for whisker motion and touch. *Proc. Natl. Acad. Sci. U. S. A.* **108**, 4188–93 (2011).
46. Kubota, Y. Untangling GABAergic wiring in the cortical microcircuit. *Curr. Opin. Neurobiol.* **26**, 7–14 (2014).
47. Zhang, Y. & Barres, B. A. Astrocyte heterogeneity: an underappreciated topic in neurobiology. *Curr. Opin. Neurobiol.* **20**, 588–94 (2010).
48. Miocinovic, S., Somayajula, S., Chitnis, S. & Vitek, J. L. History, Applications, and Mechanisms of Deep Brain Stimulation. *JAMA Neurol.* **70**, 163 (2013).
49. Herrington, T. M. *et al.* Mechanisms of deep brain stimulation. *J. Neurophysiol.* **115**, 19–38 (2016).
50. Borton, D., Micera, S., Millán, J. del R. & Courtine, G. Personalized Neuroprosthetics. *Sci. Transl. Med.* **5**, (2013).
51. Jennings, J. H. & Stuber, G. D. Tools for resolving functional activity and connectivity within intact neural circuits. *Curr. Biol.* **24**, R41–R50 (2014).
52. Prasad, A. *et al.* Comprehensive characterization and failure modes of tungsten microwire arrays in chronic neural implants. *J. Neural Eng.* **9**, 056015 (2012).
53. Barrese, J. C. *et al.* Failure mode analysis of silicon-based intracortical microelectrode arrays in non-human primates. *J. Neural Eng.* **10**, 066014 (2013).
54. Ludwig, K. A. *et al.* Poly(3,4-ethylenedioxythiophene) (PEDOT) polymer coatings facilitate smaller neural recording electrodes. *J. Neural Eng.* **8**, 014001 (2011).
55. McCreery, D. B., Yuen, T. G. H., Agnew, W. F. & Bullara, L. A. A characterization of the effects on neuronal excitability due to prolonged microstimulation with chronically implanted microelectrodes. *IEEE Trans. Biomed. Eng.* **44**, 931–939 (1997).
56. McCreery, D. B., Agnew, W. F. & Bullara, L. a. The effects of prolonged intracortical

- microstimulation on the excitability of pyramidal tract neurons in the cat. *Ann. Biomed. Eng.* **30**, 107–119 (2002).
57. Prasad, A. *et al.* Abiotic-biotic characterization of Pt/Ir microelectrode arrays in chronic implants. *Front. Neuroeng.* **7**, 2 (2014).
 58. Cahoy, J. D. *et al.* A Transcriptome Database for Astrocytes, Neurons, and Oligodendrocytes: A New Resource for Understanding Brain Development and Function. *J. Neurosci.* **28**, 264–278 (2008).
 59. Pannasch, U. & Rouach, N. Emerging role for astroglial networks in information processing: from synapse to behavior. *Trends Neurosci.* **36**, 405–17 (2013).
 60. Virchow, R. *Gesammelte abhandlungen zur wissenschaftlichen medicin.* Frankfurt: Meidinger (1856).
 61. Nishiyama, A., Komitova, M., Suzuki, R. & Zhu, X. Polydendrocytes (NG2 cells): multifunctional cells with lineage plasticity. *Nat. Rev. Neurosci.* **10**, 9–22 (2009).
 62. Richardson, W. D., Young, K. M., Tripathi, R. B. & McKenzie, I. NG2-glia as multipotent neural stem cells: fact or fantasy? *Neuron* **70**, 661–73 (2011).
 63. Dimou, L. & Gallo, V. NG2-Glia and Their Functions in the Central Nervous System. *Glia* **63**, 1429–1451 (2015).
 64. Crisan, M. *et al.* A Perivascular Origin for Mesenchymal Stem Cells in Multiple Human Organs. *Cell Stem Cell* **3**, 301–313 (2008).
 65. Scadden, D. T. The stem-cell niche as an entity of action. *Nature* **441**, 1075–1079 (2006).
 66. Saxena, T. *et al.* The impact of chronic blood–brain barrier breach on intracortical electrode function. *Biomaterials* **34**, 4703–4713 (2013).
 67. Kozai, T. D. Y., Eles, J. R., Vazquez, A. L. & Cui, X. T. Two-photon imaging of chronically implanted neural electrodes: Sealing methods and new insights. *J. Neurosci. Methods* **258**, 46–55 (2016).
 68. Jorfi, M., Skousen, J. L., Weder, C. & Capadona, J. R. Progress towards biocompatible intracortical microelectrodes for neural interfacing applications. *J. Neural Eng.* **12**, 011001 (2015).
 69. Kozai, T. D. Y., Jaquins-Gerstl, Andrea S. Vazquez, A. L., Michael, A. C. & Cui, X. T. Brain Tissue Responses to Neural Implants Impact Signal Sensitivity and Intervention Strategies. *ACS Chem. Neurosci.* **6**, 48–67 (2015).

70. Hall, C. N. *et al.* Capillary pericytes regulate cerebral blood flow in health and disease. *Nature* **508**, 55–60 (2014).
71. Attwell, D. *et al.* Glial and neuronal control of brain blood flow. *Nature* **468**, 232–243 (2010).
72. Fidler, P. S. *et al.* Comparing astrocytic cell lines that are inhibitory or permissive for axon growth: the major axon-inhibitory proteoglycan is NG2. *J. Neurosci.* **19**, 8778–88 (1999).
73. Zhong, Y. & Bellamkonda, R. V. Dexamethasone-coated neural probes elicit attenuated inflammatory response and neuronal loss compared to uncoated neural probes. *Brain Res.* **1148**, 15–27 (2007).
74. Rivers, L. E. *et al.* PDGFRA/NG2 glia generate myelinating oligodendrocytes and piriform projection neurons in adult mice. *Nat. Neurosci.* **11**, 1392–1401 (2008).
75. Kozai, T. D. Y., Vazquez, A. L., Weaver, C. L., Kim, S.-G. & Cui, X. T. In vivo two-photon microscopy reveals immediate microglial reaction to implantation of microelectrode through extension of processes. *J. Neural Eng.* **9**, 066001 (2012).
76. Vedam-Mai, V. *et al.* The national DBS brain tissue network pilot study: need for more tissue and more standardization. *Cell Tissue Bank.* **12**, 219–231 (2011).
77. Malaga, K. A. *et al.* Data-driven model comparing the effects of glial scarring and interface interactions on chronic neural recordings in non-human primates. *J. Neural Eng.* **13**, 016010 (2016).
78. Kipke, D. R., Vetter, R. J., Williams, J. C. & Hetke, J. F. Silicon-substrate intracortical microelectrode arrays for long-term recording of neuronal spike activity in cerebral cortex. *IEEE Trans. Neural Syst. Rehabil. Eng.* **11**, 151–5 (2003).
79. Kindlmann, G. *et al.* Imaging of Utah Electrode Array, Implanted in Cochlear Nerve. *Digit. Biol. Emerg. Paradig.* 6–7 (2003).
80. Moss, J., Ryder, T., Aziz, T. Z., Graeber, M. B. & Bain, P. G. Electron microscopy of tissue adherent to explanted electrodes in dystonia and Parkinson’s disease. *Brain* **127**, 2755–63 (2004).
81. Khakh, B. S. & Sofroniew, M. V. Diversity of astrocyte functions and phenotypes in neural circuits. *Nat. Neurosci.* **18**, 942–952 (2015).
82. Liddel, S. A. *et al.* Neurotoxic reactive astrocytes are induced by activated microglia. *Nature* **541**, 481–487 (2017).
83. Sofroniew, M. V. Astrogliosis. *Cold Spring Harb. Perspect. Biol.* **7**, a020420 (2014).

84. Buffo, A., Rolando, C. & Ceruti, S. Astrocytes in the damaged brain: Molecular and cellular insights into their reactive response and healing potential. *Biochemical Pharmacology* **79**, 77–89 (2010).
85. Eles, J. R. *et al.* Neuroadhesive L1 coating attenuates acute microglial encapsulation of neural electrodes as revealed by live two-photon microscopy. *Biomaterials* **113**, 279–292 (2017).
86. Kozai, T. D. Y. *et al.* Reduction of neurovascular damage resulting from microelectrode insertion into the cerebral cortex using in vivo two-photon mapping. *J. Neural Eng.* **7**, 046011 (2010).
87. Perry, V. H. & Teeling, J. Microglia and macrophages of the central nervous system: the contribution of microglia priming and systemic inflammation to chronic neurodegeneration. *Semin. Immunopathol.* **35**, 601–612 (2013).
88. Sofroniew, M. V. Molecular dissection of reactive astrogliosis and glial scar formation. *Trends Neurosci.* **32**, 638–47 (2009).
89. Chew, S. S. L., Johnson, C. S., Green, C. R. & Danesh-Meyer, H. V. Role of connexin43 in central nervous system injury. *Exp. Neurol.* **225**, 250–261 (2010).
90. Pannasch, U. *et al.* Astroglial networks scale synaptic activity and plasticity. *Proc. Natl. Acad. Sci.* **108**, 8467–8472 (2011).
91. Liu, J. Y. W. *et al.* Neuropathology of the blood–brain barrier and pharmaco-resistance in human epilepsy. *Brain* **135**, 3115–3133 (2012).
92. Nolta, N. F., Christensen, M. B., Crane, P. D., Skousen, J. L. & Tresco, P. A. BBB leakage, astrogliosis, and tissue loss correlate with silicon microelectrode array recording performance. *Biomaterials* **53**, 753–762 (2015).
93. Bekar, L. *et al.* Adenosine is crucial for deep brain stimulation–mediated attenuation of tremor. *Nat. Med.* **14**, 75–80 (2008).
94. Lempka, S. F., Miocinovic, S., Johnson, M. D., Vitek, J. L. & McIntyre, C. C. In vivo impedance spectroscopy of deep brain stimulation electrodes. *J. Neural Eng.* **6**, 046001 (2009).
95. Johnson, M. D., Otto, K. J. & Kipke, D. R. Repeated Voltage Biasing Improves Unit Recordings by Reducing Resistive Tissue Impedances. *IEEE Trans. Neural Syst. Rehabil. Eng.* **13**, 160–165 (2005).
96. Ludwig, K. A. *et al.* Chronic neural recordings using silicon microelectrode arrays electrochemically deposited with a poly(3,4-ethylenedioxythiophene) (PEDOT) film. *J. Neural Eng.* **3**, 59–70 (2006).

97. Prasad, A. *et al.* Quantifying long-term microelectrode array functionality using chronic in vivo impedance testing. *J. Neural Eng.* **9**, 026028 (2012).
98. Sofroniew, M. V. Molecular dissection of reactive astrogliosis and glial scar formation. *Trends Neurosci.* **32**, 638–47 (2009).
99. McConnell, G. C. *et al.* Implanted neural electrodes cause chronic, local inflammation that is correlated with local neurodegeneration. *J. Neural Eng.* **6**, 056003 (2009).
100. Tawfik, V. L. *et al.* Deep brain stimulation results in local glutamate and adenosine release: investigation into the role of astrocytes. *Neurosurgery* **67**, 367–75 (2010).
101. McAdams, E. T., Lacknermeier, A., McLaughlin, J. A., Macken, D. & Jossinet, J. The linear and non-linear electrical properties of the electrode-electrolyte interface. *Biosens. Bioelectron.* **10**, 67–74 (1995).
102. Mercanzini, A., Colin, P., Bensadoun, J.-C., Bertsch, A. & Renaud, P. In Vivo Electrical Impedance Spectroscopy of Tissue Reaction to Microelectrode Arrays. *IEEE Trans. Biomed. Eng.* **56**, 1909–1918 (2009).
103. Kozai, T. D. Y. *et al.* Ultrasmall implantable composite microelectrodes with bioactive surfaces for chronic neural interfaces. *Nat. Mater.* **11**, 1065–73 (2012).
104. Robblee, L. S., McHardy, J., Agnew, W. F. & Bullara, L. A. Electrical stimulation with Pt electrodes. VII. Dissolution of Pt electrodes during electrical stimulation of the cat cerebral cortex. *J. Neurosci. Methods* **9**, 301–308 (1983).
105. Wei, X. F. *et al.* Impedance characteristics of deep brain stimulation electrodes *in vitro* and *in vivo*. *J. Neural Eng.* **6**, 046008 (2009).
106. Merrill, D. R., Bikson, M. & Jefferys, J. G. R. Electrical stimulation of excitable tissue: design of efficacious and safe protocols. *J. Neurosci. Methods* **141**, 171–198 (2005).
107. Otto, K. J., Johnson, M. D. & Kipke, D. R. Voltage Pulses Change Neural Interface Properties and Improve Unit Recordings With Chronically Implanted Microelectrodes. *IEEE Trans. Biomed. Eng.* **53**, 333–340 (2006).
108. Keese, C. R., Wegener, J., Walker, S. R. & Giaever, I. Electrical wound-healing assay for cells in vitro. *Proc. Natl. Acad. Sci. U. S. A.* **101**, 1554–9 (2004).
109. Kilgore, K. L. & Bhadra, N. Nerve conduction block utilising high-frequency alternating current. *Med. Biol. Eng. Comput.* **42**, 394–406 (2004).
110. McIntyre, C. C. *et al.* Extracellular stimulation of central neurons: influence of stimulus waveform and frequency on neuronal output. *J. Neurophysiol.* **88**, 1592–604 (2002).

111. Nowak, L. G. & Bullier, J. Axons, but not cell bodies, are activated by electrical stimulation in cortical gray matter. *Exp. Brain Res.* **118**, 477–488 (1998).
112. Williams, J. C., Rennaker, R. L. & Kipke, D. R. Long-term neural recording characteristics of wire microelectrode arrays implanted in cerebral cortex. *Brain Res. Protoc.* **4**, 303–313 (1999).
113. Preda, F. *et al.* Switching from constant voltage to constant current in deep brain stimulation: a multicenter experience of mixed implants for movement disorders. *Eur. J. Neurol.* **23**, 190–195 (2016).
114. Timmermann, L. *et al.* Multiple-source current steering in subthalamic nucleus deep brain stimulation for Parkinson’s disease (the VANTAGE study): a non-randomised, prospective, multicentre, open-label study. *Lancet Neurol.* **14**, 693–701 (2015).
115. McCreery, D. *et al.* Correlations between histology and neuronal activity recorded by microelectrodes implanted chronically in the cerebral cortex. *J. Neural Eng.* **13**, 036012 (2016).
116. Williams, J. C., Hippensteel, J. A., Dilgen, J., Shain, W. & Kipke, D. R. Complex impedance spectroscopy for monitoring tissue responses to inserted neural implants. *J. Neural Eng.* **4**, 410–423 (2007).
117. Ludwig, K. A. *et al.* Using a Common Average Reference to Improve Cortical Neuron Recordings From Microelectrode Arrays. *J. Neurophysiol.* **101**, (2009).
118. Suner, S., Fellows, M. R., Vargas-Irwin, C., Nakata, G. K. & Donoghue, J. P. Reliability of Signals From a Chronically Implanted, Silicon-Based Electrode Array in Non-Human Primate Primary Motor Cortex. *IEEE Trans. Neural Syst. Rehabil. Eng.* **13**, 524–541 (2005).
119. Jiang, J., Willett, F. R. & Taylor, D. M. Relationship between microelectrode array impedance and chronic recording quality of single units and local field potentials. in *2014 36th Annual International Conference of the IEEE Engineering in Medicine and Biology Society* 3045–3048 (IEEE, 2014). doi:10.1109/EMBC.2014.6944265
120. Kozai, T. D. Y. *et al.* Mechanical failure modes of chronically implanted planar silicon-based neural probes for laminar recording. *Biomaterials* **37**, 25–39 (2015).
121. Jiang, J., Willett, F. R. & Taylor, D. M. Relationship between microelectrode array impedance and chronic recording quality of single units and local field potentials. in *2014 36th Annual International Conference of the IEEE Engineering in Medicine and Biology Society* 3045–3048 (IEEE, 2014). doi:10.1109/EMBC.2014.6944265
122. Malaga, K. A. *et al.* Data-driven model comparing the effects of glial scarring and interface interactions on chronic neural recordings in non-human primates. *J. Neural*

- Eng.* **13**, 016010 (2016).
123. Humphrey, D. R. & Schmidt, E. M. Extracellular Single-Unit Recording Methods. in *Neurophysiological Techniques, II* 1–64 (Humana Press, 1990). doi:10.1385/0-89603-185-3:1
 124. Shoham, S. & Nagarajan, S. The theory of central nervous system recording. in *Neuroprosthetics: theory and practice* 448–465 (2003).
 125. Alivisatos, A. P. *et al.* Nanotools for neuroscience and brain activity mapping. *ACS Nano* **7**, 1850–66 (2013).
 126. Clark, J. J. *et al.* Chronic microsensors for longitudinal, subsecond dopamine detection in behaving animals. *Nat. Methods* **7**, 126–129 (2010).
 127. Grahn, P. J. *et al.* A neurochemical closed-loop controller for deep brain stimulation: toward individualized smart neuromodulation therapies. *Front. Neurosci.* **8**, 169 (2014).
 128. Hascup, E. R. *et al.* Histological studies of the effects of chronic implantation of ceramic-based microelectrode arrays and microdialysis probes in rat prefrontal cortex. *Brain Res.* **1291**, 12–20 (2009).
 129. Phillips, P. E. M. & Wightman, R. M. Critical guidelines for validation of the selectivity of in-vivo chemical microsensors. *TrAC Trends Anal. Chem.* **22**, 509–514 (2003).
 130. Roitbak, T. & Sykov, E. Diffusion Barriers Evoked in the Rat Cortex by Reactive Astrogliosis. *Glia* **28**, 40–48 (1999).
 131. Hascup, E. R. *et al.* Rapid microelectrode measurements and the origin and regulation of extracellular glutamate in rat prefrontal cortex. *J. Neurochem.* **115**, 1608–1620 (2010).
 132. Melendez, R. I., Vuthiganon, J. & Kalivas, P. W. Regulation of Extracellular Glutamate in the Prefrontal Cortex: Focus on the Cystine Glutamate Exchanger and Group I Metabotropic Glutamate Receptors. *J. Pharmacol. Exp. Ther.* **314**, 139–147 (2005).
 133. Hille, B. *Ion channels of excitable membranes.* **507**, (Sinauer Sunderland, MA, 2001).
 134. Pietrobon, D. & Moskowitz, M. A. Chaos and commotion in the wake of cortical spreading depression and spreading depolarizations. *Nat. Rev. Neurosci.* **15**, 379–393 (2014).
 135. Haupt, C., Witte, O. W. & Frahm, C. Up-regulation of Connexin43 in the glial scar following photothrombotic ischemic injury. *Mol. Cell. Neurosci.* **35**, 89–99 (2007).

136. Karumbaiah, L. *et al.* Relationship between intracortical electrode design and chronic recording function. *Biomaterials* **34**, 8061–8074 (2013).
137. Karumbaiah, L. *et al.* The upregulation of specific interleukin (IL) receptor antagonists and paradoxical enhancement of neuronal apoptosis due to electrode induced strain and brain micromotion. *Biomaterials* **33**, 5983–5996 (2012).
138. Kozai, T. D. Y. *et al.* Effects of caspase-1 knockout on chronic neural recording quality and longevity: insight into cellular and molecular mechanisms of the reactive tissue response. *Biomaterials* **35**, 9620–34 (2014).
139. Vezzani, A. & Viviani, B. Neuromodulatory properties of inflammatory cytokines and their impact on neuronal excitability. *Neuropharmacology* **96**, 70–82 (2015).
140. Vezzani, A., French, J., Bartfai, T. & Baram, T. Z. The role of inflammation in epilepsy. *Nat. Rev. Neurol.* **7**, 31–40 (2011).
141. Zhou, C. *et al.* Interleukin-1 β Inhibits Voltage-Gated Sodium Currents in a Time- and Dose-Dependent Manner in Cortical Neurons. *Neurochem. Res.* **36**, 1116–1123 (2011).
142. Li, X., Chen, W., Sheng, J., Cao, D. & Wang, W. Interleukin-6 inhibits voltage-gated sodium channel activity of cultured rat spinal cord neurons. *Acta Neuropsychiatr.* **26**, 170–177 (2014).
143. Zhou, C., Ye, H.-H., Wang, S.-Q. & Chai, Z. *Interleukin-1 β regulation of N-type Ca²⁺ channels in cortical neurons.* *Neuroscience Letters* **403**, (2006).
144. Ma, S.-H., Li, B., Huang, H.-W., Peng, Y.-P. & Qiu, Y.-H. Interleukin-6 inhibits L-type calcium channel activity of cultured cerebellar granule neurons. *J. Physiol. Sci.* **62**, 385–392 (2012).
145. Liu, Z., Qiu, Y.-H., Li, B., Ma, S.-H. & Peng, Y.-P. Neuroprotection of Interleukin-6 Against NMDA-Induced Apoptosis and Its Signal-Transduction Mechanisms. *Neurotox. Res.* **19**, 484–495 (2011).
146. Baldwin, K. T. & Eroglu, C. Molecular mechanisms of astrocyte-induced synaptogenesis. *Curr. Opin. Neurobiol.* **45**, 113–120 (2017).
147. Salatino, J. W., Winter, B. M., Drazin, M. H. & Purcell, E. K. Functional remodeling of subtype-specific markers surrounding implanted neuroprostheses. *J. Neurophysiol.* **118**, (2017).
148. Weissberg, I. *et al.* Albumin induces excitatory synaptogenesis through astrocytic TGF- β /ALK5 signaling in a model of acquired epilepsy following blood-brain barrier dysfunction. *Neurobiol. Dis.* **78**, 115–25 (2015).

149. Diniz, L. P. *et al.* Astrocyte transforming growth factor beta 1 promotes inhibitory synapse formation via CaM kinase II signaling. *Glia* **62**, 1917–1931 (2014).
150. Lin, T. -n. *et al.* Differential Regulation of Thrombospondin-1 and Thrombospondin-2 After Focal Cerebral Ischemia/Reperfusion. *Stroke* **34**, 177–186 (2003).
151. Carsten Möller, J. *et al.* Regulation of thrombospondin in the regenerating mouse facial motor nucleus. *Glia* **17**, 121–132 (1996).
152. Tran, M. D. & Neary, J. T. Purinergic signaling induces thrombospondin-1 expression in astrocytes. *Proc. Natl. Acad. Sci.* **103**, 9321–9326 (2006).
153. Christopherson, K. S. *et al.* Thrombospondins are astrocyte-secreted proteins that promote CNS synaptogenesis. *Cell* **120**, 421–33 (2005).
154. Kerchner, G. A. & Nicoll, R. A. Silent synapses and the emergence of a postsynaptic mechanism for LTP. *Nat. Rev. Neurosci.* **9**, 813–825 (2008).
155. Stellwagen, D. & Malenka, R. C. Synaptic scaling mediated by glial TNF- α . *Nature* **440**, 1054–1059 (2006).
156. Beattie, E. C. *et al.* Control of synaptic strength by glial TNF α . *Science* **295**, 2282–5 (2002).
157. Salatino, J. W., Ludwig, K. A., Kozai, T. D. Y. & Purcell, E. K. Glial responses to implanted electrodes in the brain. *Nat. Biomed. Eng.* **1**, 862–877 (2017).
158. Chang, S.-Y., Shon, Y. M., Agnesi, F. & Lee, K. H. Microthalamotomy effect during deep brain stimulation: Potential involvement of adenosine and glutamate efflux. in *2009 Annual International Conference of the IEEE Engineering in Medicine and Biology Society* 3294–3297 (IEEE, 2009). doi:10.1109/IEMBS.2009.5333735
159. Dunwiddie, T. V, Diao, L. & Proctor, W. R. Adenine nucleotides undergo rapid, quantitative conversion to adenosine in the extracellular space in rat hippocampus. *J. Neurosci.* **17**, 7673–82 (1997).
160. FREDHOLM, B. & DUNWIDDIE, T. How does adenosine inhibit transmitter release? *Trends Pharmacol. Sci.* **9**, 130–134 (1988).
161. Dunwiddie, T. V & Fredholm, B. B. Adenosine A1 receptors inhibit adenylate cyclase activity and neurotransmitter release and hyperpolarize pyramidal neurons in rat hippocampus. *J. Pharmacol. Exp. Ther.* **249**, 31–7 (1989).
162. Stone, T. W., Ceruti, S. & Abbracchio, M. P. Adenosine Receptors and Neurological Disease: Neuroprotection and Neurodegeneration. in 535–587 (Springer, Berlin, Heidelberg, 2009). doi:10.1007/978-3-540-89615-9_17

163. Ben Achour, S. & Pascual, O. Glia: the many ways to modulate synaptic plasticity. *Neurochem. Int.* **57**, 440–5 (2010).
164. Gradinaru, V., Mogri, M., Thompson, K. R., Henderson, J. M. & Deisseroth, K. Optical deconstruction of parkinsonian neural circuitry. *Science* **324**, 354–9 (2009).
165. Amiri, M., Montaseri, G. & Bahrami, F. On the role of astrocytes in synchronization of two coupled neurons: a mathematical perspective. *Biol. Cybern.* **105**, 153–166 (2011).
166. Agulhon, C., Fiacco, T. A. & McCarthy, K. D. Hippocampal short- and long-term plasticity are not modulated by astrocyte Ca²⁺ signaling. *Science* **327**, 1250–4 (2010).
167. Strogatz, S. H. Exploring complex networks. *Nature* **410**, 268–276 (2001).
168. Perea, G. & Araque, A. Astrocytes potentiate transmitter release at single hippocampal synapses. *Science* **317**, 1083–6 (2007).
169. Newman, E. A. New roles for astrocytes: Regulation of synaptic transmission. *Trends Neurosci.* **26**, 536–542 (2003).
170. Wetherington, J., Serrano, G. & Dingledine, R. Astrocytes in the Epileptic Brain. *Neuron* (2008). doi:10.1016/j.neuron.2008.04.002
171. Fellin, T. *et al.* Neuronal Synchrony Mediated by Astrocytic Glutamate through Activation of Extrasynaptic NMDA Receptors. *Neuron* **43**, 729–743 (2004).
172. Silchenko, A. N. & Tass, P. A. Computational modeling of paroxysmal depolarization shifts in neurons induced by the glutamate release from astrocytes. *Biol. Cybern.* **98**, 61–74 (2008).
173. Uhlhaas, P. J. & Singer, W. Neural Synchrony in Brain Disorders: Relevance for Cognitive Dysfunctions and Pathophysiology. *Neuron* **52**, 155–168 (2006).
174. Norden, D. M., Muccigrosso, M. M. & Godbout, J. P. Microglial priming and enhanced reactivity to secondary insult in aging, and traumatic CNS injury, and neurodegenerative disease. *Neuropharmacology* **96**, 29–41 (2015).
175. Vedam-Mai, V. *et al.* Deep brain stimulation and the role of astrocytes. *Mol. Psychiatry* **17**, 124–31, 115 (2012).
176. McIntyre, C. C. & Anderson, R. W. Deep brain stimulation mechanisms: the control of network activity via neurochemistry modulation. *J. Neurochem.* **139**, 338–345 (2016).
177. Fenoy, A. J., Goetz, L., Chabard?s, S. & Xia, Y. Deep Brain Stimulation: Are Astrocytes a Key Driver Behind the Scene? *CNS Neurosci. Ther.* **20**, 191–201 (2014).

178. Sun, D. A. *et al.* Postmortem analysis following 71 months of deep brain stimulation of the subthalamic nucleus for Parkinson disease. *J. Neurosurg.* **109**, 325–329 (2008).
179. van Kuyck, K., Welkenhuysen, M., Arckens, L., Sciot, R. & Nuttin, B. Histological Alterations Induced by Electrode Implantation and Electrical Stimulation in the Human Brain: A Review. *Neuromodulation Technol. Neural Interface* **10**, 244–261 (2007).
180. Chang, S.-Y. *et al.* Wireless Fast-Scan Cyclic Voltammetry to Monitor Adenosine in Patients With Essential Tremor During Deep Brain Stimulation. *Mayo Clin. Proc.* **87**, 760–765 (2012).
181. Van Gompel, J. J. *et al.* Increased cortical extracellular adenosine correlates with seizure termination. *Epilepsia* **55**, 233–44 (2014).
182. Santello, M. & Volterra, A. TNF α in synaptic function: switching gears. *Trends Neurosci.* **35**, 638–647 (2012).
183. Gellner, A.-K., Reis, J. & Fritsch, B. Glia: A Neglected Player in Non-invasive Direct Current Brain Stimulation. *Front. Cell. Neurosci.* **10**, 188 (2016).
184. Monai, H. *et al.* Calcium imaging reveals glial involvement in transcranial direct current stimulation-induced plasticity in mouse brain. *Nat. Commun.* **7**, 11100 (2016).
185. Sasaki, T. *et al.* Application of an optogenetic byway for perturbing neuronal activity via glial photostimulation. *Proc. Natl. Acad. Sci. U. S. A.* **109**, 20720–5 (2012).
186. Braun, R. *et al.* Transcranial direct current stimulation accelerates recovery of function, induces neurogenesis and recruits oligodendrocyte precursors in a rat model of stroke. *Exp. Neurol.* **279**, 127–136 (2016).
187. Arsenault, D. *et al.* A novel combinational approach of microstimulation and bioluminescence imaging to study the mechanisms of action of cerebral electrical stimulation in mice. *J. Physiol.* **593**, 2257–2278 (2015).
188. Matsuo, H. *et al.* Early transcutaneous electrical nerve stimulation reduces hyperalgesia and decreases activation of spinal glial cells in mice with neuropathic pain. *Pain* **155**, 1888–1901 (2014).
189. Peruzzotti-Jametti, L. *et al.* Safety and Efficacy of Transcranial Direct Current Stimulation in Acute Experimental Ischemic Stroke. *Stroke* **44**, 3166–3174 (2013).
190. Iwasa, S. N., Babona-Pilipos, R. & Morshead, C. M. Environmental Factors That Influence Stem Cell Migration: An “Electric Field”. *Stem Cells Int.* **2017**, 4276927 (2017).

191. Vedam-Mai, V. *et al.* Increased Precursor Cell Proliferation after Deep Brain Stimulation for Parkinson's Disease: A Human Study. *PLoS One* **9**, e88770 (2014).
192. Toda, H., Hamani, C., Fawcett, A. P., Hutchison, W. D. & Lozano, A. M. The regulation of adult rodent hippocampal neurogenesis by deep brain stimulation. *J. Neurosurg.* **108**, 132–138 (2008).
193. Encinas, J. M., Hamani, C., Lozano, A. M. & Enikolopov, G. Neurogenic hippocampal targets of deep brain stimulation. *J. Comp. Neurol.* **519**, 6–20 (2011).
194. Babona-Pilipos, R., Pritchard-Oh, A., Popovic, M. R. & Morshead, C. M. Biphasic monopolar electrical stimulation induces rapid and directed galvanotaxis in adult subependymal neural precursors. *Stem Cell Res. Ther.* **6**, 67 (2015).
195. Rueger, M. A. *et al.* Multi-session transcranial direct current stimulation (tDCS) elicits inflammatory and regenerative processes in the rat brain. *PLoS One* **7**, e43776 (2012).
196. Zhao, H., Steiger, A., Nohner, M. & Ye, H. Specific Intensity Direct Current (DC) Electric Field Improves Neural Stem Cell Migration and Enhances Differentiation towards β III-Tubulin+ Neurons. *PLoS One* **10**, e0129625 (2015).
197. Khaindrava, V. *et al.* High frequency stimulation of the subthalamic nucleus impacts adult neurogenesis in a rat model of Parkinson's disease. *Neurobiol. Dis.* **42**, 284–291 (2011).
198. Zonta, M. *et al.* Neuron-to-astrocyte signaling is central to the dynamic control of brain microcirculation. *Nat. Neurosci.* (2003). doi:10.1038/nn980
199. Filosa, J. A., Bonev, A. D. & Nelson, M. T. Calcium Dynamics in Cortical Astrocytes and Arterioles During Neurovascular Coupling. *Circ. Res.* **95**, (2004).
200. Takano, T. *et al.* Astrocyte-mediated control of cerebral blood flow. doi:10.1038/nn1623
201. Ke, B., Liu, T.-T., Liu, C., Xiang, H. & Xiong, J. Dorsal subthalamic nucleus electrical stimulation for drug/treatment-refractory epilepsy may modulate melanocortinerbic signaling in astrocytes. *Epilepsy Behav.* **36**, 6–8 (2014).
202. Seymour, J. P., Wu, F., Wise, K. D. & Yoon, E. State-of-the-art MEMS and microsystem tools for brain research. *Microsystems Nanoeng.* **3**, 16066 (2017).
203. Seymour, J. P. & Kipke, D. R. Neural probe design for reduced tissue encapsulation in CNS. *Biomaterials* **28**, 3594–3607 (2007).
204. Loane, D. J. *et al.* Progressive neurodegeneration after experimental brain trauma: association with chronic microglial activation. *J. Neuropathol. Exp. Neurol.* **73**, 14–29 (2014).

205. Johnson, V. E. *et al.* Inflammation and white matter degeneration persist for years after a single traumatic brain injury. *Brain* **136**, 28–42 (2013).
206. Perry, V. H., Nicoll, J. A. R. & Holmes, C. Microglia in neurodegenerative disease. *Nat. Rev. Neurol.* **6**, 193–201 (2010).
207. Glass, C. K., Saijo, K., Winner, B., Marchetto, M. C. & Gage, F. H. Mechanisms Underlying Inflammation in Neurodegeneration. *Cell* **140**, 918–934 (2010).
208. Frank, M. G. *et al.* mRNA up-regulation of MHC II and pivotal pro-inflammatory genes in normal brain aging. *Neurobiol. Aging* **27**, 717–722 (2006).
209. Henry, C. J., Huang, Y., Wynne, A. M. & Godbout, J. P. Peripheral lipopolysaccharide (LPS) challenge promotes microglial hyperactivity in aged mice that is associated with exaggerated induction of both pro-inflammatory IL-1 β and anti-inflammatory IL-10 cytokines. *Brain. Behav. Immun.* **23**, 309–317 (2009).
210. Cunningham, C., Wilcockson, D. C., Champion, S., Lunnon, K. & Perry, V. H. Central and Systemic Endotoxin Challenges Exacerbate the Local Inflammatory Response and Increase Neuronal Death during Chronic Neurodegeneration. *J. Neurosci.* **25**, 9275–9284 (2005).
211. Vezzani, A., French, J., Bartfai, T. & Baram, T. Z. The role of inflammation in epilepsy. *Nat. Rev. Neurol.* **7**, 31–40 (2011).
212. Moshayedi, P. *et al.* The relationship between glial cell mechanosensitivity and foreign body reactions in the central nervous system. *Biomaterials* **35**, 3919–3925 (2014).
213. Velliste, M., Perel, S., Spalding, M. C., Whitford, A. S. & Schwartz, A. B. Cortical control of a prosthetic arm for self-feeding. *Nature* **453**, 1098–101 (2008).
214. Collinger, J. L. *et al.* High-performance neuroprosthetic control by an individual with tetraplegia. *Lancet* **381**, 557–564 (2013).
215. Nguyen, J. K. *et al.* Mechanically-compliant intracortical implants reduce the neuroinflammatory response. *J. Neural Eng.* **11**, 056014 (2014).
216. Kolarcik, C. L. *et al.* Elastomeric and soft conducting microwires for implantable neural interfaces. *Soft Matter* **11**, 4847–61 (2015).
217. Hess, A. E. *et al.* Development of a stimuli-responsive polymer nanocomposite toward biologically optimized, MEMS-based neural probes. *J. Micromechanics Microengineering* **21**, 054009 (2011).
218. Ware, T. *et al.* Thiol-ene/acrylate substrates for softening intracortical electrodes. *J. Biomed. Mater. Res. Part B Appl. Biomater.* **102**, 1–11 (2014).

219. Ware, T. *et al.* Fabrication of responsive, softening neural interfaces. *Adv. Funct. Mater.* **22**, 3470–3479 (2012).
220. Capadona, J. R. *et al.* Mechanically adaptive nanocomposites for neural interfacing. *MRS Bull.* **37**, 581–589 (2012).
221. Hess, A. E. *et al.* Development of a stimuli-responsive polymer nanocomposite toward biologically optimized, MEMS-based neural probes. *J. Micromechanics Microengineering* **21**, 054009 (2011).
222. Capadona, J. R., Shanmuganathan, K., Tyler, D. J., Rowan, S. J. & Weder, C. Stimuli-responsive polymer nanocomposites inspired by the sea cucumber dermis. *Science (80-.)*. **319**, 1370–1374 (2008).
223. Harris, J. P. *et al.* Mechanically adaptive intracortical implants improve the proximity of neuronal cell bodies. *J. Neural Eng.* **8**, 066011 (2011).
224. Ware, T. *et al.* Three-Dimensional Flexible Electronics Enabled by Shape Memory Polymer Substrates for Responsive Neural Interfaces. *Macromol. Mater. Eng.* **297**, 1193–1202 (2012).
225. Seymour, J. P. & Kipke, D. R. Neural probe design for reduced tissue encapsulation in CNS. *Biomaterials* **28**, 3594–607 (2007).
226. Hong, G. *et al.* Syringe Injectable Electronics: Precise Targeted Delivery with Quantitative Input/Output Connectivity. *Nano Lett.* **15**, 6979–6984 (2015).
227. Fu, T.-M. *et al.* Stable long-term chronic brain mapping at the single-neuron level. *Nat. Methods* (2016). doi:10.1038/nmeth.3969
228. Chen, R., Canales, A. & Anikeeva, P. Neural recording and modulation technologies. *Nat. Rev. Mater.* **2**, 16093 (2017).
229. Luan, L. *et al.* Ultraflexible nanoelectronic probes form reliable, glial scar-free neural integration. *Sci. Adv.* **3**, (2017).
230. Kim, B. J. *et al.* 3D Parylene sheath neural probe for chronic recordings. *J. Neural Eng.* **10**, 45002 (2013).
231. Metallo, C. & Trimmer, B. A. Silk coating as a novel delivery system and reversible adhesive for stiffening and shaping flexible probes. *J. Biol. Methods* **2**, e13 (2015).
232. Kozai, T. D. Y. *et al.* Chronic tissue response to carboxymethyl cellulose based dissolvable insertion needle for ultra-small neural probes. *Biomaterials* **35**, 9255–9268 (2014).

233. Seymour, J. P., Langhals, N. B., Anderson, D. J. & Kipke, D. R. Novel multi-sided, microelectrode arrays for implantable neural applications. *Biomed. Microdevices* **13**, 441–51 (2011).
234. Skousen, J. L. *et al.* Reducing surface area while maintaining implant penetrating profile lowers the brain foreign body response to chronically implanted planar silicon microelectrode arrays. *Prog. Brain Res.* **194**, 167–80 (2011).
235. Chen, C. S., Mrksich, M., Huang, S., Whitesides, G. M. & Ingber, D. E. Geometric Control of Cell Life and Death. *Science (80-.)*. **276**, (1997).
236. Chen, C. S., Tan, J. & Tien, J. Mechanotransduction at Cell-Matrix and Cell-Cell Contacts. *Annu. Rev. Biomed. Eng.* **6**, 275–302 (2004).
237. Turner, A. M. P. *et al.* Attachment of astroglial cells to microfabricated pillar arrays of different geometries. *J. Biomed. Mater. Res.* **51**, 430–441 (2000).
238. Sanders, J. E., Stiles, C. E. & Hayes, C. L. Tissue response to single-polymer fibers of varying diameters: Evaluation of fibrous encapsulation and macrophage density. *J. Biomed. Mater. Res.* **52**, 231–237 (2000).
239. Bernatchez, S., Parks, P. J. & Gibbons, D. F. Interaction of macrophages with fibrous materials in vitro. *Biomaterials* **17**, 2077–2086 (1996).
240. Gällentoft, L. *et al.* Size-dependent long-term tissue response to biostable nanowires in the brain. *Biomaterials* **42**, 172–183 (2015).
241. Kim, T. *et al.* Injectable, cellular-scale optoelectronics with applications for wireless optogenetics. *Science* **340**, 211–6 (2013).
242. Skousen, J. L., Bridge, M. J. & Tresco, P. A. A strategy to passively reduce neuroinflammation surrounding devices implanted chronically in brain tissue by manipulating device surface permeability. *Biomaterials* **36**, 33–43 (2015).
243. Saxena, T. & Bellamkonda, R. V. Implantable electronics: A sensor web for neurons. *Nat Mater* **14**, 1190–1191 (2015).
244. Xie, C. *et al.* Three-dimensional macroporous nanoelectronic networks as minimally invasive brain probes. (2015). doi:10.1038/NMAT4427
245. Liu, J. *et al.* Syringe-injectable electronics. *Nat. Nanotechnol.* **10**, 629–36 (2015).
246. Fattahi, P., Yang, G., Kim, G. & Abidian, M. R. A review of organic and inorganic biomaterials for neural interfaces. *Adv. Mater.* **26**, 1846–85 (2014).
247. Green, R. & Abidian, M. R. Conducting Polymers for Neural Prosthetic and Neural

- Interface Applications. *Adv. Mater.* **27**, 7620–7637 (2015).
248. Kolarcik, C. L. *et al.* In vivo effects of L1 coating on inflammation and neuronal health at the electrode–tissue interface in rat spinal cord and dorsal root ganglion. *Acta Biomater.* **8**, 3561–3575 (2012).
 249. Rao, L., Zhou, H., Li, T., Li, C. & Duan, Y. Y. Polyethylene glycol-containing polyurethane hydrogel coatings for improving the biocompatibility of neural electrodes. *Acta Biomater.* **8**, 2233–2242 (2012).
 250. Kim, D.-H. *et al.* Dissolvable films of silk fibroin for ultrathin conformal bio-integrated electronics. *Nat. Mater.* **9**, 511–517 (2010).
 251. Tien, L. W. *et al.* Silk as a Multifunctional Biomaterial Substrate for Reduced Glial Scarring around Brain-Penetrating Electrodes. *Adv. Funct. Mater.* **23**, 3185–3193 (2013).
 252. He, W., McConnell, G. C., Schneider, T. M. & Bellamkonda, R. V. A Novel Anti-inflammatory Surface for Neural Electrodes. *Adv. Mater.* **19**, 3529–3533 (2007).
 253. Mercanzini, A. *et al.* Controlled release nanoparticle-embedded coatings reduce the tissue reaction to neuroprostheses. *J. Control. Release* **145**, 196–202 (2010).
 254. Abidian, M. R. & Martin, D. C. Multifunctional Nanobiomaterials for Neural Interfaces. *Adv. Funct. Mater.* **19**, 573–585 (2009).
 255. Bezuidenhout, D. *et al.* Covalent incorporation and controlled release of active dexamethasone from injectable polyethylene glycol hydrogels. *J. Biomed. Mater. Res. Part A* **101A**, 1311–1318 (2013).
 256. Gutowski, S. M. *et al.* Protease-degradable PEG-maleimide coating with on-demand release of IL-1Ra to improve tissue response to neural electrodes. *Biomaterials* **44**, 55–70 (2015).
 257. Wadhwa, R., Lagenaur, C. F. & Cui, X. T. Electrochemically controlled release of dexamethasone from conducting polymer polypyrrole coated electrode. *J. Control. Release* **110**, 531–541 (2006).
 258. Abidian, M. R., Ludwig, K. A., Marzullo, T. C., Martin, D. C. & Kipke, D. R. Interfacing Conducting Polymer Nanotubes with the Central Nervous System: Chronic Neural Recording using Poly(3,4-ethylenedioxythiophene) Nanotubes. *Adv. Mater.* **21**, 3764–3770 (2009).
 259. Kim, Y. *et al.* Stretchable nanoparticle conductors with self-organized conductive pathways. *Nature* **500**, 59–63 (2013).

260. Keefer, E. W., Botterman, B. R., Romero, M. I., Rossi, A. F. & Gross, G. W. Carbon nanotube coating improves neuronal recordings. *Nat. Nanotechnol.* **3**, 434–439 (2008).
261. Abidian, M. R., Corey, J. M., Kipke, D. R. & Martin, D. C. Conducting-polymer nanotubes improve electrical properties, mechanical adhesion, neural attachment, and neurite outgrowth of neural electrodes. *Small* **6**, 421–9 (2010).
262. Singh, A. V *et al.* Astrocytes increase ATP exocytosis mediated calcium signaling in response to microgroove structures. *Sci. Rep.* **5**, 7847 (2015).
263. Min, S. K. *et al.* Effect of topography of an electrospun nanofiber on modulation of activity of primary rat astrocytes. *Neurosci. Lett.* **534**, 80–84 (2013).
264. Zuidema, J. M. *et al.* Enhanced GLT-1 mediated glutamate uptake and migration of primary astrocytes directed by fibronectin-coated electrospun poly-l-lactic acid fibers. *Biomaterials* **35**, 1439–1449 (2014).
265. Vishwakarma, A. *et al.* Engineering Immunomodulatory Biomaterials To Tune the Inflammatory Response. *Trends Biotechnol.* **34**, 470–482 (2016).
266. Webber, M. J., Appel, E. A., Meijer, E. W. & Langer, R. Supramolecular biomaterials. *Nat. Mater.* **15**, 13–26 (2016).
267. Lu, Y., Aimetti, A. A., Langer, R. & Gu, Z. Bioresponsive materials. *Nat. Rev. Mater.* **2**, 16075 (2016).
268. Jackson, A., Mavoori, J. & Fetz, E. E. Long-term motor cortex plasticity induced by an electronic neural implant. **444**, 2–6 (2006).
269. Hampson, R. E. *et al.* NIH Public Access. **10**, 1–26 (2014).
270. Herrington, T. M., Cheng, J. J. & Eskandar, E. N. Mechanisms of deep brain stimulation. *J. Neurophysiol.* **115**, 19–38 (2016).
271. Fishell, G. & Heintz, N. The Neuron Identity Problem: Form Meets Function. *Neuron* **80**, 602–612 (2013).
272. Bullmore, E. & Sporns, O. Complex brain networks: graph theoretical analysis of structural and functional systems. *Nat. Rev. Neurosci.* **10**, 186–198 (2009).
273. Yu, S., Huang, D., Singer, W. & Nikolic, D. A small world of neuronal synchrony. *Cereb. Cortex* **18**, 2891–901 (2008).
274. Huang, D. & Pipa, G. Achieving synchronization of networks by an auxiliary hub. *EPL* **77**, (2007).

275. Yizhar, O., Fenno, L. E., Davidson, T. J., Mogri, M. & Deisseroth, K. Optogenetics in Neural Systems. *Neuron* **71**, 9–34 (2011).
276. Izhikevich, E. M. Simple Model of Spiking Neurons. *IEEE Trans. NEURAL NETWORKS* **14**, (2003).
277. Zamanian, J., Xu, L. & Foo, L. Genomic Analysis of Reactive Astroglia. *J. ...* **32**, 6391–6410 (2012).
278. Martín, R., Bajo-Grañeras, R., Moratalla, R., Perea, G. & Araque, A. Circuit-specific signaling in astrocyte-neuron networks in basal ganglia pathways. *Science (80-.)*. **349**, (2015).
279. Araque, A. *et al.* Gliotransmitters Travel in Time and Space. *Neuron* **81**, 728–739 (2014).
280. Robel, S. *et al.* Reactive astroglia causes the development of spontaneous seizures. *J. Neurosci.* **35**, 3330–45 (2015).
281. Ortinski, P. I. *et al.* Selective induction of astrocytic gliosis generates deficits in neuronal inhibition. *Nat. Neurosci.* **13**, 584–91 (2010).
282. Cardin, J. A. *et al.* Driving fast-spiking cells induces gamma rhythm and controls sensory responses. *Nature* **459**, 663–667 (2009).
283. Roux, L. & Buzsáki, G. Tasks for inhibitory interneurons in intact brain circuits. *Neuropharmacology* **88**, 10–23 (2015).
284. Fries, P., Nikolić, D. & Singer, W. The gamma cycle. *Trends Neurosci.* **30**, 309–316 (2007).
285. Neto, J. P. *et al.* Validating silicon polytrodes with paired juxtacellular recordings: method and dataset. *J. Neurophysiol.* **116**, (2016).
286. Liu, X.-B. & Murray, K. D. Neuronal excitability and calcium/calmodulin-dependent protein kinase type II: Location, location, location. *Epilepsia* **53**, 45–52 (2012).
287. McCreery, D., Cogan, S., Kane, S. & Pikov, V. Correlations between histology and neuronal activity recorded by microelectrodes implanted chronically in the cerebral cortex. *J. Neural Eng.* **13**, 036012 (2016).
288. Su-Youne Chang, S.-Y., Young Min Shon, Y. M., Agnesi, F. & Lee, K. H. Microthalamotomy effect during deep brain stimulation: Potential involvement of adenosine and glutamate efflux. in *2009 Annual International Conference of the IEEE Engineering in Medicine and Biology Society* 3294–3297 (IEEE, 2009). doi:10.1109/IEMBS.2009.5333735

289. Minelli, A., Edwards, R. H., Manzoni, T. & Conti, F. *Postnatal development of the glutamate vesicular transporter VGLUT1 in rat cerebral cortex. Developmental Brain Research* **140**, (2003).
290. Wilson, N. R. *et al.* Presynaptic Regulation of Quantal Size by the Vesicular Glutamate Transporter VGLUT1. *J. Neurosci.* **25**, (2005).
291. Sánchez-Mendoza, E. *et al.* Transient focal cerebral ischemia significantly alters not only EAATs but also VGLUTs expression in rats: relevance of changes in reactive astroglia. *J. Neurochem.* **113**, 1343–1355 (2010).
292. Jones, E., Huntley, G. & Benson, D. Alpha calcium/calmodulin-dependent protein kinase II selectively expressed in a subpopulation of excitatory neurons in monkey sensory- motor cortex: comparison with GAD-67 expression. *J. Neurosci.* **14**, (1994).
293. Hamilton, N. B. & Attwell, D. Do astrocytes really exocytose neurotransmitters? *Nat. Publ. Gr.* **11**, (2010).
294. Lee, S. *et al.* Channel-mediated tonic GABA release from glia. *Science* **330**, 790–6 (2010).
295. Le Meur, K., Mendizabal-Zubiaga, J., Grandes, P. & Audinat, E. GABA release by hippocampal astrocytes. *Front. Comput. Neurosci.* **6**, 59 (2012).
296. Kozlov, A. S., Angulo, M. C., Audinat, E. & Charpak, S. Target cell-specific modulation of neuronal activity by astrocytes. *Proc. Natl. Acad. Sci. U. S. A.* **103**, 10058–63 (2006).
297. Lee, M., McGeer, E. G. & McGeer, P. L. Mechanisms of GABA release from human astrocytes. *Glia* **59**, 1600–1611 (2011).
298. Jo, S. *et al.* GABA from reactive astrocytes impairs memory in mouse models of Alzheimer’s disease. *Nat. Med.* **20**, 886–896 (2014).
299. Bean, B. P. The action potential in mammalian central neurons. *Nat. Rev. Neurosci.* **8**, 451–465 (2007).
300. Perge, J. A. *et al.* Intra-day signal instabilities affect decoding performance in an intracortical neural interface system. *J. Neural Eng.* **10**, 036004 (2013).
301. Gilja, V. *et al.* Challenges and Opportunities for Next-Generation Intracortically Based Neural Prostheses. *IEEE Trans. Biomed. Eng.* **58**, 1891–1899 (2011).
302. Salatino, J. W., Ludwig, K. A., Kozai, T. D. Y. & Purcell, E. K. Glial responses to implanted electrodes in the brain. *Nat. Biomed. Eng.* (2017). doi:10.1038/s41551-017-0154-1
303. Mao, Q. *et al.* The up-regulation of voltage-gated sodium channel nav1.6 expression

- following fluid percussion traumatic brain injury in rats. *Neurosurgery* **66**, 1134–1139 (2010).
304. Bolkvadze, T. & Pitkänen, A. Development of Post-Traumatic Epilepsy after Controlled Cortical Impact and Lateral Fluid-Perfusion-Induced Brain Injury in the Mouse. *J. Neurotrauma* (2012). doi:10.1089/neu.2011.1954
 305. Lei, Z., Deng, P., Li, J. & Xu, Z. C. Alterations of A-type potassium channels in hippocampal neurons after traumatic brain injury. *J. Neurotrauma* **29**, 235–45 (2012).
 306. Huang, X.-J. *et al.* Blockage of the Upregulation of Voltage-Gated Sodium Channel Nav1.3 Improves Outcomes after Experimental Traumatic Brain Injury. *J. Neurotrauma* **12**, 1–12 (2013).
 307. Vezzani, A., Maroso, M., Balosso, S., Sanchez, M.-A. & Bartfai, T. IL-1 receptor/Toll-like receptor signaling in infection, inflammation, stress and neurodegeneration couples hyperexcitability and seizures. *Brain. Behav. Immun.* **25**, 1281–1289 (2011).
 308. Viviani, B., Gardoni, F. & Marinovich, M. Cytokines and Neuronal Ion Channels in Health and Disease. *Int. Rev. Neurobiol.* **82**, 247–263 (2007).
 309. Buffo, A., Rolando, C. & Ceruti, S. Astrocytes in the damaged brain: molecular and cellular insights into their reactive response and healing potential. *Biochem. Pharmacol.* **79**, 77–89 (2010).
 310. Heinemann, U., Kaufer, D. & Friedman, A. Blood-brain barrier dysfunction, TGF β signaling, and astrocyte dysfunction in epilepsy. *Glia* **60**, 1251–7 (2012).
 311. Jin, X., Prince, D. A. & Huguenard, J. R. Enhanced excitatory synaptic connectivity in layer v pyramidal neurons of chronically injured epileptogenic neocortex in rats. *J. Neurosci.* **26**, 4891–900 (2006).
 312. Greer, J. E., Povlishock, J. T. & Jacobs, K. M. Electrophysiological Abnormalities in Both Axotomized and Nonaxotomized Pyramidal Neurons following Mild Traumatic Brain Injury. *J. Neurosci.* **32**, 6682–6687 (2012).
 313. Caldwell, J. H., Schaller, K. L., Lasher, R. S., Peles, E. & Levinson, S. R. Sodium channel Nav1.6 is localized at nodes of Ranvier, dendrites, and synapses. *PNAS* **97**, 5616–5620 (2000).
 314. Smart, S. L. *et al.* Deletion of the KV1.1 Potassium Channel Causes Epilepsy in Mice. *Neuron* **20**, 809–819 (1998).
 315. Figueiro-Silva, J. *et al.* Neuronal Pentraxin 1 Negatively Regulates Excitatory Synapse Density and Synaptic Plasticity. *J. Neurosci.* **35**, 5504–5521 (2015).

316. Guatteo, E., Franceschetti, S., Bacci, A., Avanzini, G. & Wanke, E. A TTX-sensitive conductance underlying burst firing in isolated pyramidal neurons from rat neocortex. *Brain Res.* **741**, 1–12 (1996).
317. Yuen, T. J., Browne, K. D., Iwata, A. & Smith, D. H. Sodium channelopathy induced by mild axonal trauma worsens outcome after a repeat injury. *J. Neurosci. Res.* **87**, 3620–3625 (2009).
318. Diem, R., Hobom, M., Grötsch, P., Kramer, B. & Bähr, M. Interleukin-1 β protects neurons via the interleukin-1 (IL-1) receptor-mediated Akt pathway and by IL-1 receptor-independent decrease of transmembrane currents in vivo. *Mol. Cell. Neurosci.* **22**, 487–500 (2003).
319. Zhou, C. *et al.* Interleukin-1 β Inhibits Voltage-Gated Sodium Currents in a Time- and Dose-Dependent Manner in Cortical Neurons. *Neurochem. Res.* **36**, 1116–1123 (2011).
320. Nashmi, R., Jones, O. T. & Fehlings, M. G. Abnormal axonal physiology is associated with altered expression and distribution of Kv1.1 and Kv1.2 K⁺ channels after chronic spinal cord injury. *Eur. J. Neurosci.* **12**, 491–506 (2000).
321. Nashmi, R. & Fehlings, M. G. Mechanisms of axonal dysfunction after spinal cord injury: With an emphasis on the role of voltage-gated potassium channels. *Brain Res. Rev.* **38**, 165–191 (2001).
322. Blumenfeld, H. *et al.* Role of hippocampal sodium channel Nav1.6 in kindling epileptogenesis. *Epilepsia* **50**, 44–55 (2009).
323. Xie, C. *et al.* Three-dimensional macroporous nanoelectronic networks as minimally invasive brain probes. *Nat. Mater.* **14**, 1286–1292 (2015).
324. Purcell, E. K., Seymour, J. P., Yandamuri, S. & Kipke, D. R. In vivo evaluation of a neural stem cell-seeded prosthesis. *J. Neural Eng.* **6**, 026005 (2009).
325. Kozai, T. D. Y., Jaquins-gerstl, A. S., Vazquez, A. L., Michael, A. C. & Cui, X. T. Biomaterials Dexamethasone retrodialysis attenuates microglial response to implanted probes in vivo. *Biomaterials* **87**, 157–169 (2016).
326. Michelson, N. J. *et al.* Multi-scale, multi-modal analysis uncovers complex relationship at the brain tissue-implant neural interface: New emphasis on the biological interface. *J. Neural Eng.* **15**, (2018).
327. Jackson, A. & Fetz, E. E. Compact Movable Microwire Array for Long-Term Chronic Unit Recording in Cerebral Cortex of Primates. *J. Neurophysiol.* **98**, (2007).
328. Prince, D. A., Parada, I. & Graber, K. *Traumatic Brain Injury and Posttraumatic Epilepsy. Jasper's Basic Mechanisms of the Epilepsies* (National Center for Biotechnology Information (US), 2012).

329. Eles, J. R., Vazquez, A. L., Kozai, T. D. Y. & Cui, X. T. In vivo imaging of neuronal calcium during electrode implantation: Spatial and temporal mapping of damage and recovery. *Biomaterials* **174**, 79–94 (2018).
330. Carrasquillo, Y., Burkhalter, A. & Nerbonne, J. M. A-type K⁺ channels encoded by Kv4.2, Kv4.3 and Kv1.4 differentially regulate intrinsic excitability of cortical pyramidal neurons. *J. Physiol.* **590**, 3877–3890 (2012).
331. Wang, H. S. *et al.* KCNQ2 and KCNQ3 potassium channel subunits: molecular correlates of the M-channel. *Science* **282**, 1890–3 (1998).
332. Hansen, H. H. *et al.* Kv7 channels: interaction with dopaminergic and serotonergic neurotransmission in the CNS. *J. Physiol.* **586**, 1823–1832 (2008).
333. Hernandez, C. C., Zaika, O., Tolstykh, G. P. & Shapiro, M. S. Regulation of neural KCNQ channels: signalling pathways, structural motifs and functional implications. *J. Physiol.* **586**, 1811–1821 (2008).
334. Martire, M. *et al.* M Channels Containing KCNQ2 Subunits Modulate Norepinephrine, Aspartate, and GABA Release from Hippocampal Nerve Terminals. (2004). doi:10.1523/JNEUROSCI.3143-03.2004
335. Martire, M. *et al.* Involvement of KCNQ2 subunits in [³H]dopamine release triggered by depolarization and pre-synaptic muscarinic receptor activation from rat striatal synaptosomes. *J. Neurochem.* **102**, 179–193 (2007).
336. Buzsáki, G. Large-scale recording of neuronal ensembles. *Nat. Neurosci.* **7**, 446–451 (2004).
337. Buzsáki, G., Anastassiou, C. a. & Koch, C. The origin of extracellular fields and currents — EEG, ECoG, LFP and spikes. *Nat. Rev. Neurosci.* **13**, 407–420 (2012).
338. Reimann, M. W. *et al.* A biophysically detailed model of neocortical local field potentials predicts the critical role of active membrane currents. *Neuron* **79**, 375–390 (2013).
339. Gold, C., Henze, D. A., Koch, C. & Buzsáki, G. On the Origin of the Extracellular Action Potential Waveform: A Modeling Study. *J. Neurophysiol.* **95**, 3113–3128 (2006).
340. Wu, C.-Y., Kaur, C., Sivakumar, V., Lu, J. & Ling, E.-A. Kv1.1 expression in microglia regulates production and release of proinflammatory cytokines, endothelins and nitric oxide. *Neuroscience* **158**, 1500–1508 (2009).
341. Bagchi, B. *et al.* Disruption of Myelin Leads to Ectopic Expression of KV1.1 Channels with Abnormal Conductivity of Optic Nerve Axons in a Cuprizone-Induced Model of Demyelination. *PLoS One* **9**, e87736 (2014).

342. Liu, Y. *et al.* CDYL suppresses epileptogenesis in mice through repression of axonal Nav1.6 sodium channel expression. *Nat. Commun.* **8**, 355 (2017).
343. Arancibia-Cárcamo, I. L. *et al.* Node of Ranvier length as a potential regulator of myelinated axon conduction speed. *Elife* **6**, (2017).
344. Burkhalter, A., Gonchar, Y., Mellor, R. & Nerbonne, J. Differential Expression of IA Channel Subunits Kv4.2 and Kv4.3 in Mouse Visual Cortical Neurons and Synapses. *J. Neurosci.* **26**, 12274–12282 (2006).
345. Rizwan, A. P., Zhan, X., Zamponi, G. W. & Turner, R. W. Long-Term Potentiation at the Mossy Fiber-Granule Cell Relay Invokes Postsynaptic Second-Messenger Regulation of Kv4 Channels. *J. Neurosci.* **36**, 11196–11207 (2016).
346. Bekku, Y. *et al.* Bral1: Its Role in Diffusion Barrier Formation and Conduction Velocity in the CNS. *J. Neurosci.* **30**, 3113–3123 (2010).
347. Gascón, S. *et al.* Excitotoxicity and focal cerebral ischemia induce truncation of the NR2A and NR2B subunits of the NMDA receptor and cleavage of the scaffolding protein PSD-95. (2008). doi:10.1038/sj.mp
348. Golabchi, A. *et al.* Melatonin improves quality and longevity of chronic neural recording. *Biomaterials* **180**, 225–239 (2018).
349. Kozai, T. D. Y., Jaquins-Gerstl, A. S., Vazquez, A. L., Michael, A. C. & Cui, X. T. Dexamethasone retrodialysis attenuates microglial response to implanted probes in vivo. *Biomaterials* **87**, 157–169 (2016).
350. Thompson, C. H., Zoratti, M. J., Langhals, N. B. & Purcell, E. K. Regenerative Electrode Interfaces for Neural Prostheses. *Tissue Eng. Part B Rev.* **22**, 125–135 (2016).
351. Winter, B. M., Daniels, S. R., Salatino, J. W. & Purcell, E. K. Genetic Modulation at the Neural Microelectrode Interface: Methods and Applications. *Micromachines* **9**, 476 (2018).
352. Winter, B. M. *et al.* Control of cell fate and excitability at the neural electrode interface: Genetic reprogramming and optical induction. in *2017 IEEE Life Sciences Conference (LSC)* 157–161 (IEEE, 2017). doi:10.1109/LSC.2017.8268167
353. Halassa, M. M., Fellin, T. & Haydon, P. G. The tripartite synapse: roles for gliotransmission in health and disease. *Trends Mol. Med.* **13**, 54–63 (2007).
354. Halassa, M. M. & Haydon, P. G. Integrated brain circuits: astrocytic networks modulate neuronal activity and behavior. *Annu. Rev. Physiol.* **72**, 335–55 (2010).
355. Perea, G., Navarrete, M. & Araque, A. Tripartite synapses: astrocytes process and

- control synaptic information. *Trends Neurosci. (Cell Rev.)* (2009). doi:10.1016/j.tins.2009.05.001
356. Araque, A., Parpura, V., Sanzgiri, R. P. & Haydon, P. G. Tripartite synapses: glia, the unacknowledged partner. *Trends Neurosci.* **22**, 208–215 (1999).
357. Balosso, S. *et al.* Tumor necrosis factor- α inhibits seizures in mice via p75 receptors. *Ann. Neurol.* **57**, 804–812 (2005).
358. Shen, Y. *et al.* Postnatal activation of TLR4 in astrocytes promotes excitatory synaptogenesis in hippocampal neurons. *J. Cell Biol.* **215**, 719–734 (2016).
359. Henry, C. J., Huang, Y., Wynne, A. M. & Godbout, J. P. Peripheral lipopolysaccharide (LPS) challenge promotes microglial hyperactivity in aged mice that is associated with exaggerated induction of both pro-inflammatory IL-1 β and anti-inflammatory IL-10 cytokines. *Brain Behav. Immun.* **23**, 309–317 (2008).
360. Bedell, H. W. *et al.* Targeting CD14 on blood derived cells improves intracortical microelectrode performance. *Biomaterials* **163**, 163–173 (2018).
361. Bennett, C. *et al.* Neuroinflammation, oxidative stress, and blood-brain barrier (BBB) disruption in acute Utah electrode array implants and the effect of deferoxamine as an iron chelator on acute foreign body response. *Biomaterials* **188**, 144–159 (2019).
362. Bennett, C. *et al.* Blood brain barrier (BBB)-disruption in intracortical silicon microelectrode implants. *Biomaterials* **164**, 1–10 (2018).
363. Hermann, J. K. *et al.* Inhibition of the cluster of differentiation 14 innate immunity pathway with IAXO-101 improves chronic microelectrode performance. *J. Neural Eng.* **15**, 025002 (2018).
364. Tzour, A. *et al.* KV7/M channels as targets for lipopolysaccharide-induced inflammatory neuronal hyperexcitability. *J. Physiol.* **595**, 713–738 (2017).
365. Gamper, N. & Shapiro, M. S. Calmodulin mediates Ca²⁺-dependent modulation of M-type K⁺ channels. *J. Gen. Physiol.* **122**, 17–31 (2003).
366. Wen, H. & Levitan, I. B. Calmodulin is an auxiliary subunit of KCNQ2/3 potassium channels. *J. Neurosci.* **22**, 7991–8001 (2002).
367. Christensen, R. K. *et al.* Spinal dorsal horn astrocytes release GABA in response to synaptic activation. *J. Physiol.* **596**, 4983–4994 (2018).
368. Lee, M., McGeer, E. G. & McGeer, P. L. Mechanisms of GABA release from human astrocytes. *Glia* **59**, 1600–1611 (2011).

369. Pascual, O. *et al.* Astrocytic Purinergic Signaling Coordinates Synaptic Networks. *Haydon Source Sci. New Ser.* **310**, 113–116 (2005).
370. Zhang, Q. *et al.* Fusion-related release of glutamate from astrocytes. *J. Biol. Chem.* **279**, 12724–33 (2004).
371. Ormel, L., Stensrud, M. J., Bergersen, L. H. & Gundersen, V. VGLUT1 is localized in astrocytic processes in several brain regions. *Glia* **60**, 229–238 (2012).
372. Araque, A., Li, N., Doyle, R. T. & Haydon, P. G. SNARE Protein-Dependent Glutamate Release from Astrocytes. *J. Neurosci.* **20**, 666–673 (2000).
373. Burrone, J., Li, Z. & Murthy, V. N. Studying vesicle cycling in presynaptic terminals using the genetically encoded probe synaptopHluorin. *Nat. Protoc.* **1**, 2970–2978 (2006).
374. Allen, T. G. J. The ‘sniffer-patch’ technique for detection of neurotransmitter release. *Trends Neurosci.* **20**, 192–197 (1997).
375. Michelson, N. J. *et al.* Multi-scale, multi-modal analysis uncovers complex relationship at the brain tissue-implant neural interface: new emphasis on the biological interface. *J. Neural Eng.* **15**, 033001 (2018).
376. Russo, M. V & McGavern, D. B. Inflammatory neuroprotection following traumatic brain injury. *Science* **353**, 783–5 (2016).
377. Christopherson, K. S. *et al.* Thrombospondins are astrocyte-secreted proteins that promote CNS synaptogenesis. *Cell* **120**, 421–33 (2005).
378. Allen, N. J. *et al.* Astrocyte glypicans 4 and 6 promote formation of excitatory synapses via GluA1 AMPA receptors. *Nat. 2012 4867403* **486**, 410 (2012).
379. Garrett, A. M. & Weiner, J. A. Control of CNS synapse development by {gamma}-protocadherin-mediated astrocyte-neuron contact. *J. Neurosci.* **29**, 11723–31 (2009).
380. Sultan, S. *et al.* Synaptic Integration of Adult-Born Hippocampal Neurons Is Locally Controlled by Astrocytes. *Neuron* **88**, 957–972 (2015).
381. O’Brien, R. J. *et al.* Synaptic Clustering of AMPA Receptors by the Extracellular Immediate-Early Gene Product Narp. *Neuron* **23**, 309–323 (1999).
382. O’Brien, R. *et al.* Synaptically targeted narp plays an essential role in the aggregation of AMPA receptors at excitatory synapses in cultured spinal neurons. *J. Neurosci.* **22**, 4487–98 (2002).
383. Chu, Y. *et al.* Enhanced synaptic connectivity and epilepsy in C1q knockout mice. *Proc. Natl. Acad. Sci.* **107**, 7975–7980 (2010).

384. Huh, G. S. *et al.* Functional requirement for class I MHC in CNS development and plasticity. *Science* **290**, 2155–2159 (2000).
385. Stevens, B. *et al.* The Classical Complement Cascade Mediates CNS Synapse Elimination. *Cell* **131**, 1164–1178 (2007).
386. Elmariah, S. B., Oh, E. J., Hughes, E. G. & Balice-Gordon, R. J. Astrocytes regulate inhibitory synapse formation via Trk-mediated modulation of postsynaptic GABAA receptors. *J. Neurosci.* **25**, 3638–50 (2005).
387. Elmariah, S. B., Hughes, E. G., Oh, E. J. & Balice-Gordon, R. J. Neurotrophin signaling among neurons and glia during formation of tripartite synapses. *Neuron Glia Biol.* **1**, 1–11 (2004).
388. Chen, Z. *et al.* Microglial displacement of inhibitory synapses provides neuroprotection in the adult brain. *Nat. Commun.* **5**, 4486 (2014).
389. Maroso, M. *et al.* Toll-like receptor 4 and high-mobility group box-1 are involved in ictogenesis and can be targeted to reduce seizures. *Nat. Med.* **16**, 413–419 (2010).
390. Ravizza, T. *et al.* Interleukin Converting Enzyme inhibition impairs kindling epileptogenesis in rats by blocking astrocytic IL-1 β production. *Neurobiol. Dis.* **31**, 327–333 (2008).
391. Balosso, S. *et al.* A novel non-transcriptional pathway mediates the proconvulsive effects of interleukin-1. *Brain* **131**, 3256–3265 (2008).
392. Iori, V. *et al.* Receptor for Advanced Glycation Endproducts is upregulated in temporal lobe epilepsy and contributes to experimental seizures. *Neurobiol. Dis.* **58**, 102–114 (2013).
393. Li, T., Quan Lan, J., Fredholm, B. B., Simon, R. P. & Boison, D. Adenosine dysfunction in astrogliosis: cause for seizure generation? *Neuron Glia Biol.* **3**, (2007).
394. Chen, C. & Bazan, N. G. Lipid signaling: Sleep, synaptic plasticity, and neuroprotection. *Prostaglandins Other Lipid Mediat.* **77**, 65–76 (2005).
395. Yang, S. *et al.* Interleukin-1 β enhances NMDA receptor-mediated current but inhibits excitatory synaptic transmission. *Brain Research* **1034**, (2005).
396. Viviani, B. *et al.* Interleukin-1beta enhances NMDA receptor-mediated intracellular calcium increase through activation of the Src family of kinases. *J. Neurosci.* **23**, 8692–700 (2003).
397. Ogoshi, F. *et al.* Tumor necrosis-factor-alpha (TNF- α) induces rapid insertion of Ca²⁺-permeable α -amino-3-hydroxyl-5-methyl-4-isoxazole-propionate (AMPA)/kainate

- (Ca-A/K) channels in a subset of hippocampal pyramidal neurons. *Exp. Neurol.* **193**, 384–393 (2005).
398. Eid, T. *et al.* Loss of glutamine synthetase in the human epileptogenic hippocampus: possible mechanism for raised extracellular glutamate in mesial temporal lobe epilepsy. *Lancet* **363**, 28–37 (2004).
399. Plata-Salamán, C. R. & French-Mullen, J. M. H. Interleukin-1 β inhibits Ca²⁺ channel currents in hippocampal neurons through protein kinase C. *Eur. J. Pharmacol. Mol. Pharmacol.* **266**, 1–10 (1994).
400. Zhou, C. *et al.* Interleukin-1 β downregulates the L-type Ca²⁺ channel activity by depressing the expression of channel protein in cortical neurons. *J. Cell. Physiol.* **206**, 799–806 (2006).
401. Kochanek, P. M. *et al.* Adenosine A1 receptor knockout mice develop lethal status epilepticus after experimental traumatic brain injury. *J. Cereb. Blood Flow Metab.* **26**, 565–75 (2006).
402. Cunningham, A. J., Murray, C. A., O'Neill, L. A. J., Lynch, M. A. & O'Connor, J. J. Interleukin-1 β (IL-1 β) and tumour necrosis factor (TNF) inhibit long-term potentiation in the rat dentate gyrus in vitro. *Neurosci. Lett.* **203**, 17–20 (1996).
403. Katsuki, H. *et al.* Interleukin-1 β inhibits long-term potentiation in the CA3 region of mouse hippocampal slices. *Eur. J. Pharmacol.* **181**, 323–326 (1990).
404. Miller, L. G., Galpern, W. R., Dunlap, K., Dinarello, C. A. & Turner, T. J. Interleukin-1 augments gamma-aminobutyric acidA receptor function in brain. *Mol. Pharmacol.* **39**, 105–8 (1991).
405. Fedele, D. E., Li, T., Lan, J. Q., Fredholm, B. B. & Boison, D. Adenosine A1 receptors are crucial in keeping an epileptic focus localized. *Exp. Neurol.* **200**, 184–190 (2006).
406. Martín, E. D. *et al.* Adenosine released by astrocytes contributes to hypoxia-induced modulation of synaptic transmission. *Glia* **55**, 36–45 (2007).
407. Fellin, T., Pascual, O. & Haydon, P. G. Astrocytes coordinate synaptic networks: balanced excitation and inhibition. *Physiology (Bethesda)*. **21**, 208–15 (2006).